Phototransistors based on InP HEMTs and HBTs, and their applications to fiber-optic/millimeter-wave data transmission systems

Chang-Soon Choi

THE GRADUATE SCHOOL

YONSEI UNIVERSITY

Department of Electrical and Electronic Engineering

Phototransistors based on InP HEMTs and HBTs, and their applications to fiber-optic/millimeter-wave data transmission systems

by

Chang-Soon Choi

Submitted to the Department of Electrical and Electronic Engineering
in partial fulfillment of the requirements for the degree of

Doctor of Philosophy

at the

THE GRADUATE SCHOOL

YONSEI UNIVERSITY

January 2005

This certificates that the dissertation of

Chang-Soon Choi is approved.

____

Thesis Supervisor: Woo-Young Choi

____

Sang-Kook Han

____

Ilgu Yun

____

Kwang-Seok Seo

____

Jeha Kim

THE GRADUATE SCHOOL

YONSEI UNIVERSITY

January 2005

Abstract

Phototransistors based on InP HEMTs and InP HBTs are investigated and practically implemented to fiber-optic/millimeter-wave data transmission systems. The physical origins involved in photodetection characteristics of the fabricated InP HEMT are clarified through the consideration of its phototransistor operations. Based on the understanding of these photodetection mechanisms, the important device parameters including phototransistor internal gain and optical gain cutoff frequency are determined for the InP HEMT. It is experimentally shown for the first time that they are applicable to millimeter-wave subharmonic optoelectronic mixers that have the possibility to use low frequency local oscillator (LO) for millimeter-wave frequency up-conversion. To evaluate InP HEMT optoelectronic mixer performances, an internal conversion gain is introduced and characterized at 60GHz band. Nonlinear distortion characteristics and usable LO ranges for InP HEMT subharmonic optoelectronic mixers are also investigated. Utilizing them, fiber-optic/millimeter-wave data transmission system is constructed and 622Mbps data transmission over 30km fiber-optic link and 3m wireless link at 60GHz band is demonstrated. Their other applications, direct optically injection-locked oscillators are introduced with expecting their potentials to offer high-power and low phase-noise LO source. By endowing them with harmonic optoelectronic mixing functions, a novel antenna base station architecture is proposed

for fiber-optic/millimeter-wave downlinks. It is made up of an InP HEMT oscillator, in which the InP HEMT device simultaneously provides the functions of optically injection-locked oscillation and harmonic optoelectronic mixing. Fiber-optic/30GHz data transmission systems employing the proposed scheme are presented and 16QAM downlink data transmission in these systems is successfully demonstrated with the help of its low phase-noise characteristics. For achieving gigabit transmission in fiber-optic/millimeter-wave links, InP HBTs which are expected to provide wide photonic bandwidth are also exploited. It is experimentally shown that an InP HBT exhibits higher optical responsivity and wider optical 3dB bandwidth in comparison with InP HEMT. Utilizing it as a broadband optoelectronic mixer, 1.25Gbps data transmission in both fiber-optic wireline and 60GHz wireless links is achieved and their applicability to broadband fiber-optic/millimeter-wave convergence networks are given.

KEYWORDS: Phototransistor, InP-based HEMT, InP-based HBT, Photodetector, Millimeter-wave, Microwave photonics, Radio-on-fiber system, Fiber-optic/millimeter-wave data transmission system, Broadband convergence network

STUDENT NUMBER: 10120135

Table of Contents

TABLE OF CONTENTS ..... **VI**

1. INTRODUCTION **1**

1-1. FIBER-OPTIC/MILLIMETER-WAVE DATA TRANSMISSION SYSTEMS FOR BROADBAND CONVERGENCE NETWORKS 1

1-2. DESIGN CONSIDERATION OF FIBER-OPTIC/MILLIMETER-WAVE DATA TRANSMISSION SYSTEMS 6

1-3. THREE-TERMINAL PHOTOTRANSISTORS 13

1-4. OUTLINE OF DISSERTATION 18

REFERENCES 20

2. PHOTOTRANSISTORS BASED ON INP HEMTS **24**

2-1. INTRODUCTION 24

2-1-1. InP HEMT for optoelectronic MMIC *24*

2-1-2. Simulation analysis of InP HEMT *27*

2-2. 0.1μM INP PHEMT USED IN THIS WORK 31

2-2-1. InP pseudomorphic HEMT structure *31*

2-2-2. Device characteristics of InP pHEMT. *34*

2-3. EXPERIMENTAL SETUP 38

2-4. PHOTODETECTION CHARACTERISTICS OF INP HEMT 41

2-4-1. Motivation *41*

2-4-2. Photodetection mechanisms in InP HEMT *42*

2-4-3. DC photodetection characteristics of InP pHEMT *47*

2-4-4. Optical modulation response of InP HEMT *54*

2-4-5. 60GHz photodetection with optimization process *57*

2-4-6. Fiber-optic transmission demonstration using InP HEMT *60*

2-5. CONCLUSION 62

REFERENCES 64

3. FIBER-OPTIC/MILLIMETER-WAVE DATA TRANSMISSION SYSTEMS BASED ON INP HEMTS **67**

3-1. INTRODUCTION 67

3-1-1. Direct optical control of microwave devices and circuits for fiber-optic/millimeter-wave

systems *67*
3-1-2. Optically controlled amplifiers *68*
3-1-3. Optoelectronic mixers *69*
3-1-4. Optical control of oscillators *69*
3-2. SUBHARMONIC OPTOELECTRONIC MIXER 74
3-2-1. Motivation *74*
3-2-2. Features of InP HEMT subharmonic optoelectronic mixers *75*
3-2-3. Optimum bias conditions and internal conversion gain *78*
3-2-4. Usable LO ranges *82*
3-2-5. Nonlinear distortion characteristics *84*
3-3. FIBER-OPTIC/60GHZ DATA TRANSMISSION SYSTEMS BASED ON INP HEMT SUBHARMONIC OPTOELECTRONIC MIXERS 88
3-4. DIRECT OPTICAL INJECTION-LOCKED OSCILLATOR 92
3-4-1. Motivation *92*
3-4-2. Characteristics of direct optical injection-locked oscillators *95*
3-5. FIBER-OPTIC/MILLIMETER-WAVE DATA TRANSMISSION SYSTEMS BASED ON OPTICALLY CONTROLLED INP HEMT OSCILLATORS 100
3-5-1. Proposed scheme *100*
3-5-2. Fiber-optic/30GHz data transmission demonstration *103*
3-6. CONCLUSION 111
REFERENCES 113

4. PHOTOTRANSISTORS BASED ON INP HBTS AND THEIR APPLICATIONS TO GIGABIT DATA TRANSMISSION LINKS 116

4-1. INTRODUCTION 116
4-1-1. InP HBT for optoelectronic MMIC *116*
4-1-2. InP/InGaAs HBT used in this work *119*
4-1-3. Device characteristics of InP/InGaAs HBT *123*
4-2. EXPERIMENTAL SETUP 126
4-3. PHOTODETECTION CHARACTERISTICS OF INP HBT 127
4-3-1. Photodetection mechanism in InP HBT *127*
4-3-2. DC photodetection characteristics of InP HBT *129*
4-3. OPTOELECTRONIC MIXER 134
4-3-1. Features of InP HBT optoelectronic mixer *134*
4-3-2. Usable LO frequency ranges *137*
4-4. GIGABIT DATA TRANSMISSION IN FIBER-OPTIC WIRELINE AND 60GHZ WIRELESS LINKS 138

4-4-1. Motivation ... *138*
4-4-2. Gigabit data transmission in fiber-optic and 60GHz links ... *140*
4-5. CONCLUSION ... 145
REFERENCES ... 146

5. SUMMARY AND FUTURE WORKS ... 147

5-1. SUMMARY ... 147
5-2. COMPARISON BETWEEN TWO TYPES OF PHOTOTRANSISTORS, INP HEMTS AND HBTS ... 150
5-3. FUTURE WORKS ... 154

APPENDICE ... 155

A. HIGH-SPEED PHOTODIODE AS AN OPTOELECTRONIC MIXER FOR FIBER-OPTIC/MILLIMETER-WAVE UPLINK DATA TRANSMISSION ... 155
B. MEDICI SIMULATION CODE FOR LATTICE-MATCHED INP HEMT ... 162

PUBLICATION LISTS ... 167

Chapter 1

Introduction

1-1. Fiber-optic/millimeter-wave data transmission systems for broadband convergence networks

Since analog cellular phone services were first commercialized, personal mobile communication services have made great progress in the past two decades. Through the digital voice telephony services, much attention is now moving toward next-generation mobile networks which are expected to service not only voice stream but also broadband multimedia data such as high-quality video stream [1]. Concurrently, the exploding growth of mobile internet subscribers have stimulated considerable interest in broadband wireless services such as high-speed wireless local-area networks (LAN), broadband wireless access (BWA) and intelligent traffic systems (ITS).

Millimeter-wave frequency bands, depicted in Fig. 1-1-(A), have been regarded as one of the promising frequency bands for these future broadband wireless communication systems [2]. They had been exclusively utilized in military applications including missile guidance systems and high-resolution radars. Radiometry and radio-telescope had been other major applications of millimeter-wave frequency bands until the 1980's. As a variety of wireless services have launched from the 1990's, low

frequency bands below 5GHz become congested and higher frequencies above tens of gigahertz are getting much attention. The potential to provide wide transmission bandwidth is the foremost reason to use these millimeter-wave frequency bands in broadband wireless fixed/mobile communication systems.

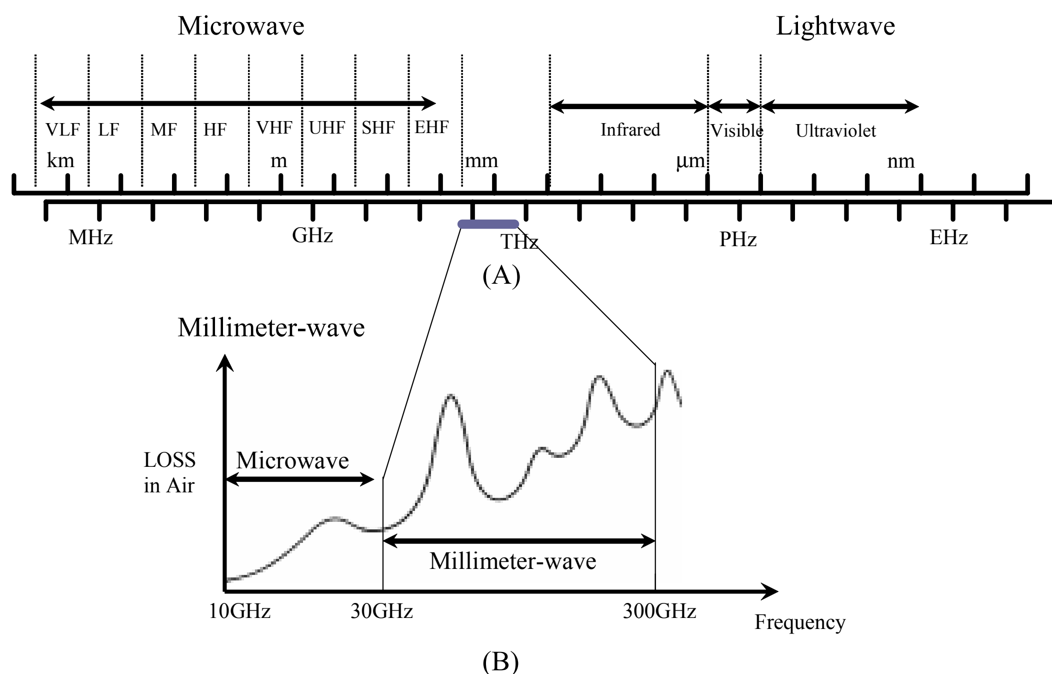

Figure 1-1. (A) Electromagnetic spectrums, (B) Signal attenuation as a function of millimeter-wave frequency

In addition to their wide bandwidth characteristics, there are several other factors making millimeter-wave frequency bands to be very attractive in broadband wireless networks. One important reason originates from the high atmospheric loss at millimeter-wave frequency bands, especially, at 60GHz band. Figure 1-1-(B) shows the signal attenuation (dB/km) as a function of signal frequency. Attenuation caused by oxygen resonance is about 10-16dB/km at 60GHz, which is much higher than any other

frequency bands below 100GHz. The high-attenuation characteristics of 60GHz band allow wireless communication systems to have enhanced frequency re-use capability and suppressed interference to adjacent cells. Another reason is a result of the smaller wavelength which makes RF components and radiation antennas to be smaller and provides higher imaging resolution, particularly attractive in automotive radar applications [3]. Finally, the millimeter-wave frequency bands around 60GHz provide large unlicensed spectral bandwidth, which is favorable to service providers. For example, the U.S. Federal Communications Commission (FCC) opens the 59-64 frequency bands for unlicensed applications [4].

In spite of these many advantages, millimeter-wave wireless communication systems are not yet widespread due to the difficulties in millimeter-wave generation, processing and transmission. Since these systems inherently use microcells or picocells in order to compensate high transmission loss of millimeter-wave, the interconnection between existing backbone networks and many antenna base stations in each cell is another critical factor for their practical implementations.

Fiber-optic technologies have been introduced as solutions to these problems, resulting in fiber-optic/millimeter-wave data transmission systems [5]. The mergence of fiber-optic wireline and micro/millimeter-wave wireless links can be also referred to radio-on-fiber systems which transmit RF signals with data to antenna base stations through optical fiber [6-7]. The main advantage of these approaches is that they are able to perform the above-mentioned micro/millimeter-wave functions by fiber-optic techniques even at very high frequencies. They also offer not only low loss and huge bandwidth wireline transmission medium by optical fiber but also incorporation with previously deployed fiber-optic networks, which makes it an ideal candidate for

realizing micro/pico cellular networks in millimeter-wave wireless communication systems such as high-speed wireless LANs, wireless personal networks (WPN) and road-to-vehicle communications in ITS. Figure 1-2 illustrates the applications of fiber-optic technologies to broadband millimeter-wave wireless links.

Recently, service providers of personal mobile communications begin to utilize these fiber-optic technologies for the wireless services in closed areas where subscribers cannot access to antenna base stations, for example, in shadow of building, in-building and underground area. Since an optical fiber is inherently small size, light-weight and flexible, it is easy to deploy many optical fiber cables in these closed area lying here and there. Figure 1-3 shows the example of fiber-optic technologies for closed area wireless service.

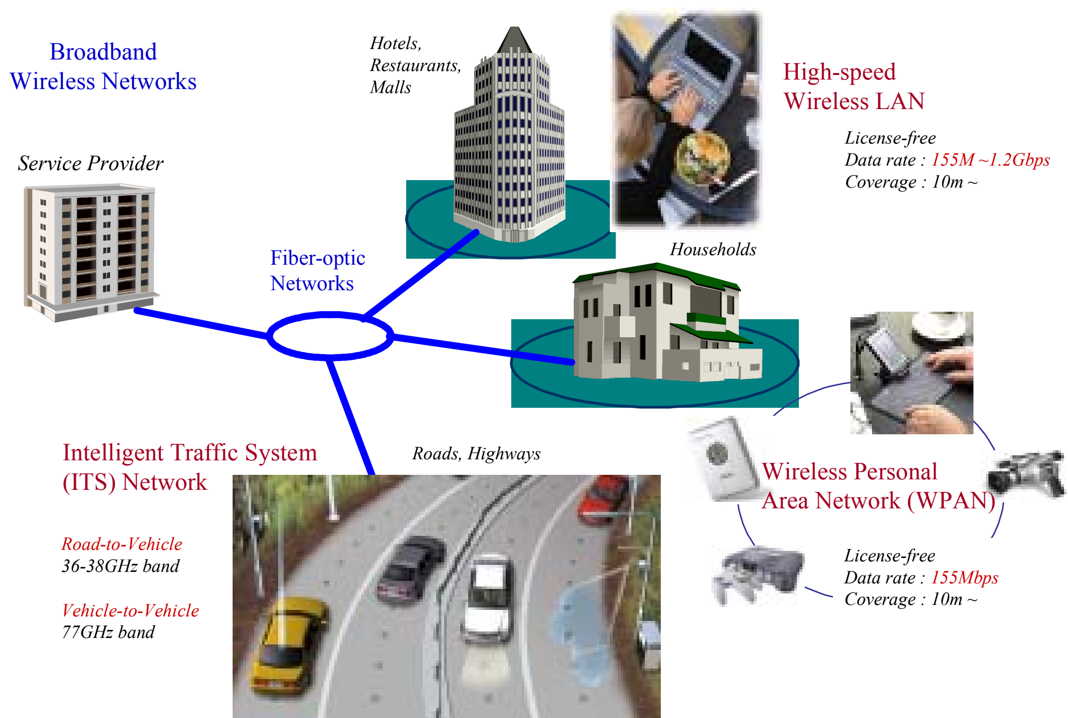

Figure 1-2. Applications of fiber-optic technologies to millimeter-wave wireless links

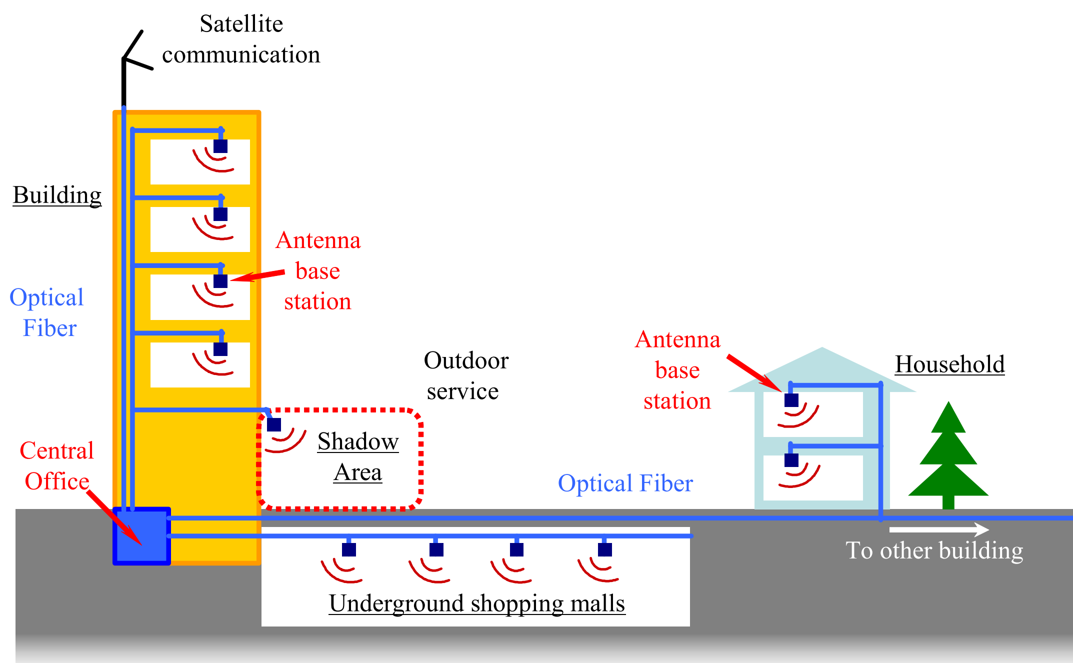

Figure 1-3. Applications of fiber-optic technologies to closed-area wireless services

1-2. Design consideration of fiber-optic/millimeter-wave data transmission systems

Figure 1-4 shows the typical layout of simplified fiber-optic/millimeter-wave downlink systems. In a central office (CO), input electrical signals can be converted to optical signals by several types of optical devices such as laser diodes and external modulators. In most cases, light sources have a wavelength of either 1300nm or 1550nm, however, some latest works have investigated 850nm vertical-cavity surface emitting laser (VCSEL)-based radio-on-fiber links for short-range communication [8-9]. Because the direct modulation frequency of commercially available laser diode is limited below a few tens of gigahertz, only baseband data or intermediate frequency (IF) modulations are practicable [10]. For the optical modulation of millimeter-wave signals, high-speed external optical modulators such as electro-optic modulators or electro-absorption modulators should be used, which also give us the possibility to independently optimize optical source for high-power and low-noise characteristics [10-12]. Other techniques having the potential to optically generate higher frequency have been also developed such as optical heterodyning techniques [14], mode-locked lasers [15] and dual-mode lasers [16].

The optical fiber may be multi-mode or single-mode, although the latter is favorable for long-distance optical communication due to its low dispersion properties. Although it provides extremely low loss (0.2dB/km at 1550nm) and wide bandwidth, fiber dispersion and nonlinearity may deteriorate the system performances of fiber-optic/millimeter-wave systems. In addition, optical amplifiers including erbium-doped fiber amplifiers (EDFA) and semiconductor optical amplifiers (SOA) should be

carefully used due to their inherent noise and nonlinear characteristics.

After optical transmission, optical receivers in antenna base stations (BS) convert optical signals back into corresponding RF signals. In a conventional vertical *p-i-n* photodiode, there is the fundamental limitation of bandwidth-efficiency product, basically attributed to its structure. To overcome this limitation, many works have been concentrated to the development of high-speed waveguide photodiodes and traveling-wave photodiodes which can detect millimeter-wave modulated optical signals without sacrificing absorption efficiency [17]. High saturation power is another key factor because the use of optical amplifier can eliminate the expensive electrical post-amplifier if a photodetector accommodates high input optical power [18]. For achieving high performance and low cost optical receivers, the one-chip integration is essential, which requires a photodetector to allow simple optoelectronic integration with other electrical circuitries.

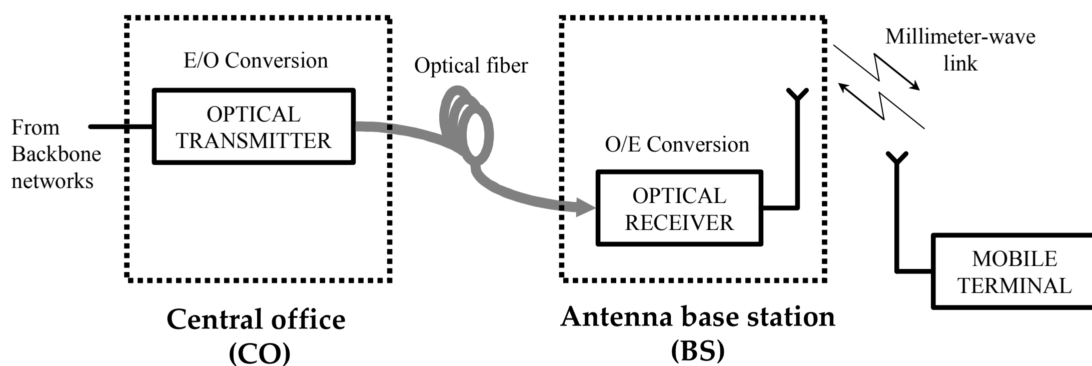

Figure 1-4. Typical layout of simplified fiber-optic/millimeter-wave downlink system

There are two major approaches to construct these fiber-optic/millimeter-wave data transmission systems. In one configuration, called optical millimeter-wave system shown in figure 1-5-(A), millimeter-wave signals are optically generated and transmitted over optical fiber, and converted back to millimeter-wave at antenna base station [12-13]. Although this scheme can provide a simple antenna base station architecture composed of only a photodetector, an amplifier and a radiation antenna, a high-speed photodetector operating at millimeter-wave is essential.[1] In addition, these intensity-modulation and direct-detection (IM-DD) schemes are unfortunately susceptible to fiber chromatic dispersion, particularly at high frequency modulated optical signal transmission. After the intensity-modulation, RF signals generate lower and upper sidebands which are separated from an optical carrier by the modulation frequency. During its propagation through optical fiber, these two sidebands experience a different phase-shift due to fiber chromatic dispersions. After direct detection, it results in the decreased carrier-to-noise ratio and increased phase noises in photodetected RF signals [19]. From the simulated results shown in the inset of figure 1-5-(A), it can be found that the dispersion-induced carrier-to-noise suppression is more severe if higher frequency modulated optical signal is transmitted.

These problems can be overcome by the optical heterodyning of frequency offsets between two single-mode laser outputs. This technique, however, generates a microwave signal with the large spectral width that is equal to the sum of linewidths of two lasers. In order to achieve low phase-noise characteristics of optically generated microwave signals, novel schemes in which two lasers are phase-locked, such as optical

[1] The 60GHz photodiode is available in Discovery Semiconductor, however, the price is higher than $10000/unit. (http://www.chipsat.com)

sideband injection-locking [20] and optical phase-locked loop [21] have been proposed but further improvements are necessary in terms of frequency stability and tunability.

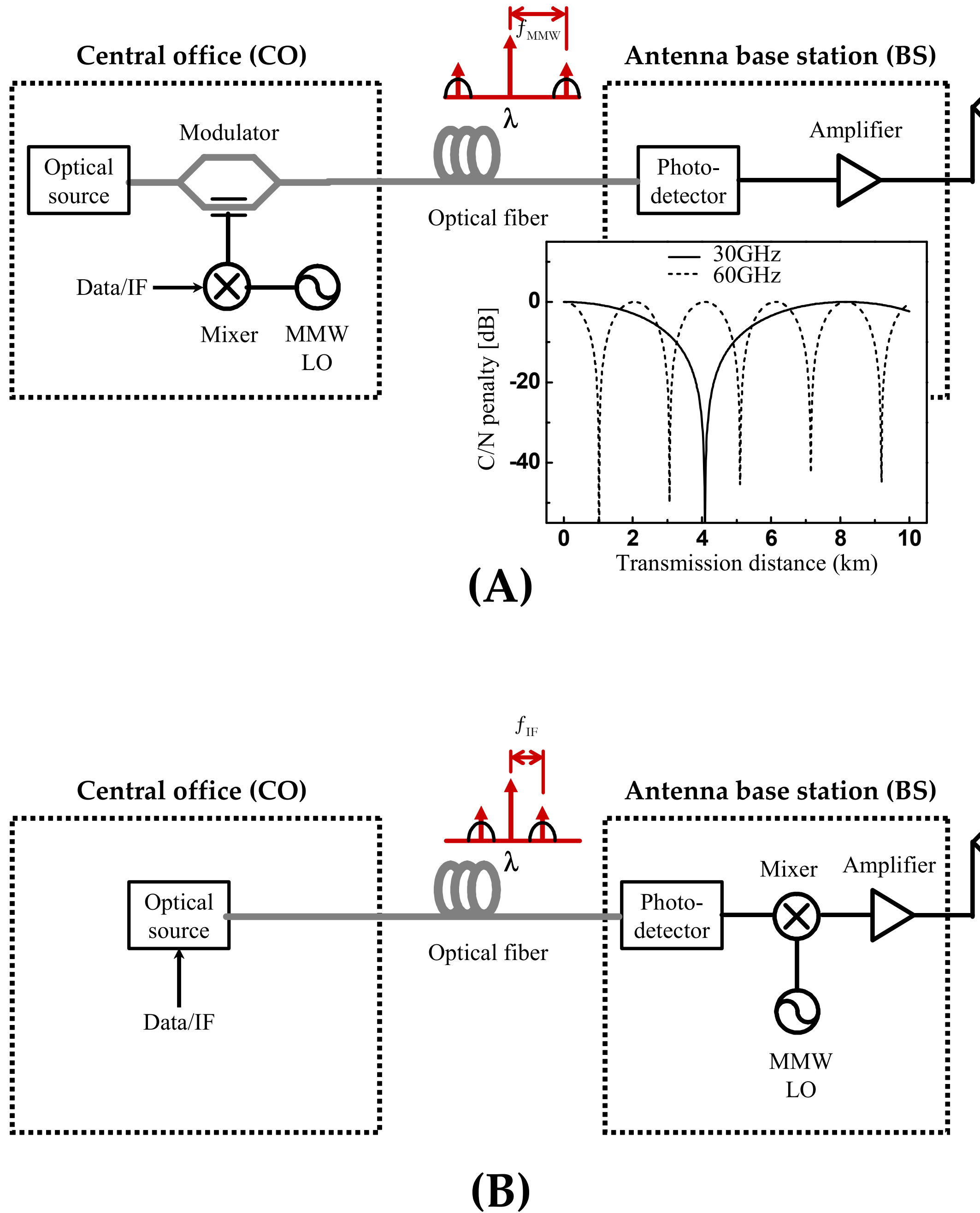

Figure 1-5. Two configurations of fiber-optic/millimeter-wave data transmission system (A) optical millimeter-wave system (B) remote up-conversion system. The inset shows the dispersion-induced C/N penalty as a function of optical transmission distance with a 1550nm wavelength and 17ps/km·nm dispersion parameter

In another scheme termed remote up-conversion system, low frequency data/IF modulated optical signals are transmitted over a fiber, and remotely frequency up-converted to millimeter-wave at the antenna base station as shown in figure 1-5-(B) [22-24]. This remote up-conversion scheme mitigates the above-mentioned problems and provides compatibility to wavelength division multiplexing (WDM) networks. However, complex antenna base station architecture is inevitable because it requires many millimeter-wave components including frequency mixers and phase-locked oscillators and filters. Therefore, the one-chip integration of photodetector, RF components and other matching circuitries on a single substrate is indispensable for reducing system construction cost in this remote up-conversion scheme.

For designing optical receivers of broadband optical communication systems, optoelectronic integrated circuit (OEIC) technologies have been studied for suppressing the parasitic effects in optical receiver and pursuing simple packaging [25-26]. However, they have not been widespread because additional fabrication steps such as epitaxial layer re-growth and careful circuit design techniques are required as shown in figure 1-6-(A). Furthermore, they are designed for signal processing of ultra-wide bandwidth incoming optical data signals exceeding tens of gigabit per second. It is different from the optical receiver in above-mentioned fiber-optic/millimeter-wave systems where many RF components such as low-noise amplifier, frequency mixer, oscillator and filter are required for the wireless transmission of RF signals. Therefore, monolithic microwave integrated circuits (MMIC) technologies are favorable for the integration of antenna base station if MMIC compatible photodetectors are employed.

There are two types of photodetectors having the compatibility to MMIC fabrication processes. Metal-semiconductor-metal photodiodes (MSM-PD) are most

common photodetectors used in MMIC integration because they provide simplicity of device fabrication and small capacitance which results in large photonic bandwidth. However, they have a low responsivity, the tradeoff between bandwidth and driving voltage, and the difficulties to achieving MSM-PD on small bandgap materials including InGaAs [27]. Three-terminal phototransistors are another alternative to MMIC compatible photodetectors which offer many useful characteristics in optical signal processing of fiber-optic/millimeter-wave systems. As shown in figure 1-6-(B), these phototransistors do not require additional epitaxial layers for photodetector, which results in the simplicity of optoelectronic integration called optoelectronic MMIC in this work. This dissertation focuses on three-terminal phototransistors having the potential to be utilized in optoelectronic MMIC and their applications to fiber-optic/millimeter-wave systems.

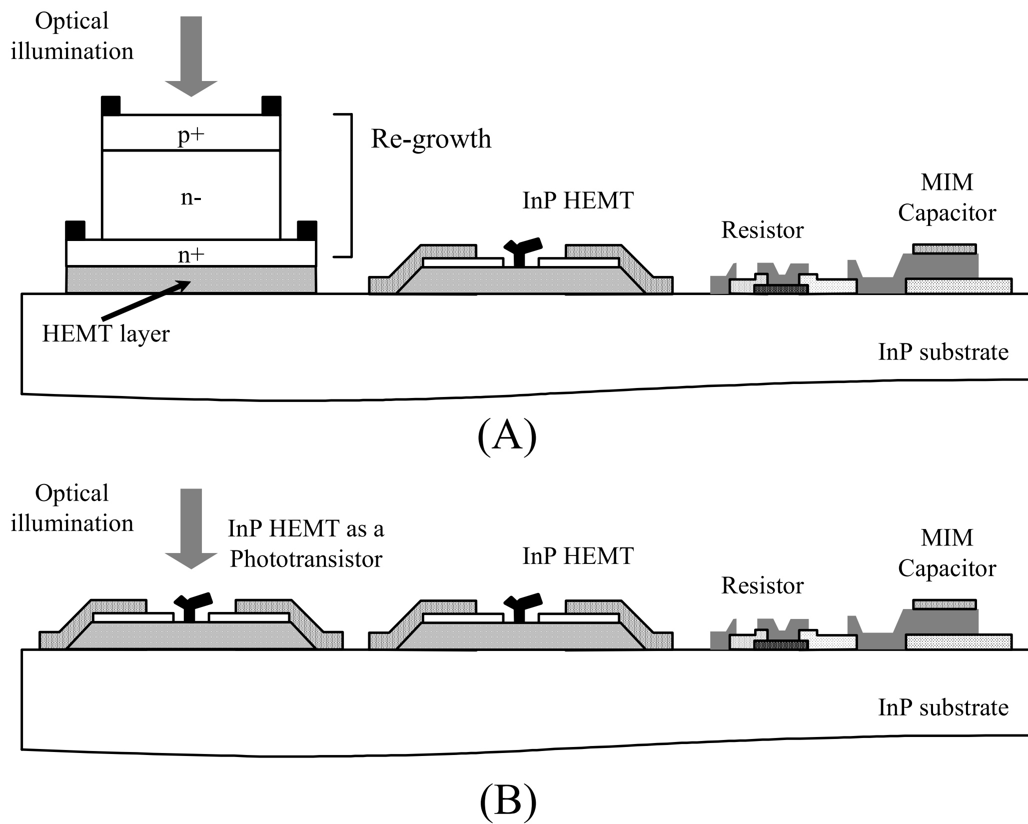

Figure 1-6. Schematic cross sections of (A) optoelectronic integrated circuit (OEIC) having PIN diode on HEMT layer and (B) optoelectronic monolithic microwave integrated circuit (MMIC) having phototransistor based on InP HEMT

1-3. Three-terminal phototransistors

The word of "phototransistor" is the compound of "photo" representing light and "transistor" indicating a device providing gain of input signals. From the origin of this word, we can easily see that phototransistor performs the photodetection of input optical signals followed by the amplification of these photodetected signals. It was first proposed by William Shockley who introduced the bipolar configuration for phototransistor operation [28]. After two years, Shive et al. made the first demonstration of phototransistor having the n-p-n structure with germanium (Ge) material, which provides optical gain of about 100 [28].

Since silicon (Si) materials have dominated the semiconductor industries, a various kinds of Si-based phototransistors based on Metal-Oxide-Semiconductor Field-Effect-Transistors (MOSFETs) and Bipolar Junction Transistors (BJTs) have been developed because of their low cost and fabrication simplicities. Although they exhibit high optical responsivity, the speed limitations make them unsuitable for high-speed optical communication. At present, these Si-based phototransistors have been extensively investigated in CMOS image sensor applications.

With the progress of gallium arsenide (GaAs) MMIC technologies, many works have devoted to the development of GaAs-based phototransistors which can be integrated with high-speed microwave transistors on a single GaAs substrate. A MEtal-Semiconductor Field-Effect Transistor (MESFET) is one of the first type GaAs-based transistors investigated as phototransistors [31-32]. The realization of AlGaAs/GaAs heterojunction has accelerated the development of phototransistors, which makes many research groups study on the optical characteristics of GaAs-based high-electron

mobility transistors (HEMTs) and heterojunction bipolar transistors (HBTs) [33-34]. At that time, from the different point of view, there have been initiative studies to utilize an optical signal as another input port of a microwave transistor [35]. These techniques are called "optical control of microwave devices" which have been extended to microwave circuits including amplifiers, oscillators and phase-shifters [36-37]. They can provide many useful features for optical signal processing in fiber-optic/millimeter-wave systems, detailed descriptions and experimental demonstration on these techniques will be discussed in chapter 3.

As mentioned in previous section, most of optical communication systems including fiber-optic/millimeter-wave systems discussed in this dissertation use the lightwave having the wavelength of 1300nm or 1550nm due to their low dispersion and low loss characteristics in silica single-mode optical fiber. Si or GaAs phototransistors cannot afford to detect these long wavelength optical signals, which have spurred the research on indium-phosphide (InP)-based phototransistors. Figure 1-7 shows the relationship between the energy gap and the corresponding wavelength as a function of the lattice constants for a variety of binary and ternary compound semiconductor materials [38]. We should focus InP-based material systems, especially $In_xGa_{1-x}As$ ternary alloy with the indium mole fraction (x) of 0.53, which is widely used in active channel of InP-based high-speed transistors. It has the bandgap of 0.73eV which is suitable for the photodetection to optical wavelength up to 1.6μm. Due to the narrow bandgap and the small effective mass, electrons in the $In_{0.53}Ga_{0.47}As$ exhibit a mobility over than 1000cm^2/v·s and the saturation velocity of about 2.4x10^{7}cm/s at room temperature. In addition, InAlAs/InGaAs and InP/InGaAs lattice-matched heterostructures provide large conduction and valence band discontinuities,

respectively. Combination of these attractive features makes it possible to achieve high performance of HEMTs and HBTs providing transistor gain even at hundreds of gigahertz. Therefore, InP-based phototransistors are one of the best candidates for the antenna base station in fiber-optic/millimeter-wave systems, where the photodetection of 1.55μm long wavelength and the high-speed operation up to millimeter-wave are simultaneously required [24, 39].

Three-terminal phototransistors are classified into two groups: field-effect-transistor structures and bipolar structures. HEMTs belong to the former, and HBTs to the latter. Choosing device technology depends on several factors including system specification, system application and system cost. For microwave signal processing applications, there is a good comparison of the relative merits of each microwave three-terminal devices described in Table 1-1 [40]. Generally, InP HEMTs are known to be suitable for high frequency low-noise amplifiers (LNAs) [41], while InP HBTs are widely used for voltage-controlled oscillators (VCOs) [42] because of their low flicker noise. In a viewpoint of device fabrication cost, InP HBTs require more fabrication steps than HEMT, but they do not require expensive electron-beam lithography which makes nano-meter resolution gates for InP HEMT. In addition, it has been reported that the fabrication process of InP HBT provide higher threshold voltage uniformity and yield than that of HEMT, which is indispensable to digital circuit applications [40]. However, in choosing phototransistor structure for fiber-optic/millimeter-wave system applications, other important factors should be considered such as photonic characteristics of 1.55μm lightwave. Many works have tried to report a comparison of these two types of phototransistors but answer is not clear. The object of this dissertation is to investigate the device characteristics of phototransistors and to

provide a guideline when choosing a phototransistor for realizing optoelectronic MMIC. It also includes how to utilize these phototransistors in fiber-optic/millimeter-wave broadband data transmission systems. In final chapter, a brief comparison of two phototransistors will be given with the consideration of photonic and microwave characteristics.

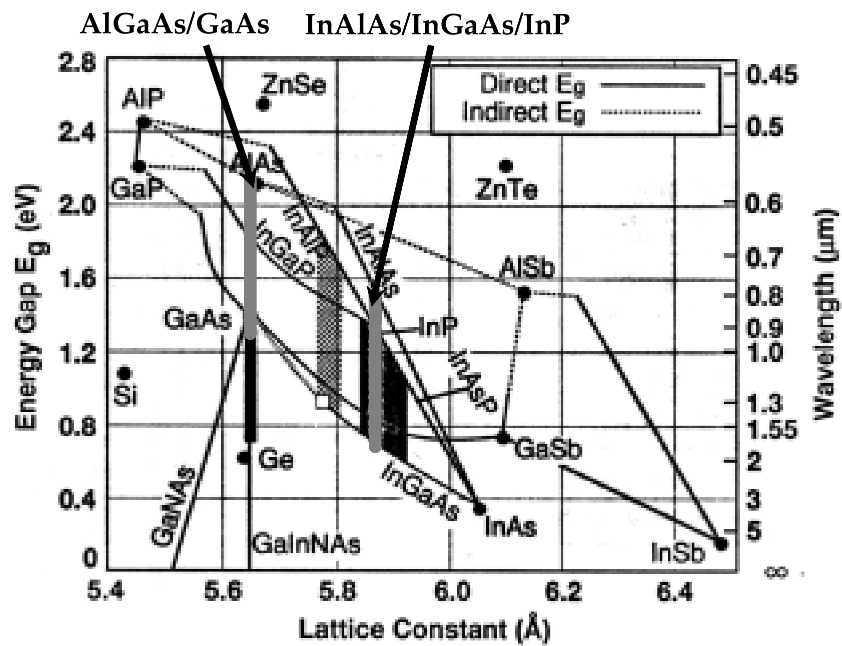

Figure 1-7. Energy gap and the corresponding wavelength as a function of the lattice constant for binary and ternary compound semiconductor materials. Adapted from reference [38]

Merit parameters	Si CMOS	Si BJT	SiGe HBT	GaAs MESFET	GaAs HEMT	GaAs HBT	InP HEMT	InP HBT
Operation frequency	poor	poor	average	average	good	average	very good	very good
Breakdown voltage	poor	poor	average	average	average	good	poor	average
V_{th} uniformity	average	good	good	average	poor	good	poor	good
Output power density	poor	good	average	average	average	good	average	good
Low freq. noise	average	good	good	poor	poor	good	poor	good
High freq. noise	poor	poor	average	average	good	poor	very good	poor
Lithography requirements	poor	average	average	poor	poor	good	poor	good
Maturity	good	good	average	good	good	good	poor	poor
Cost	good	good	good	average	average	average	poor	poor

Table 1-1. Comparison between HEMT and HBT in the viewpoint of microwave signal processing applications

1-4. Outline of dissertation

This dissertation will be dedicated to characteristics of InP-based three-terminal phototransistors and demonstration of fiber-optic/millimeter-wave data transmission systems utilizing them. The remainder of this dissertation is organized as follows.

The primary emphasis is placed on the phototransistors based on InP HEMTs. Chapter 2 begins with the introduction of an InP-based HEMT and describes DC and RF characteristics of 0.1μm $In_{0.4}Al_{0.6}As/In_{0.65}Ga_{0.35}As$ pseudomorphic HEMT used in the work. The first accomplishment of this work is to clarify the photodetection mechanism in InP HEMTs. Based on these studies, the phototransistor internal gain provided by transistor operation and optical gain cutoff frequency are determined.

In chapter 3, their applications to fiber-optic/millimeter-wave data transmission systems are presented and experimentally demonstrated. Particularly, millimeter-wave sub-harmonic optoelectronic mixers and optically injection-locked oscillators based on InP HEMTs are discussed more in detail. This is followed by the introduction to the research field "optical control of microwave devices." Section 3-3 presents the experimental demonstration of 622Mbps data transmission in fiber-optic/60GHz downlink system using InP HEMT as a sub-harmonic optoelectronic mixer. In section 3-5, novel antenna base station architecture is proposed, which performs the dual-functions of harmonic optoelectronic mixing and optical injection-locked oscillation by a single InP HEMT. For its validation, the experimental demonstration of 16QAM data transmission in fiber-optic/millimeter-wave downlink system is achieved.

Chapter 4 introduces phototransistors based on InP/InGaAs HBTs with an emphasis on their high responsivity and wide photonic bandwidth. After investigating

their utilizations as optoelectronic mixers, this chapter ends with the experimental demonstration of 1.25Gbps data transmission in both fiber-optic wireline and 60GHz wireless links.

Finally, in chapter 5, comparison between InP HEMT and HBT for the applications to fiber-optic/millimeter-wave data transmission system is given. Summary and outlines for future works are also described in this chapter.

References

[1] *Annual reports on telecommunications in Korea*, 2003, Ministry of Information and Communication of Korea.

[2] Holger H. Meinel, “Commercial applications of millimeterwaves history, present status, and future trends,” *IEEE Trans. Microwave Theory Tech*., vol. 43, no. 7, pp.1639, Jul. 1995.

[3] L. Raffaelli, “Millimeter-wave automotive radars and related technology,” *IEEE MTT-S Int. Microwave Symp. Tech. Dig*., pp.35, 1996.

[4] R. L. Van Tuyl, “Unlicensed millimeter-wave communications, a new opportunity for MMIC technology at 60GHz,” *IEEE GaAs IC Symp. Tech. Dig*., pp.3, 1996.

[5] H. Al-Raweshidy and Shozo Komaki, *Radio-over-fiber technologies for mobile communications networks*, Artech House, Norwood, MA, 2002

[6] Anne Vilcot, Beatrice Cabon and Jean Chazelas, *Microwave photonics from components to applications and systems*, Kluwer Academic Publisher, 2003.

[7] Alwyn J. Seeds, “Microwave photonics,” *IEEE Trans. Microwave Theory Tech.*, vol. 50, no. 3, pp.877, Mar. 2002.

[8] C. Carlsson, A. Larsson and A. Alping, “RF transmission over multimode fibers using VCSELs – comparing standard and high-bandwidth multimode fibers,” *J. Lightwave Technol*., vol. 22, no. 7, pp. 1694, Jul. 2004.

[9] H.-H. Lu, P.-C. Lai and W.-S. Tsai, “Radio-on-multimode fiber systems based on VCSELs and external light injection technique,” *IEEE Photon. Technol. Lett*., vol. 16, no. 4, Apr. 2004.

[10] N. Dagli, “Wide-bandwidth lasers and modulators for RF photonics,” *IEEE Trans. Microwave Theory Tech.*, vol. 47, no. 7, pp.1151, Jul. 1999.

[11] G. L. Li and P. K. L. Yu, “Optical intensity modulators for digital and analog applications,” *J. Lightwave Technol*., vol. 21, no. 9, pp. 2010, Sep. 2003.

[12] T. Kuri, K.-I. Kitayama, A. Stohr and Y. Ogawa, “Fiber-optic millimeter-wave downlink system using 60GHz-band external modulation,” *J. Lightwave Technol*., vol. 17, no. 5, pp. 799, May. 1999.

[13] R.-P. Braun, G. Grosskopf, H. Heidrich, C. Helmolt, R. Kaiser, K. Kruger, U. Kruger, D. Rohde, F. Schmidt, R. Stenzel and D. Trommer, “Optical microwave generation and

transmission experiments in the 12- and 60-GHz region for wireless communication," *IEEE Trans. Microwave Theory Tech*., vol. 46, no. 4., pp. 320, Apr. 1998.

[14] E. Hashimoto, A. Takada and Y. Katagiri, "High-frequency synchronized signal generation using semiconductor lasers," *IEEE Trans. Microwave Theory Tech*., vol. 47, no. 7, pp. 1206, Jul. 1999.

[15] T. Ohno, K. Sato, S. Fukushima, Y. Doi and Y. Matshoka, "Application of DBR mode-locked lasers in millimeter-wave fiber-radio system," *J. Lightwave Technol*., vol. 18, no. 1, pp. 44, Jan. 2000.

[16] D. Wake, C. R. Lima and P. A. Davies, "Optical generation of millimeter-wave signals for fiber-radio systems using a dual-mode DFB semiconductor laser," *IEEE Trans. Microwave Theory Tech*., vol. 43, no. 9, pp. 2270, Sep. 1995.

[17] K. Kato, "Ultrawide-band/High-frequency photodetectors," *IEEE Trans. Microwave Theory Tech*., vol. 47, no. 7, pp.1265, Jul. 1999.

[18] T. Ishibashi, T. Furuta, H. Fushimi, S. Kodama, H. Ito, T. Natatsuma, N. Shimizu and Y. Miyamoto, "InP/InGaAs uni-traveling-carrier photodiodes," *IEICE Trans. Electron*., vol. E83-C, no. 6, pp. 938, Jun. 2000.

[19] U. Gliese, S. Norskov and T. N. Nielsen, "Chromatic dispersion in fiber-optic microwave and millimet-wave links," *IEEE Trans. Microwave Theory Tech*., vol. 44, no. 10, pp. 1716, Oct. 1996.

[20] Y. J. Wen, H. F. Liu and D. Novak, "Optical signal generation at millimeter-wave repetition rates using semiconductor lasers with pulsed subharmonic optical injection," *IEEE Trans. Microwave Theory Tech*., vol. 37, no. 9, pp. 1183, Sep. 2001.

[21] L. N. Langley, M. D. Elkin, C. Edge, M. J. Wale, U. Gliese, X. Huang and A. J. Seeds, "Packaged semiconductor laser optical phase-locked loop (OPLL) for photonic generation and transmission of microwave signals," *IEEE Trans. Microwave Theory Tech*., vol. 47, no. 7, pp. 1257, Jul. 1999.

[22] E. Suematsu and N. Imai, "A fiber optic/millimeter-wave radio transmission link using HBT as direct photodetector and an optoelectronic up-converter," *IEEE Trans. Microwave Theory Tech*., vol. 44, no. 1, pp. 133, Jan. 1996.

[23] H. Ogawa, D. Polifko and S. Banba, "Millimeter-wave fiber optics systems for personal radio communication," *IEEE Trans. Microwave Theory Tech*., vol. 40, no. 12, pp. 2285, Dec. 1992.

[24] C.-S. Choi, H.-S. Kang, W.-Y. Choi, D.-H. Kim and K.-S. Seo, “Phototransistors based on InP HEMTs and their applications to millimeter-wave radio-on-fiber systems,” *IEEE Trans. Microwave Theory Tech.*, vol. 53. no. 1, Jan. 2005.

[25] P. Fay, C. Caneau and I. Adesida, “High-Speed MSM/HEMT and p-i-n/HEMT Monolithic Photoreceivers,” *IEEE Trans. Microwave Theory Tech.*, vol. 50, no. 1, pp. 62, Jan. 2002

[26] G. G. Mekonnen, W. Schllak, H.-G. Bach, R. Steingruber, A. Seeger, Th. Engel, W. Passenberg, A. Umbach, C. Schramm, G. Unterborsch and S. Van Waassen, ”37GHz bandwidth InP-based photoreceiver OEIC suitable for data rates up to 50Gbps,” *IEEE Photon. Technol. Lett.*, vol. 11, no. 2, pp. 257, Feb. 1999.

[27] J. B. D. Soole and H. Schumacher, “InGaAs metal-semiconductor-metal photodetectors for long wavelength optical communication,” *IEEE J. Quantum Electron.*, vol. 27, no. 3, pp. 737, Mar. 1991.

[28] J. C. Campbel, *Phototransistors for lightwave communication* in Semiconductor and Semimetal, vol 22, part. D, Academic Press, 1985

[29] W. Zhang, M. Chan, P. K. Ko, “Performance of the floating gate/body tied NMOSFET photodetector on SOI substrate,” *IEEE Trans. Electron Devices*, vol. 47, no. 7, pp. 1375, Jul. 2000.

[30] Y. Matsunaga, H. Yamashita, S. Manabe and N. Harada, ”A high-sensitivity MOS photo-transistor for area image sensor,” *IEEE Trans. Electron Devices*, vol. 38, no. 5, May 1991.

[31] R. B. Darling and J. P. Uyemura, “Optical gain and large-signal characteristics of illuminated GaAs MESFET’s,” *IEEE J. Quantum Eletron.*, vol. 23, no. 7, pp.1160, Jul. 1987

[32] A. Paolella, A. Madjar and P. R. Herczfeld, “Modelling the GaAs MESFET’s response to modulated light at radio and microwave frequencies,” *IEEE Trans. Microwave Theory Tech*. vol. 42, no. 7, pp. 1122, Jul. 1994.

[33] L. M. de Barros, A. Paolella, M. Y. Frankel, M. A. Romero and P. R. Herczfeld, ”Photoresponse of microwave transistors to high-frequency modulated lightwave carrier signal,” *IEEE Trans. Microwave Theory Tech.*, vol. 45, no. 8, pp. 1368, Aug. 1997.

[34] A. A. de Salles and M. A. Romero, “AlGaAs/GaAs HEMT’s under optical illumination,” *IEEE Trans. Microwave Theory Tech.*, vol. 39, no. 12, pp. 2010, Dec. 1991.

[35] R. N. Simons and K. B. Bhasin, "Analysis of optically controlled microwave/millimeter-wave device structures," *IEEE Trans. Microwave Theory Tech.*, vol. 34, no. 12, pp. 1349, Dec. 1986.

[36] A. J. Seeds and A. A. de Salles, "Optical control of microwave semiconductor devices," *IEEE Trans. Microwave Theory Tech.*, vol. 38, no. 5, pp. 577, May 1990.

[37] R. D. Esman, L. Goldberg and J. F. Weller, "Optical phase control of an optically injection-locked FET microwave oscillator," *IEEE Trans. Microwave Theory Tech.*, vol. 37, no. 10, pp. 1512, Oct. 1989.

[38] Osamu Wada and Hideki Hasegawa, *InP-based materials and devices: physics and technology,* John Willey & Son Inc., 1999.

[39] C. Rauscher and K. J. Williams, "Heterdyne reception of millimeter-wave modulated optical signals with an InP-based transistor," *IEEE Trans. Microwave Theory and Tech.*, vol. 42, no. 11, pp. 2027, Nov. 1994.

[40] F. Schwierz and J. J. Liou, *Modern Microwave Transistors*, Wiley Interscience, 2003.

[41] J. W. Archer, R. Lai, R. Grundbacher, M. Barsky, R. Tsai and P. Reid, "An indium phosphide MMIC amplifier for 180-205GHz," *IEEE Microwave and Wireless Components Lett.*, vol. 11, no. 1, pp. 4, Jan. 2001.

[42] Y. Baeyens, C. Dorschky, N. Weimann, Q. Lee, R. Kopf, G. Georgiou, J.-P. Mattia, R. Hamm and Y.-K. Chen, "Compact InP-based HBT VCOs with a wide tuning range at W-and D-band," *IEEE Trans. Microwave Theory Tech.*, vol. 48, no. 12, pp. 2403, Dec. 2000.

Chapter 2

Phototransistors based on InP HEMTs

2-1. Introduction

2-1-1. InP HEMT for optoelectronic MMIC

The High-Electron Mobility Transistor (HEMT) is a heterojunction Field-Effect Transistor (FET) that provides high electron concentration as well as extremely high electron mobility in undoped channel. As device dimensions have been scaled down for higher speed and integration levels, the channel doping in FET must be increased to maintain acceptable channel resistances and threshold voltages. Such high doping concentrations are likely to reduce electron mobility due to the increased impurity scattering. Since electron mobility determines transit-time and transconductance of a transistor, it seemed to face the limitation for improving device speed in conventional FET scaling-down approaches.

Introducing modulation doping to FET broke through this limitation. To realize it, the larger bandgap material is only doped with donors, and the lower bandgap material is left to be undoped. After forming heterojunction with lattice-matched as

shown in figure 2-1, electrons in a larger bandgap layer move into an adjacent lower bandgap undoped layer, which was first introduced by Dingle et. al in 1978 [1]. The conduction band discontinuity at heterojunction interface makes a triangular potential well at the side of lower bandgap undoped layer. The electrons transferred from larger bandgap material are confined in this potential well, which is referred to two-dimensional electron-gas (2DEG). Because electrons in 2DEG are physically separated from ionized donor, they are immune to the impurity scattering, which is conducive to high electron mobility in FET structure. For this reason, HEMT using 2DEG as an active channel is also called MOdulation-Doped Field Effect Transistor (MODFET).

Since the first HEMT was demonstrated by Mimura et. al. using n-$Al_xGa_{1-x}As$/GaAs heterojunction [2], various other material systems have been introduced for attaining high frequency performance [3]. In this dissertation, InP-based HEMTs are mainly investigated because they provide many structural advantages for the applications of optoelectronic MMICs interested in this work. The large conduction band discontinuity at InAlAs/InGaAs heterojunction has led to building up higher 2DEG densities. Furthermore, an $In_xGa_{1-x}As$ channel with high indium ($x \geq 0.53$) contents exhibits higher electron mobility and peak velocity than GaAs channel, which translates into superior advantages for millimeter-wave frequency operation. The primary important feature as a phototransistor is that the $In_xGa_{1-x}As$ channel ($x \geq 0.53$) can perform the photodetection to 1.55μm lightwave and then the detected signals are amplified by FET operation. Because the photoabsorption only takes place in InGaAs channels, additional efforts for optical window in HEMT are not required if backside illumination through InP substrate is applied [4]. In this chapter, after understanding basic operation of an InP HEMT, the photodetection characteristics and phototransistor operations of the

fabricated InP HEMT are presented.

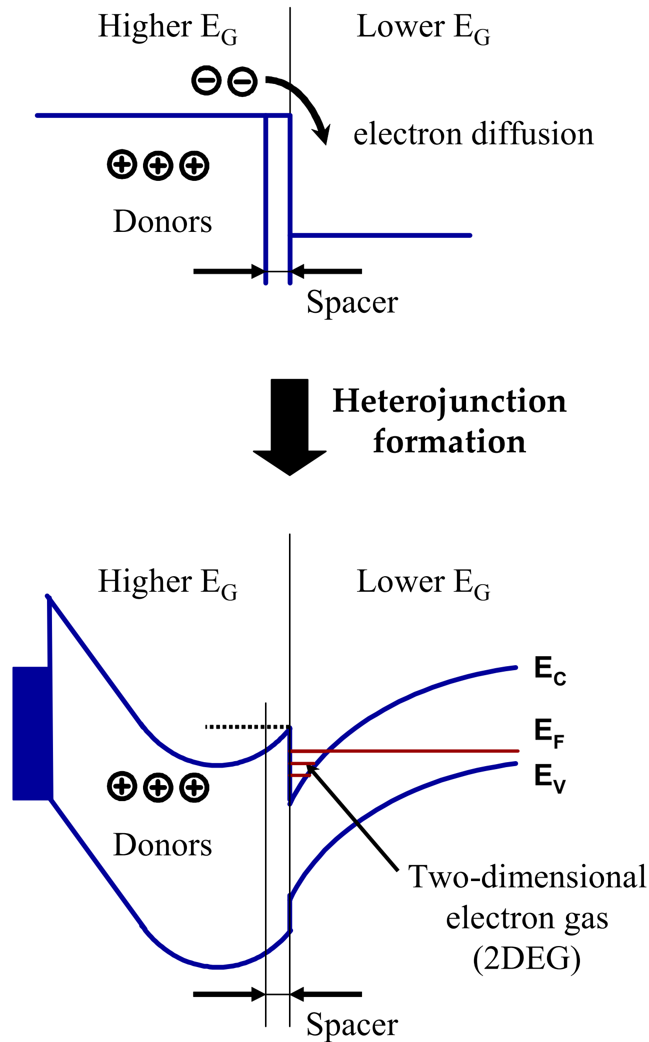

Figure 2-1. Energy band diagram for heterojunction. After heterojunction formation, electrons from remote donor in large bandgap material transfer to lower bandgap undoped material. These electrons are confined in triangular potential well, which is referred to two-dimensional electron gas (2DEG).

2-1-2. Simulation analysis of InP HEMT

Operation principles of an InP HEMT differ slightly from those of MESFET. The prime difference lies in the fact that the 2DEG density in InGaAs channel is controlled by gate bias condition. Figure 2-2 gives the schematic cross-section of the latticed-matched $In_{0.52}Al_{0.48}As/In_{0.53}Ga_{0.47}As/InP$ HEMT used for two-dimensional simulation analysis. Higher bandgap (E_G=1.46eV) $In_{0.52}Al_{0.48}As$ barrier layer delta-doped with n-type impurities exists on lower bandgap (E_G=0.75eV) $In_{0.53}Ga_{0.47}As$ undoped channel layer. The InP HEMT has the gate length of 0.25μm and the gate Schottky metal having the work function potential of 5.13eV. The band-diagram for InP HEMT under zero-bias condition (V_G=0V) is shown in figure 2-3-(A). For these simulation analyses, a MEDICI simulator with heterojunction AAM module was used [5]. As discussed early, triangular potential-well builds up at the side of $In_{0.53}Ga_{0.47}As$ undoped channel. Under zero-bias conditions, the conduction band is lower than the Fermi level, which means that free-electrons are filled with the potential well. When the drain bias is applied to HEMT, these electrons drift from source side toward drain side without experiencing impurity scattering in undoped channel. Increasing negative gate bias has led to the decreased depth of potential well, which lessen the 2DEG densities. Figure 2-3-(B) illustrates the band diagram for InP HEMT under turn-off condition (V_G=-1V). Electron concentration becomes negligibly small, thus no current conduction takes place even though forward drain bias is applied. Figure 2-4 shows the simulated drain-to-source currents (I_{DS}) as a function of gate-to-source voltage (V_{GS}) at the fixed drain-to-source voltage (V_{DS}).

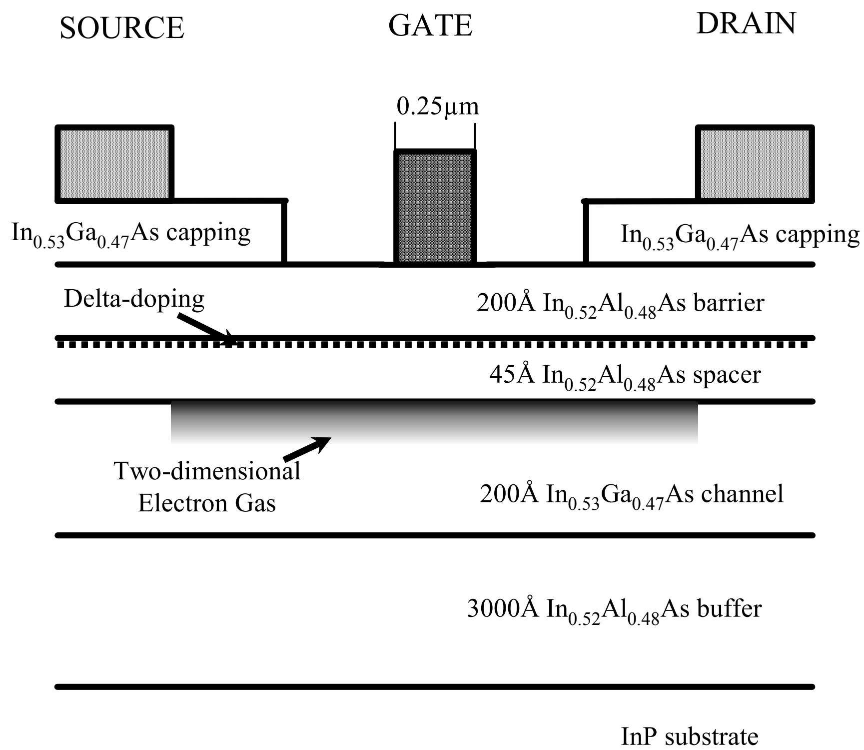

Figure 2-2. The lattice-matched $In_{0.52}Al_{0.48}As/In_{0.53}Ga_{0.47}As/InP$ HEMT used for two-dimensional simulation analysis.

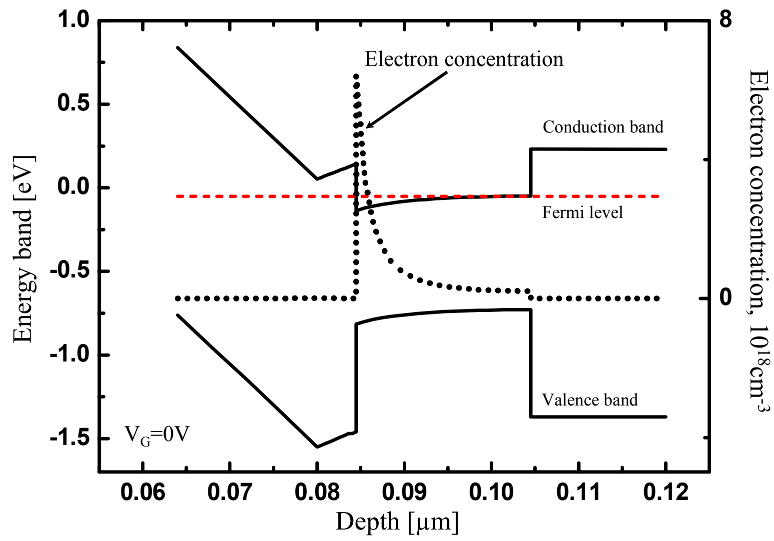

(A)

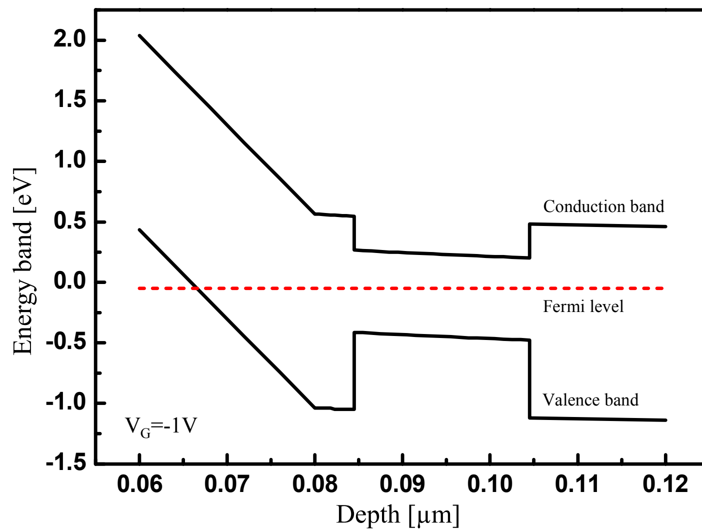

(B)

Figure 2-3. Energy band diagram for latticed-matched InP HEMT under (A) turn-on condition (V_G=0V) and (B) turn-off condition (V_G=-1V)

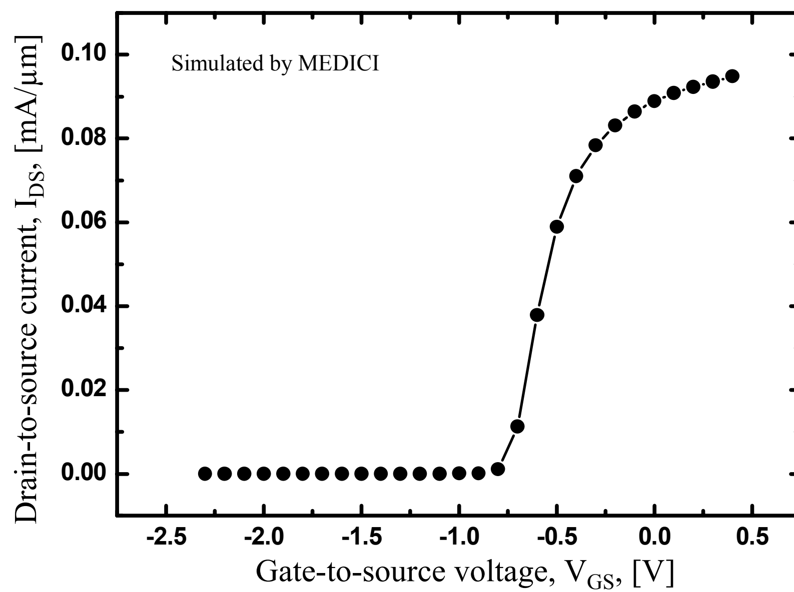

Figure 2-4. Simulated I_{DS}-V_{GS} characteristics for lattice-matched InP HEMT

2-2. 0.1μm InP pHEMT used in this work

2-2-1. InP pseudomorphic HEMT structure

There have been continuous efforts to increase operation speeds of InP HEMTs for millimeter-wave applications. It can be accomplished by reducing gate length and employing pseudomorphic channel with higher indium contents (x>0.53) of $In_xGa_{1-x}As$ channel [6]. The larger conduction band discontinuity at InAlAs/InGaAs pseudomorphic channel has led to higher 2DEG density and higher electron mobility, resulting in high frequency performance. Up to now, Fujitsu laboratories reported the record-breaking 25nm gate-length InP pseudomorphic HEMT with current gain cutoff frequency of 562GHz in 2003 [7].

In this dissertation, an InP pseudomorphic HEMT (InP pHEMT) having $In_{0.65}Ga_{0.35}As$ channel is utilized as a phototransistor. Figure 2-5 schematically illustrates the cross-section of the fabricated InP pHEMT[2] used in this work [8]. The epitaxial layers were grown on semi-insulating InP substrate by using molecular beam epitaxy (MBE). They are made of, from bottom to top, 300nm $In_{0.52}Al_{0.48}As$ buffer layer, 10nm $In_{0.53}Ga_{0.47}As$ sub-channel and 10nm $In_{0.65}Ga_{0.35}As$ pseudomorphic channel layers, 4nm $In_{0.4}Al_{0.6}As$ spacer layer with Si-delta doping ($5.8\times10^{12}cm^{-2}$), 12nm $In_{0.4}Al_{0.6}As$ barrier layer and 20nm n+ $In_{0.53}Ga_{0.47}As$ capping layers.

The heavily doped $In_{0.53}Ga_{0.47}As$ capping layer at the source/drain contacts are employed to minimize contact and series resistances. $In_{0.4}Al_{0.6}As$ strained barrier was adopted to increase conduction band discontinuity that produces better electron

[2] The InP pHEMTs were fabricated by Dr. Dae-Hyun Kim and Prof. Kwang-Seok Seo in ISRC, Seoul National University, Seoul, Korea.

confinement in 2DEG. In addition, it suppresses the gate leakage currents of the InP HEMT with the help of enhanced Schottky barrier height between gate metal and $In_{0.4}Al_{0.6}As$ barrier. The undoped $In_{0.4}Al_{0.6}As$ spacer layer serves to spatially separate 2DEG from the ionized impurity, thus it efficiently suppresses impurity scattering. The high indium contents $In_{0.65}Ga_{0.35}As$ pseudomorphic channel exhibits higher electron concentration and higher peak velocity than $In_{0.53}Ga_{0.47}As$ channel used in conventional latticed-matched InP HEMT, which results in improved millimeter-wave noise and power performances. However, it comes at the expense of higher impact ionization and early snapback breakdown characteristics due to the narrow bandgap of $In_{0.65}Ga_{0.35}As$ material. In order to solve this contradictory problem, $In_{0.65}Ga_{0.35}As/In_{0.53}Ga_{0.47}As$ composite channels were employed for improving breakdown characteristics without sacrificing high frequency performance in the fabricated InP pHEMT. The undoped $In_{0.52}Al_{0.48}As$ buffer layer below the $In_{0.53}Ga_{0.47}As$ sub-channel makes an active channel to be isolated from InP substrate. Figure 2-6 shows the simulated band-diagram of the InP pHEMT under turn-on condition (V_G=0V).

Detailed procedures for the fabrication of InP pHEMT can be found in [8]. It has T-shaped gate with the length of 0.1μm defined by the e-beam lithography. The source-to-gate spacing and the drain-to-gate spacing are 0.9μm and 2μm, respectively. On the top of InP pHEMT, silicon nitride was deposited for the passivation of the fabricated device. DC and RF characteristics of this fabricated InP pHEMT will be shown in next section.

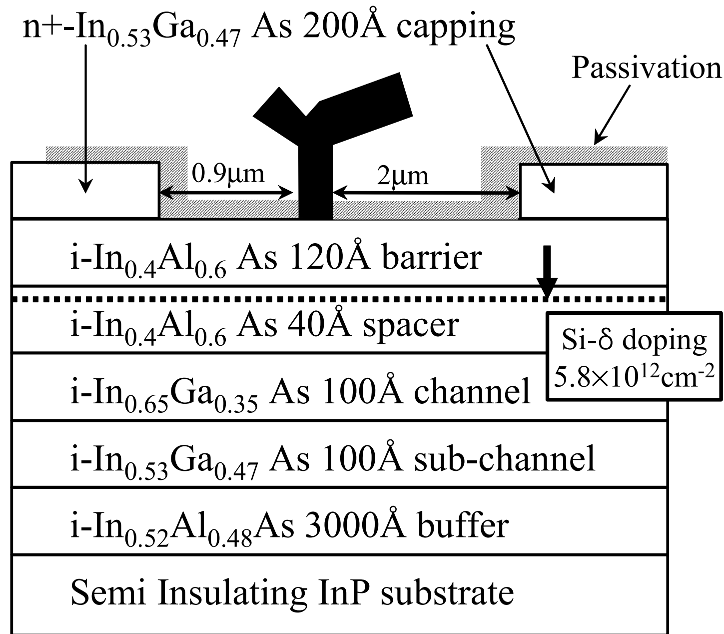

Figure 2-5. The schematic cross-section of fabricated 0.1μm InP pseudomorphic HEMT having $In_{0.4}Al_{0.6}As$ strained barrier and $In_{0.65}Ga_{0.35}$ As strained channel.

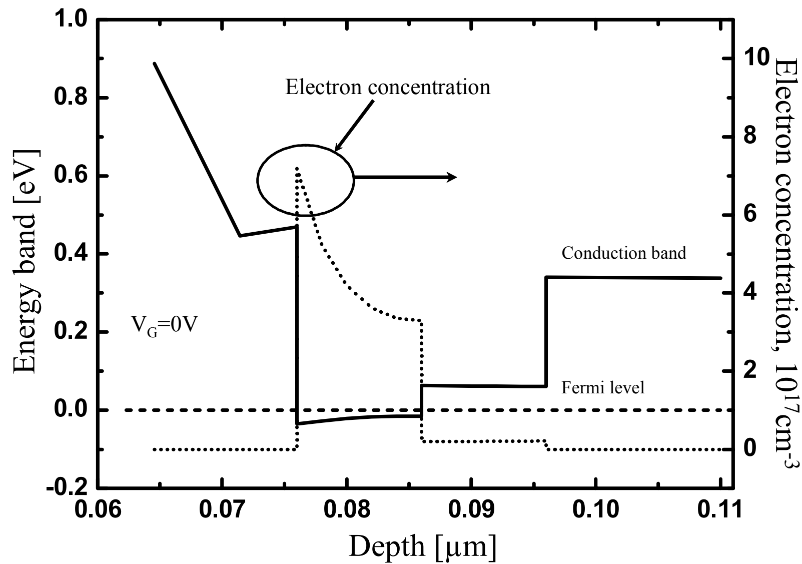

Figure 2-6. Simulated energy band diagram and electron concentration as a function of depth for the fabricated InP pHEMT under turn-on condition (V_G=0V).

2-2-2. Device characteristics of InP pHEMT.

DC characteristics of the fabricated InP pHEMT were measured using HP4145B semiconductor parameter analyzer. Figure 2-7 shows the drain-to-source currents (I_{DS}) as a function of drain-to-source voltages (V_{DS}) with the variation of gate-to-source voltage (V_{GS}). As V_{DS} increases over about 0.5V, I_{DS}-V_{DS} characteristics become collapsed. This anomalous phenomenon is called the kink effects. Although the physical origins for these kink effects are still under controversy, the interfacial traps between heterojunctions and increased holes caused by impact ionization are regarded as predominant factors for the kink effects [9].

Figure 2-8 shows I_{DS}-V_{GS} characteristics of the InP pHEMT with V_{DS} of 0.5V and 0.9V. As explained in the previous section, the electron concentration in 2DEG is controlled by the electric field of Schottky gate, which results in FET operation. The fabricated InP pHEMT has the threshold voltage (V_T) of about -0.9V which was extracted by extrapolating I_{DS}-V_{GS} curves and finding the interception point on the V_G axis. The maximum transconductance (G_m) of 705mS/mm is achieved at V_{GS} of -0.5V and V_{DS} of 1.0V. It was extracted from the derivatives of I_{DS}-V_{GS} characteristics with the respect to V_{GS} when V_{DS} is fixed, which is expressed as

$$G_m = \left. \frac{dI_{DS}}{dV_{GS}} \right|_{V_{DS}=const.}, \qquad \text{(2-1)}$$

where G_m is the transconductance.

The scattering parameters (s-parameters) of the InP pHEMT were measured using a HP8720D vector network analyzer (50MHz-40.05GHz) after the short-open-thru-load calibration of measurement setup. In microwave transistors, the current gain cutoff

frequency (f_T) and maximum oscillation frequency (f_{max}) are important parameters indicating their maximum operation frequencies. The f_T is related to short-circuit current gain, h_{21}, which is defined as the ratio of output current to input current with the short-circuited output. It is the frequency where the magnitude of h_{21} equals to 0dB. From the measured s-parameters, it can be extracted by.

$$h_{21} = \left| \frac{y_{21}}{y_{11}} \right|. \quad (2\text{-}2)$$

The f_{max} is the maximum frequency where a microwave transistor provides a power gain, therefore it is the frequency where unilateral power gain (U) equals to 0dB. U can be calculated using

$$U = \frac{\left| y_{21} - y_{12} \right|^2}{4\left[\mathrm{Re}(y_{11})\mathrm{Re}(y_{22}) - \mathrm{Re}(y_{12})\mathrm{Re}(y_{21})\right]}. \quad (2\text{-}3)$$

Figure 2-9 gives the h_{21} and the U of fabricated InP pHEMT, which were calculated from measured s-parameters. The f_T and f_{max} were not directly measured but extracted by extrapolating h_{21} and U with the slope of -20dB/decade due to the frequency limits of a vector network analyzer. The f_T of 148GHz and the f_{max} of 165GHz were obtained at at the V_{DS} of 1V and V_{GS} of -0.5V. The InP pHEMT offers excellent microwave characteristics compared with the other reported phototransistors [10-11], therefore it is expected to provide large phototransistor gain even at millimeter-wave operation.

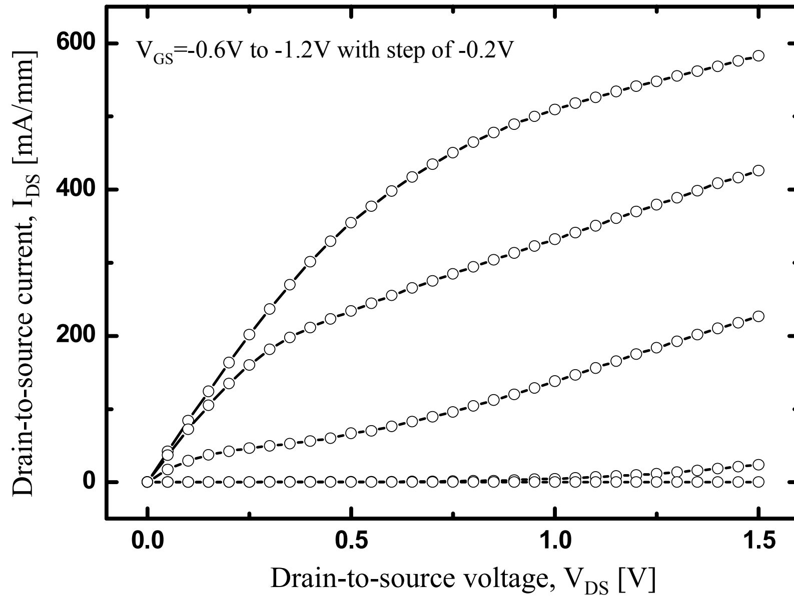

Figure 2-7. I_{DS}-V_{DS} characteristics of the fabricated InP pHEMT

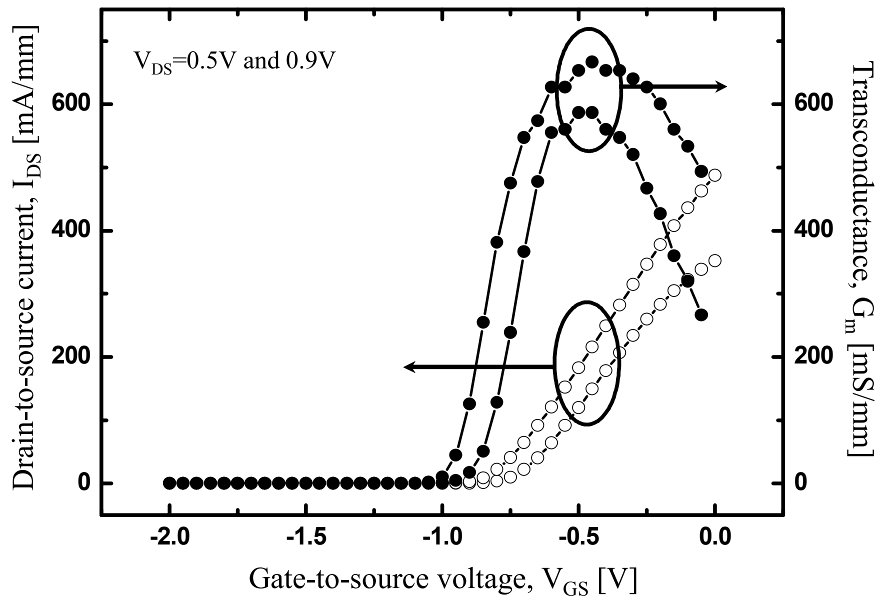

Figure 2-8. I_{DS} and G_m as a function of V_{GS} of the fabricated InP pHEMT

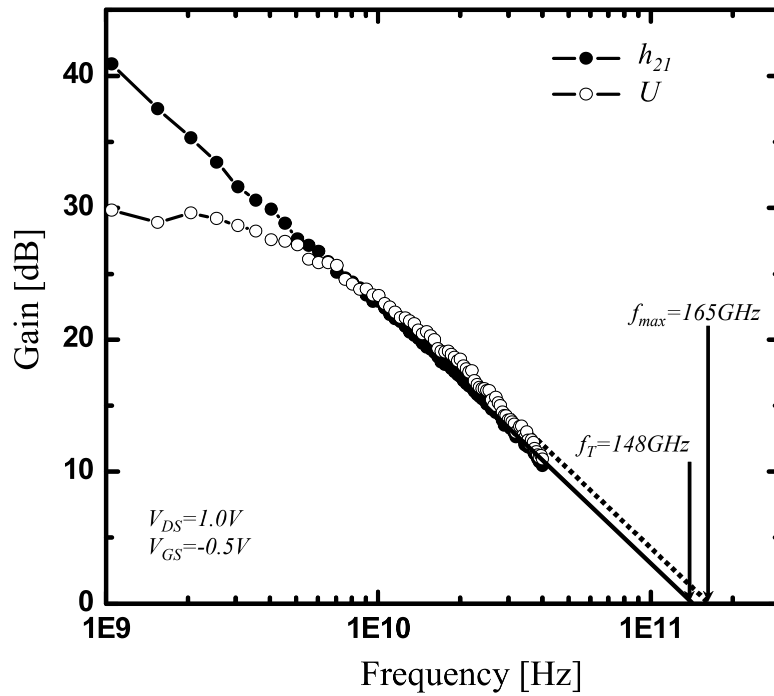

Figure 2-9. Measured short-circuit current gain (h_{21}) and unilateral power gain (U), and extrapolated f_T and f_{max} for the fabricated InP HEMT with V_{GS} of -0.5V and V_{DS} of 1V.

2-3. Experimental setup

For optical characterizations of InP HEMT, an experimental setup was constructed as depicted in figure 2-10. A distributed feedback laser diode (DFB-LD) whose wavelength is about 1553nm was used as optical source. A 40Gbps Mach-Zehnder modulator and a network analyzer (HP8720D) were used to measure optical modulation responses after careful calibration of characterization setup. After optical amplification by EDFA, the lightwave is injected to the device using a single mode lensed fiber which has the minimum spot size of 9μm and the focal length of 550μm. The positioning of beam spot to InP HEMT was determined by scanning the beam across the device with motorized picomotor translation stage and monitoring the photocurrent at drain output.

There are two methods for applying optical illumination into InP HEMT, top-side illumination and backside illumination. Although T-shaped gate metal reflects most of incident lightwave, early studies on the optical characteristics of GaAs-based HEMT could not help using top-side illumination technique because most of photoabsorption occurs in GaAs substrate if a backside illumination is applied. In the case of InP HEMT, the backside illumination through InP substrate allows to deliver optical signals into active channels because InP substrate and $In_{0.52}Al_{0.48}As$ buffer layer are transparent to 1.55μm lightwave, thus improved coupling efficiency is expected. The other important advantage of backside illumination is the improved optical modulation responses, especially at high modulation frequencies [12]. Figure 2-11 shows the experimental comparison between top and backside illumination in the respect of optical modulation response. It was measured at incident optical power of 10dBm. It can be seen that

backside illumination improves high frequency response as well as DC photoresponse compared with top-side illumination. It is because backside illumination enhances photoconductivity in the high-field channel below the gate, which results in large photoconductive gain [12]. For these reasons, the backside illumination was adopted in all experiments for InP HEMT characterization. Considering the reflection coefficients and thickness of epitaxial layers as well as the focal length and minimum beam diameter of lensed fiber, the coupling efficiency into InGaAs active channels is less than 2% of incident optical power.

All measurements were performed in common-source configuration by utilizing on-wafer GSG probes. A semiconductor parameter analyzer and two bias-Tees were used to apply gate and drain bias voltages to on-wafer devices.

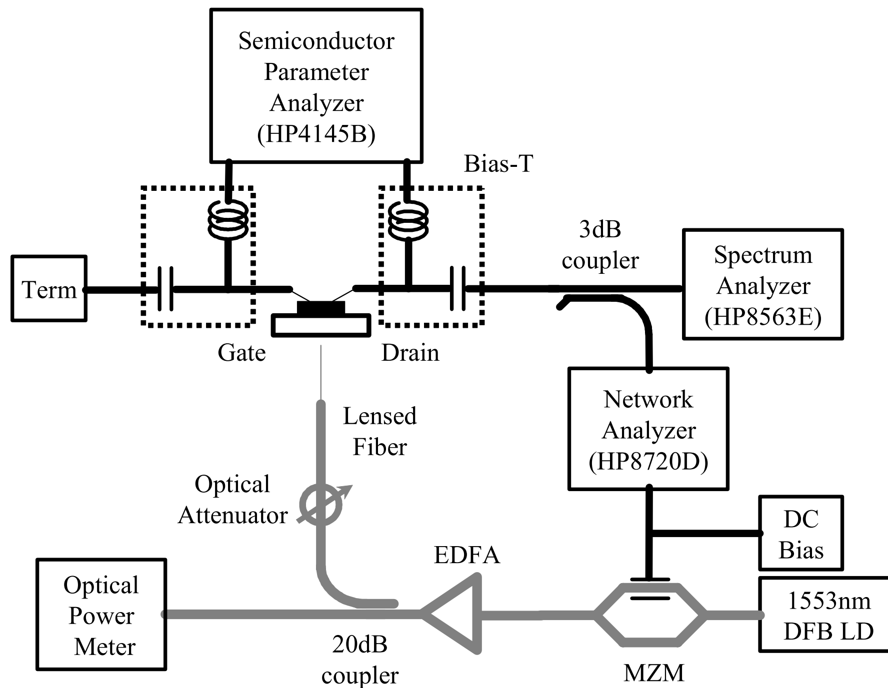

Figure 2-10. Experimental arrangements for optical characterization of InP pHEMT. Backside illumination is applied in order to improve coupling efficiency and optical modulation response

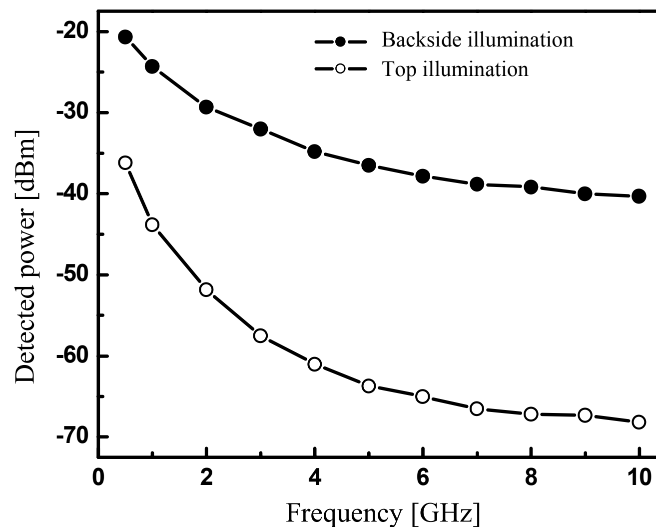

Figure 2-11. Comparison of the optical modulation responses under top and backside illumination. Backside illumination exhibits higher photoresponse than top illumination at low frequency, and this difference increases as modulation frequency increases.

2-4. Photodetection characteristics of InP HEMT

2-4-1. Motivation

Clarifying photodetection mechanism in FETs has been a crucial issue for the utilization of them as phototransistors. Many research groups have reported the photodetection characteristics and their physical origins in GaAs-based FET under 850nm or shorter wavelength optical illumination. A. A. de Salles presented that the photodetection process in a GaAs MESFET is attributed to the combination of two photoeffects, photovoltaic and photoconductive effects [13]. R. B. darling *et al.* performed the measurements of DC optical gain and suggested that the photovoltaic effects appearing as voltage drop across the gate resistance is the major origin contributing to this optical gain [14]. A. Madjar *et al*. made an analysis on optically generated current in GaAs MESFET and first discriminated internal photovoltaic effects from external photovoltaic effects [15]. In 1983, C. Y. Chen *et al*. demonstrated first type of HEMT-based photodetector with high sensitivity and speed [16]. M. Romero *et al*. established an analytical model for the photodetection in AlGaAs/GaAs HEMT and reported that nonlinear dependence of photoresponse on optical power originates from internal photovoltaic effects [17]. There are still continuing works on the photodetection mechanism and its modeling in GaAs MESFETs and HEMTs [18].

These previous works for GaAs-based FET are partially acceptable in InP-based HEMT because photo-absorption only occurs in InGaAs channels, which are different from GaAs-based FET. The first report on the photodetection in InP-based HEMT was done by Y. Takanashi et. al in 1999 [12]. It showed that the photoconductive effect can be observed at high optical frequency response in 1.3μm backside illuminated InP-

based HEMT. Although many works have been devoted to use InP-based HEMT as a phototransistor [19-20], photodetection mechanism and their identification have not been fully explained yet. In this section, photodetection mechanism of the fabricated InP pHEMT are clarified as the first step of this dissertation work. Afterward, important device performance parameters, phototransistor internal gain and optical current gain cutoff frequency are determined. Finally, their applicability to fiber-optic/millimeter-wave data transmission systems is evaluated by the demonstration for photodetections of optically transmitted broadband data and high-frequency optical signals.

2-4-2. Photodetection mechanisms in InP HEMT

A. Photoconductive effect

There are two major physical origins for the photodetection in an InP HEMT, photoconductive effect and photovoltaic effect. Figure 2-12 illustrates the photodetection process of illuminated HEMT [12]. When optical illumination is applied through backside of InP HEMT, electron-hole pairs are generated in InGaAs channels. Under the gate metal and drain side where high electric-field exists, photogenerated electrons and holes drift toward drain and source side, respectively, which increases channel conductivities resulting in increased drain currents. Photocurrents produced by this photoconductive effect (I_{PC}) are expressed as

$$I_{PC} = q\mu_n \Delta n \frac{WD \cdot V}{L}, \tag{2-4}$$

where μ_n is the electron mobility, Δn is the concentration of photogenerated

electrons, W, D and L are the photoabsorption width, depth and length, respectively.

The increased electron concentration depends on not only input optical powers but also the lifetime of electrons. In photoconductor, the electrons keep flowing until they recombine with photogenerated holes in order to preserve charge neutrality in semiconductor. This produces photoconductor gain (G_{PC}) which is expressed as

$$G_{PC} = \frac{\tau_n}{t_n}, \tag{2-5}$$

where τ_n is the lifetime of electron and t_n is the transit-time of electron.

The equation (2-4) can be also written in terms of photoconductor gain and primary photocurrent injected by optical illumination, expressed as

$$I_{PC} = q\left(\frac{\eta P_{opt}}{h\nu}\right)\cdot G_{pc} = I_{primary}\cdot G_{pc}, \tag{2-6}$$

where I_{PC} is the photocurrent produced by photoconductive effect, η is the quantum efficiency, $h\nu$ is the photon energy, $I_{primary}$ is the primary photocurrent and P_{opt} is the absorbed optical power.

The optical modulation response due to photoconductive effects ($R_{PC}(\omega)$) is dominated by τ_n, which can be described as [12]

$$R_{PC}(\omega) = \frac{R_0^{PC}}{\sqrt{1+\omega^2\tau_n^2}} \tag{2-7}$$

where R_0^{PC} is DC photocurrent produced by photoconductive effect and ω is the angular frequency.

B. Photovoltaic effect

However, in the source region where low electric field dominates, photogenerated holes are accumulated and spatially separated with electrons because of internal electric field produced by 2DEG as shown in figure 2-12-(B). These accumulated holes beneath source area effectively diminish the potential barrier between the source and the channel, as a result, a large amount of excess electrons is supplied from source contact and flows toward drain side until these accumulated holes disappear by recombination process. This gives rise to increase in drain current and provides phototransistor gain to HEMT, which is called photovoltaic effect [21]. It appears negative shift in threshold voltages which is expressed as

$$\Delta V_{TH} = \frac{nkT}{q} \ln\left(1 + \frac{q\eta P_{opt}}{I_{dark} \cdot h\nu}\right), \tag{2-8}$$

where ΔV_{TH} is the threshold voltage shift, kT/q is the thermal voltage, n is the ideality factor and I_{dark} is the dark current for holes.

Conventional FET theories indicate that small increase in gate voltage, corresponding decrease in threshold voltage, has led to large increase in drain currents described as the definition of transconductance in equation (2-1). The increase in drain current (ΔI_D) caused by threshold voltage shift is given by

$$\Delta I_D = G_m \Delta V_{TH}, \tag{2-9}$$

where G_m is the intrinsic transconductance of HEMT.

Therefore, the photocurrent caused by photovoltaic effect (I_{PV}) can be written as

$$I_{PV} = G_m \cdot \Delta V_{TH} = G_m \cdot \frac{nkT}{q} \ln\left(1 + \frac{q\eta P_{opt}}{I_{dark} \cdot h\nu}\right). \tag{2-10}$$

In contrast to case of photoconductive effect, the optical modulation response due to photovoltaic effect ($R_{PV}(\omega)$) is dominated by the lifetime of photogenerated holes, expressed as [12]

$$R_{PV}(\omega) = \frac{R_0^{PV}}{\sqrt{1 + \omega^2 \tau_p^2}}, \tag{2-11}$$

where R_0^{PV} is DC photocurrent produced by photovoltaic effect and τ_n is the lifetime of holes.

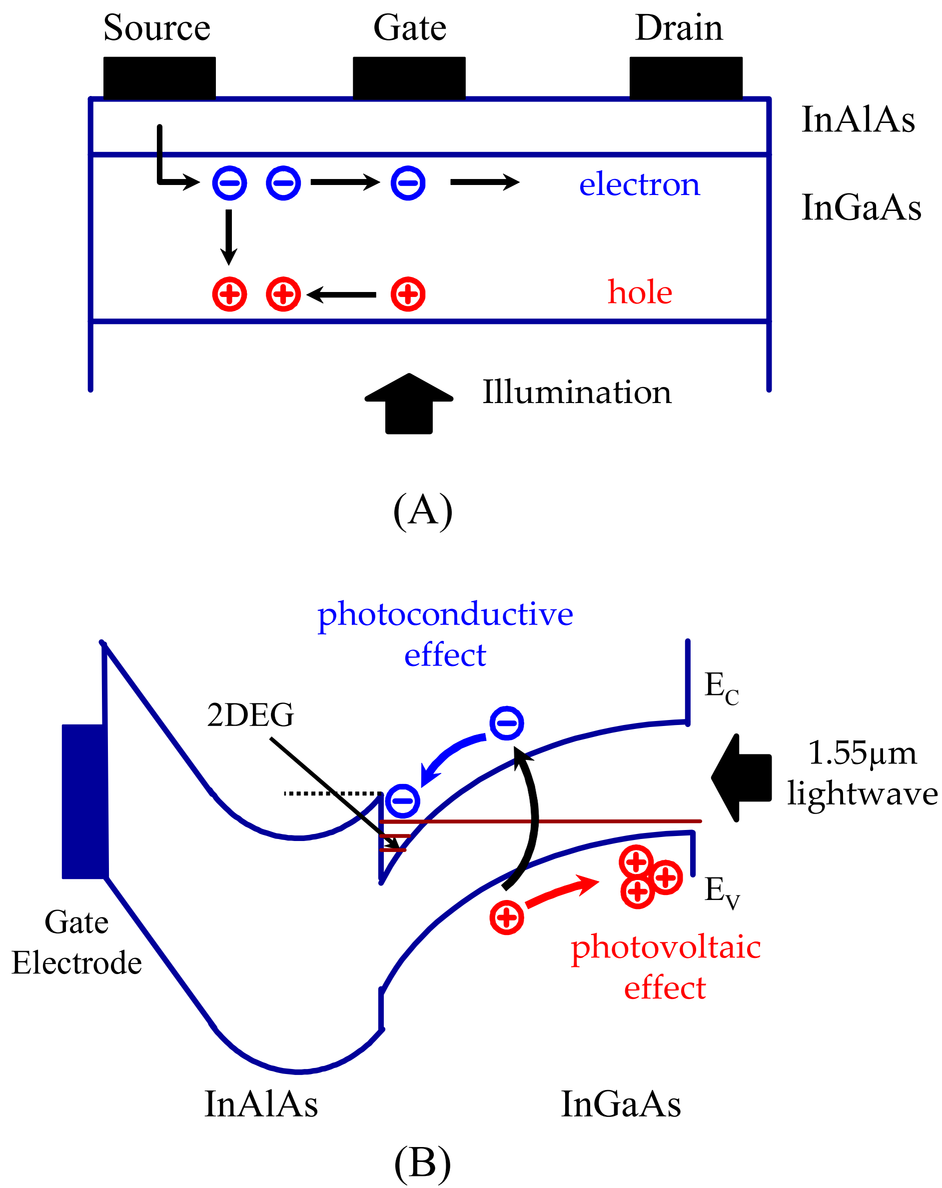

Figure 2-12. (A) Operation principle of photodetection in InP-based HEMT. (B) energy band diagram at the heterointerface at source side. When optical illumination is applied, photogenerated electrons drift toward drain side, while holes are spatially separated from electrons and accumulated beneath the source area.

2-4-3. DC photodetection characteristics of InP pHEMT

Figure 2-13 and 2-14 show the measured I_{DS}-V_{DS} and I_{DS}-V_{GS} characteristics of the 2×75μm wide InP pHEMT for different incident optical powers, respectively. The solid lines represent I_{DS} under optical illumination and the dashed lines in the dark. The InP pHEMT exhibits significant increase in I_{DS} with increasing incident optical power, which varies from -6dBm to 15dBm with the step of 3dB measured at the output of the lensed fiber. The major photodetection mechanism for InP pHEMT under turn-on condition is the photovoltaic effect which appears in threshold voltage shifts of I_{DS}-V_{GS} characteristics as explained previously.

In order to fully investigate the influence of photovoltaic effect on the increased I_{DS} of the HEMT, threshold voltage shifts and photocurrents were measured under different optical powers as shown in figure 2-15. The symbols (◇) are threshold voltage (V_T) shifts as a function of incident optical powers and the solid line is fitted result according to equation (2-8). The well-fitted line indicates that V_T shifts are attributed to the photovoltaic effect. As described in equation (2-9), the increase in I_{DS} caused by V_T shifts is the products of transconductance and V_T shift. The symbols (●) in the figure indicate the measured photocurrent (I_{PH}) at V_{DS} of 0.5V and V_{GS} of -0.5V. The symbols (○) and dashed line are the additional drain current predicted by equation (2-9) using measured V_T shifts and the intrinsic transconductance of 83mS. From the result that the measured photocurrents coincide with the calculated increase in I_{DS}, it is concluded that the major origin of photocurrent in InP HEMT under turn-on condition is the photovoltaic effect which causes the accumulation of optically generated holes at the source region to actually decrease the threshold voltage of the HEMT [22]. Since the

photovoltaic effects effectively modulate the gate voltage, they provide intrinsic gain by FET operation and make InP pHEMT operates as a phototransistor.

However, even when V_{GS} is lower than the V_T, in turn-off condition, it was observed that I_{DS} slightly increases as increasing optical power. Figure 2-16 shows the log-scale of I_{DS} as a function of V_{GS} under the same conditions of figure 2-14. Under the optical illumination, it can be seen that the InP HEMT exhibits small increase in I_{DS} even at turn-off condition. It is due to the photoconductive effect. Because the gain caused by photoconductive effects is much lower than caused by photovoltaic effects, the HEMT exhibits relatively small photocurrent under turn-off condition where it cannot provide a phototransistor gain by photovoltaic effect. This identification of photodetection mechanisms in InP HEMT can be affirmed by measuring the dependence of photocurrents on optical powers at each condition. Equation (2-10) indicates that the photocurrent caused by photovoltaic effect is a logarithmic function of input optical power. On the other hands, photoconductive effect shows the linear dependence described in equation (2-6).

Figure 2-17 shows the measured photocurrents for both turn-on (●) and turn-off (○) conditions and respectively fitted results according to the equations of (2-10) and (2-6) as a function of incident optical powers. The points are measured data and solid lines are fitted results. The well-fitted lines confirm the identification that photovoltaic effect is dominant at turn-on condition and photoconductive effect at turn-off condition. In other words, while the photodetection in InP HEMT is a superposition of these two photodetection mechanisms, the dominant one can be selectively appeared by adjusting gate bias condition of the HEMT.

The optical response of InP HEMT to 1.55μm lightwave is characterized in terms of the responsivity defined as the ratio of photocurrent to incident optical power. Figure 2-18 shows the responsivities as a function of incident optical power. Under the incident optical power of -9dBm, high DC responsivity of 14 A/W is achieved and it rapidly decreases with increasing optical power. It is because the photovoltaic effects which dominate the photodetection process at turn-on condition produce the logarithmic dependence of photocurrents on input optical power as mentioned previously.

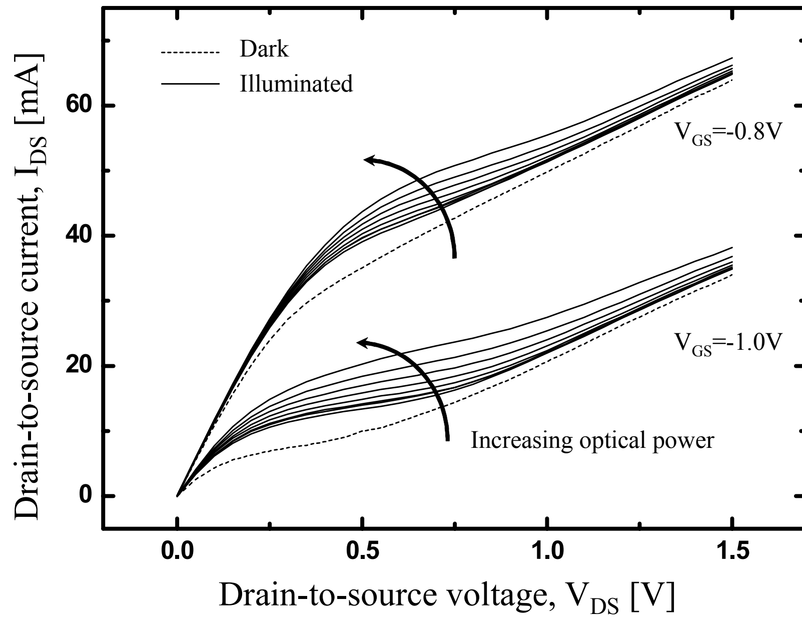

Figure 2-13. I_{DS}-V_{DS} characteristics of InP pHEMT under dark and optical illumination. Incident optical powers increase from -6dBm to 15dBm with the step of 3dB.

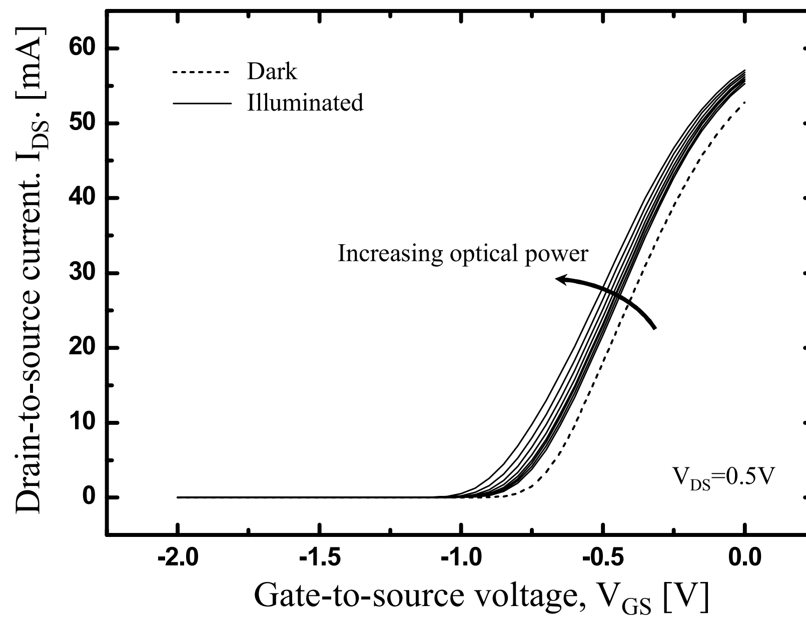

Figure 2-14. I_{DS}-V_{GS} characteristics of InP pHEMT under dark and optical illumination. Incident optical powers increase from -6dBm to 15dBm with the step of 3dB.

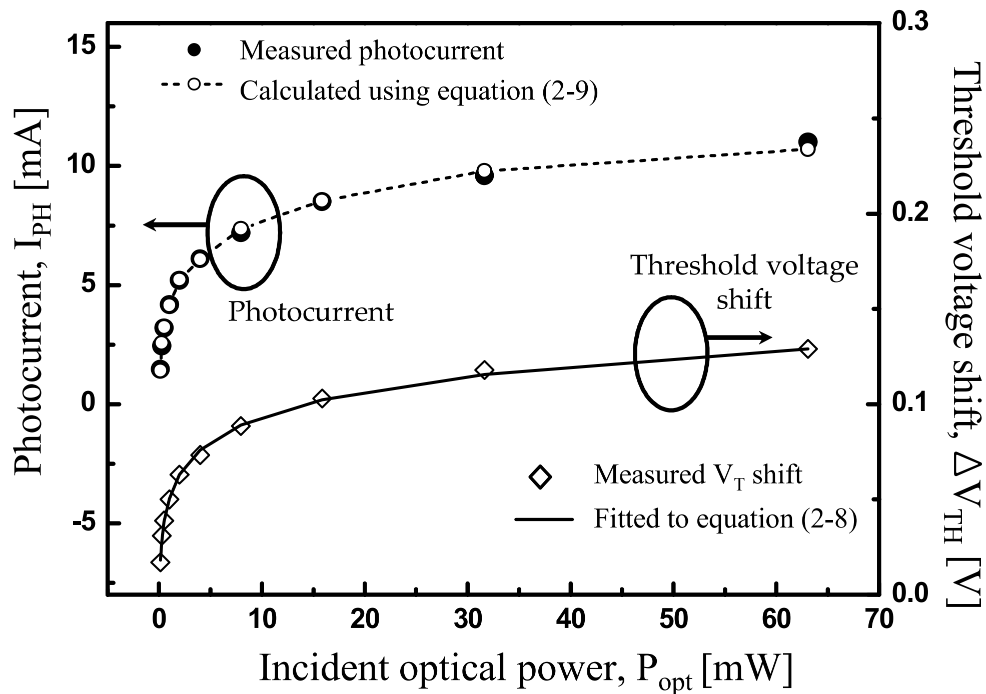

Figure 2-15. Measured photocurrent (●) and the calculated increase in drain current using equation (2-9) (--○--) as a function of incident optical power (upper curve). Measured threshold voltage shift (◇) as a function of incident optical power; solid line indicates the fitted data using equation (2-8). The V_{GS} of -0.5V and V_{DS} of 0.5V were used in the measurement of increased drain currents.

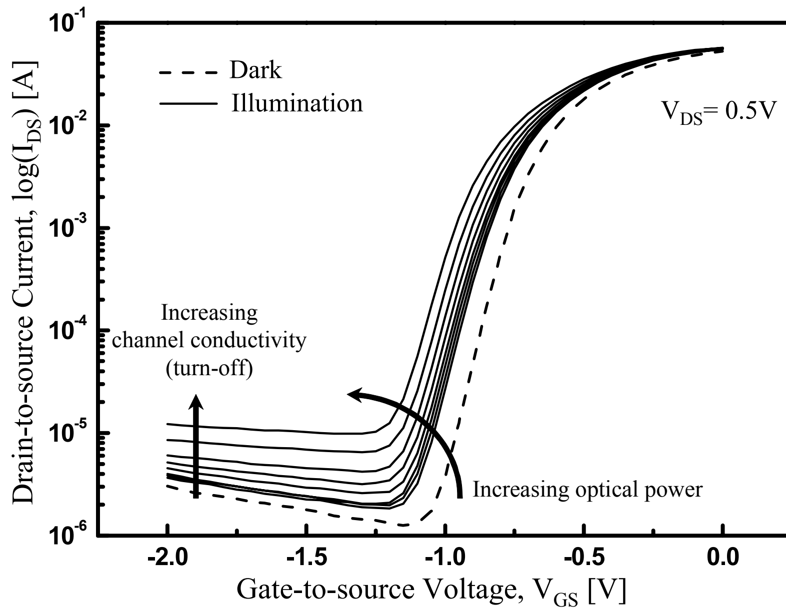

Figure 2-16. Log scale of I_{DS} as a function of V_{GS} for InP pHEMT under dark and optical illumination. Incident optical powers increase from -6dBm to 15dBm with the step of 3dB.

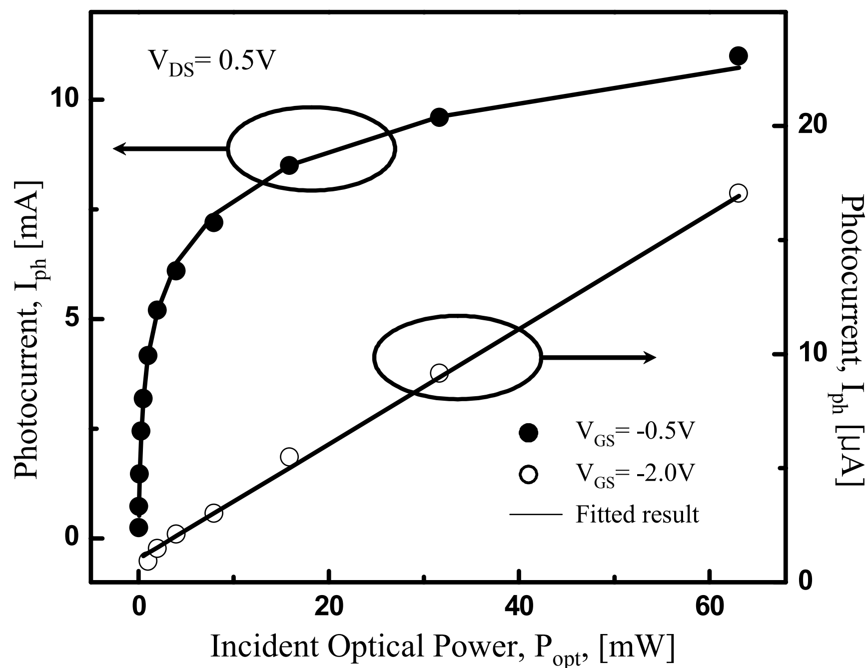

Figure 2-17. Photocurrents as a function of incident optical power to InP HEMT under turn-on (V_{GS}=-0.5V) and turn-off (V_{GS}=-2.0V) conditions. The symbols are measured data and solid lines are fitted results according to equations of (2-10) and (2-6).

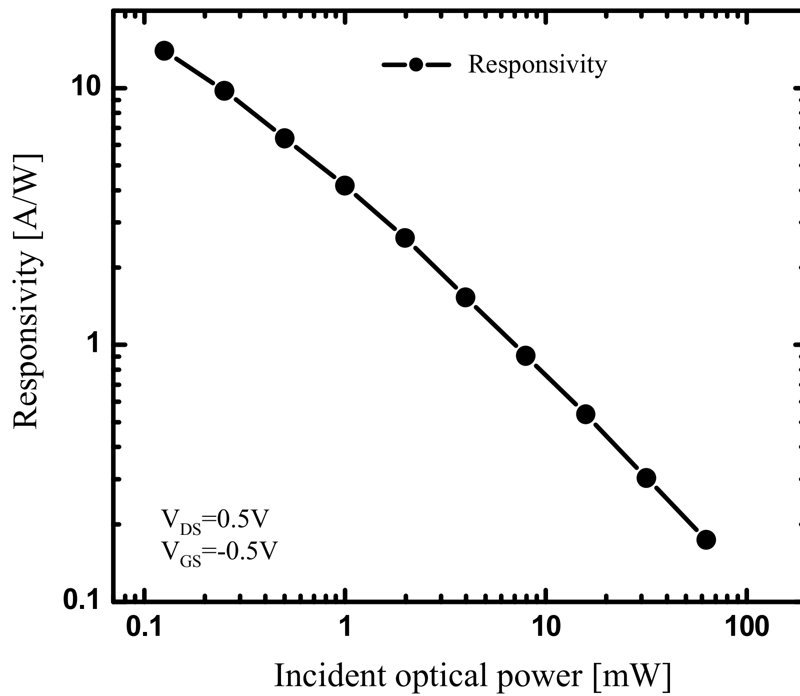

Figure 2-18. Optical responsivities of InP HEMT as a function of incident optical power under V_{GS}=-0.5V and V_{DS}=0.5V.

2-4-4. Optical modulation response of InP HEMT

The equations of (2-11) and (2-7) indicate that the optical modulation responses of photovoltaic effect and photoconductive effect are governed by lifetime of photogenerated electron and hole, respectively. Figure 2-19 shows the optical modulation response of InP HEMT under turn-on and turn-off conditions. Under turn-on condition where photovoltaic effect is dominant, the InP HEMT shows large photoresponse due to the phototransistor internal gain provided by photovoltaic effect. However, photoresponse has relatively small optical 3dB bandwidth of about 580MHz because photovoltaic effect is dominated by long lifetime of photogenerated holes accumulated beneath the source region where a small electric field exists. On the other hand, the optical modulation response at turn-off condition is small but does not fall off as fast because photoconductive effect is dominated by photogenerated electrons having much short lifetime. In this condition, InP HEMT operates as a photoconductor having InGaAs optical absorption layer [23].

Phototransistor internal gain is very important parameters which indicate how much gain an InP HEMT can be provided by phototransistor operation. It is defined as following,

$$G_{\text{int}} = \frac{I_{PV}}{I_{primary}}, \qquad (2\text{-}12)$$

where I_{PV} is the amplified photocurrent caused by photovoltaic effect and $I_{primary}$ is the primary photocurrent without any internal gain. Unfortunately, $I_{primary}$ cannot be exactly measured because actually absorbed optical power in InP HEMT is unknown due to the coupling loss. However, as described in equation (2-6), it can be estimated

by measuring photocurrent (I_{PC}) at turn-off state and calculating photoconductor gain (G_{PC}). The equation (2-6) describing photoconductor gain can be also written as

$$G_{pc} = \frac{I_{PC}}{I_{primary}} = \frac{\tau_n}{t_n} = \frac{t_p}{t_n} \approx \frac{v_n}{v_p}, \qquad (2\text{-}13)$$

where t_p and t_n are transit time of hole and electron, respectively. v_p and v_n are the velocity of hole and electron in InGaAs channel, respectively. In equation (2-13), electron lifetime can be replaced with hole transit-time because electrons are not supplied from the source until holes arrive at the source region [12]. The ratio of electron and hole transit-times can be determined by the ratio of electron to hole velocities in the strained $In_{0.65}Ga_{0.35}As$ channel under identical electric field [24]. It was estimated that the photoconductor current gain is about 2 from the other works [24-25]. From these results, the primary photodetected powers are determined as shown in Fig. 2-18. The difference between them and photodetected powers at turn-on state indicates the phototransistor internal gain (G_{int}) [26]. In the experiments, 45dB phototransistor internal gain is obtained at 100MHz optical modulation frequency.

Optical gain cutoff frequency (optical f_T) indicates maximum optical modulation frequency providing phototransistor internal gain. It is defined as the optical modulation frequency where phototransistor internal gain is 0dB as shown in figure 2-20. The fabricated InP HEMT offers the optical f_T of about 110GHz which is expected to provide high phototransistor internal gain even at high frequency modulated optical signal detections.

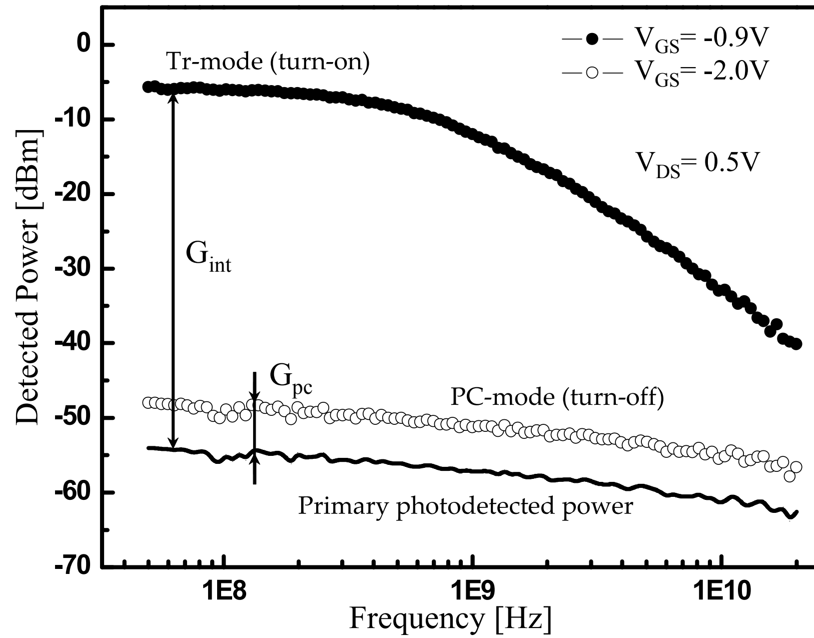

Figure 2-19. The measured optical modulation responses of InP HEMT under V_{GS} of -0.9V (turn-on) and -2V (turn-off) at fixed V_{DS} of 0.5V. The solid line is the primary photodetected power extracted from measured data at turn-off condition. G_{int} and G_{pc} represent phototransistor internal gain and photoconductor gain, respectively.

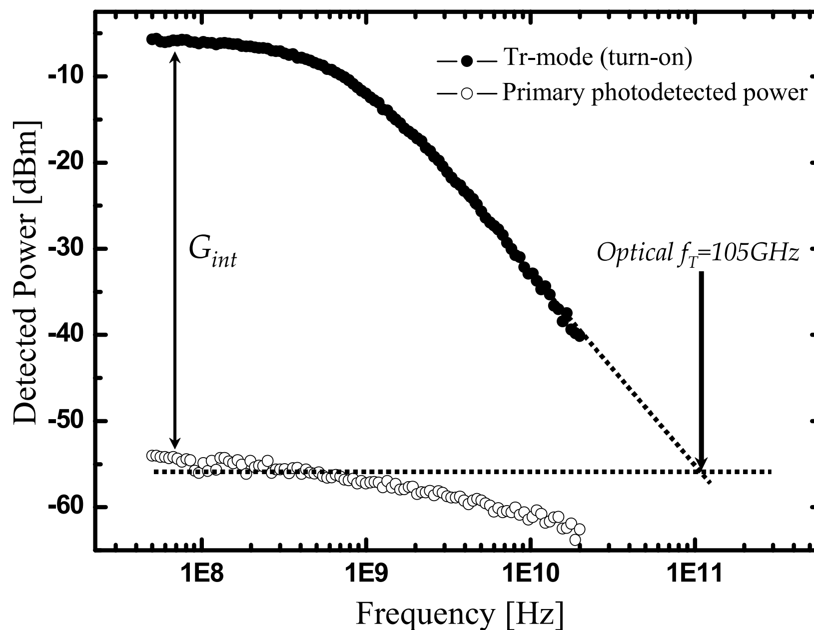

Figure 2-20. The definition of optical gain cutoff frequency (optical f_T). It is the frequency where phototransistor internal gain is 0dB. The InP HEMT exhibits the optical f_T of about 110GHz

2-4-5. 60GHz photodetection with optimization process

As presented in previous section, the fabricated InP HEMT provides high phototransistor internal gain and high optical f_T compared to the other reports. These attractive features are useful in optical millimeter-wave systems shown in figure 1-5-(A). Since the InP HEMT performs the photodetection of millimeter-wave modulated optical signals with amplification, it contributes to increase link gain of these fiber-optic/millimeter-wave system approaches. Figure 2-21 shows the photodetected 60GHz spectrum of InP HEMT. For generating 60GHz optical signal, Mach-Zehnder modulator was biased at minimum transmission point and modulated by 30GHz RF signals, which generates double-side band with suppressed carrier (DSB-SC) optical signals. For observation of 60GHz signal, low noise amplifier with 17dB gain was used at the drain port of InP HEMT.

To obtain maximum photodetection power, optimum bias conditions for InP HEMT are investigated over practical ranges of bias levels. Because the measurement sensitivity at 60GHz band is limited by high background noise level of external harmonic mixer (HP11974V), the optical modulation frequency was set to be 1GHz. Figure 2-22 shows the dependence of photodetected power on V_{DS} conditions at V_{GS} of -0.9V. As increasing V_{DS}, the output power at 1GHz initially increases and begins to saturate when V_{DS} is over than 0.5V. The dependence on V_{GS} conditions is displayed in figure 2-23. The general shapes of these results resemble that of the dependence of G_m on V_{DS} and V_{GS}, respectively. This corresponds to the equation (2-9) that photocurrents at turn-on condition are directly related to the transconductance of InP HEMT. However, this equation cannot explain the photodetection signals under turn-off

condition where G_m is zero. As clarified in the previous section, it can be explained by the introduction of photoconductive effect. From figure 2-23, phototransistor internal gain can be estimated by measuring difference between photodetection powers at turn-on condition and primary photodetection power extracted from turn-off condition.

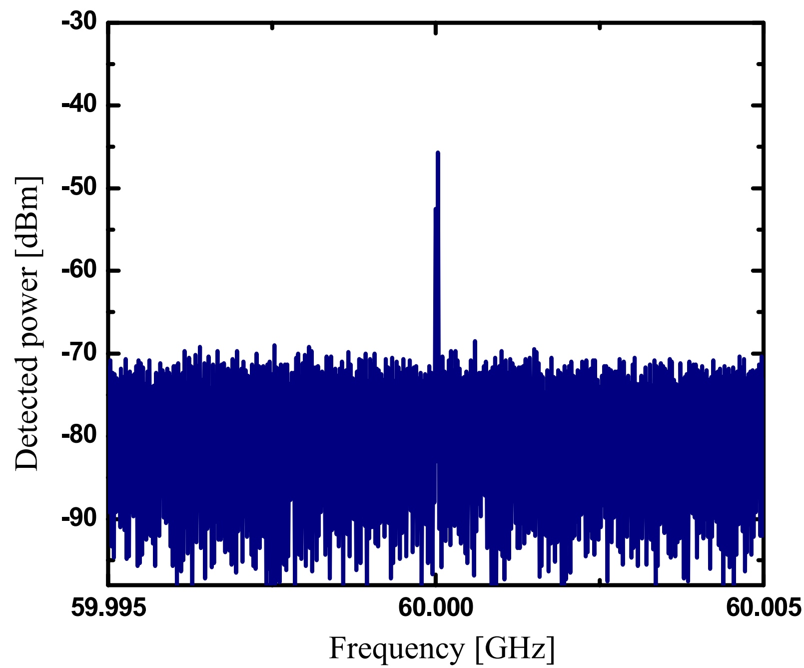

Figure 2-21. The measured spectrum of 60GHz photodetected signal using InP HEMT.

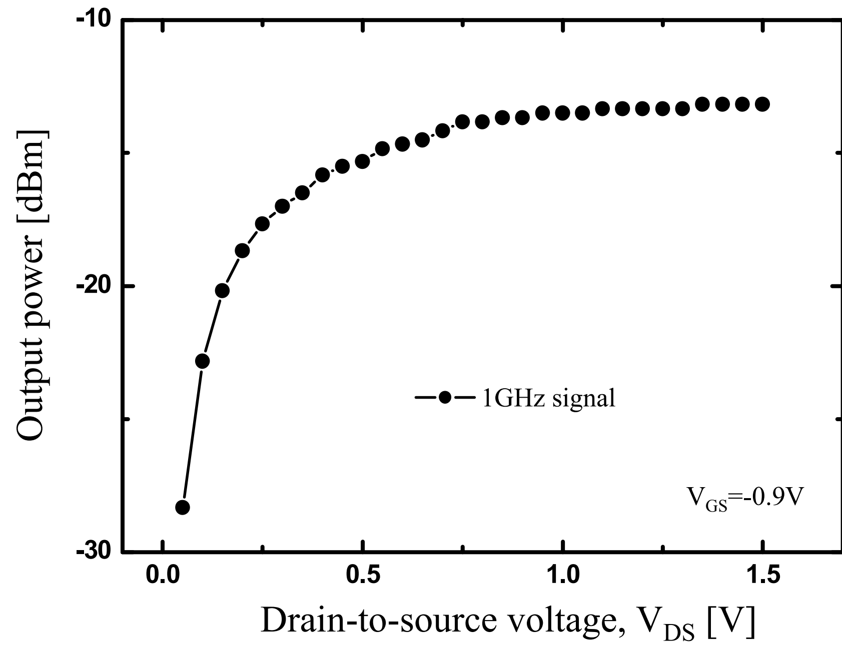

Figure 2- 22. The dependence of 1GHz photodetection signal on V_{DS} conditions.

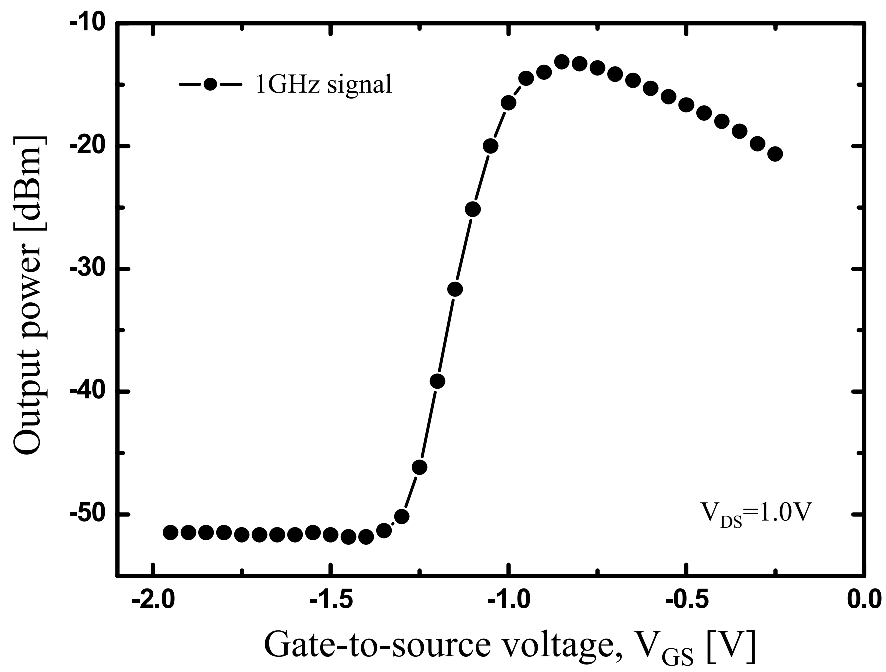

Figure 2-23. The dependence of 1GHz photodetection signal on V_{GS} conditions.

2-4-6. Fiber-optic transmission demonstration using InP HEMT

Photodetection bandwidth for optically transmitted digital data signals is determined by the optical 3dB-bandwidth of a photodetector. The InP HEMT operates as a phototransistor offer the 3dB-bandwidth of about 580MHz as described before. In order to verify its feasibility as a photodetector, a 20km fiber-optic transmission is demonstrated for photodetection of 622Mbps optical data signals. Experimental setup is depicted in figure 2-24. The DFB laser diode was directly modulated with 622Mbps nonreturn-to-zero (NRZ) data signals having the 2Vpp from bit-pattern generator (Anritsu MP1632A). After 20km optical transmission in a commercial single-mode optical fiber followed by EDFA amplification, optical signals were illuminated to InP HEMT. The photodeteted output signals from drain port were low-pass filtered and connected to sampling oscilloscope (Tektronix 11801C) for eye diagram measurements or error detector for bit-error-rate (BER) measurements. The eye-diagram shown in figure 2-24-(A) was obtained at the pseudo-random-bit-sequence (PRBS) of 2^{15}-1 when InP HEMT was biased at V_{GS} of -0.9V and V_{DS} of 1.2V. The measured BER characteristics as a function of incident optical power are plotted as shown in figure 2-24-(B). The measured sensitivity at 10^{-9} BER was achieved at the incident optical power of 9dBm. Since the actually absorbed optical power is less than 2% of incident optical power as mentioned in section 2-2, the sensitivity can be improved if more efficient optical coupling techniques are utilized. Setting aside the high coupling loss, these experimental demonstrations confirm that InP HEMTs do not have any problem to detect broadband optical data signals up to 622Mbps.

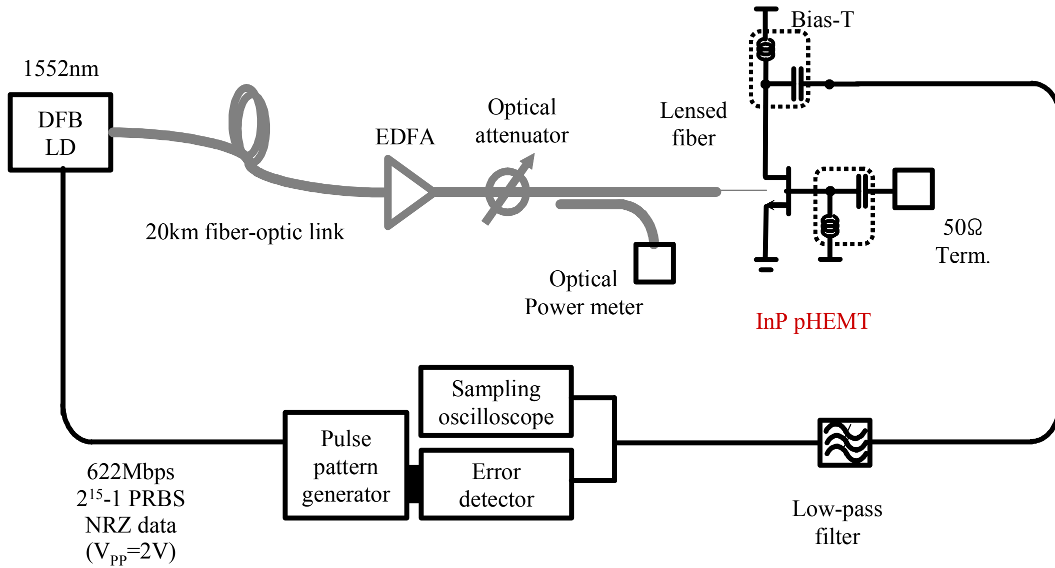

Figure 2-24. Experimental setup for fiber-optic transmission using InP HEMT as a phototransistor.

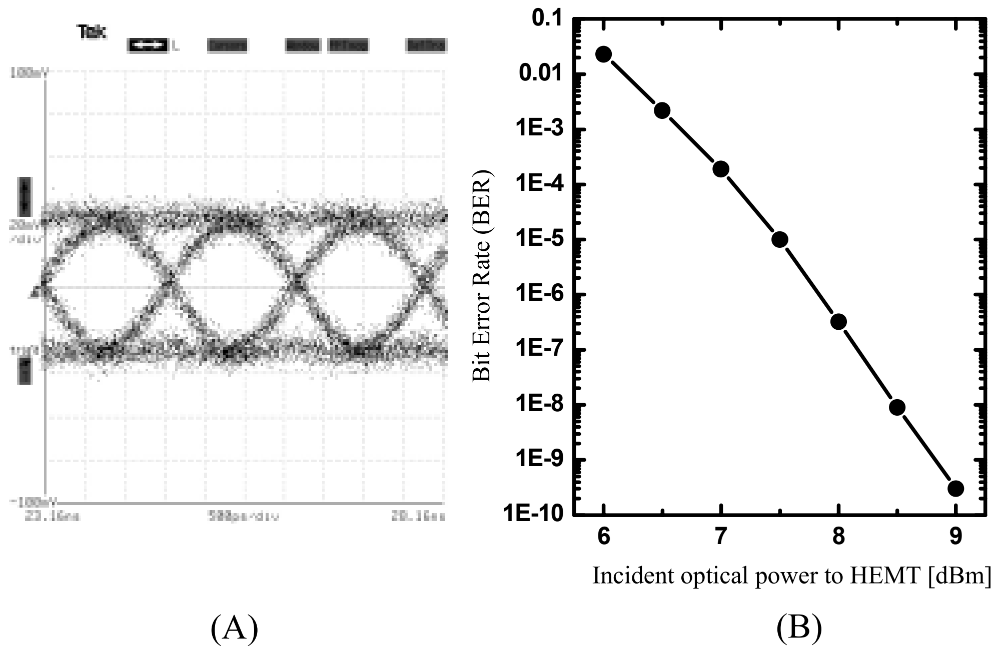

Figure 2-25. (A) Eye-diagram for photodetected 622Mbps data signal. (B) Bit-error-rate (BER) characteristics as a function of incident optical power to HEMT.

2-5. Conclusion

The photodetection characteristics of InP pHEMT to 1.55μm lightwave are experimentally investigated. Their physical origins are classified into two major photoeffects. One is a photovoltaic effect that arises from the accumulation of photogenerated holes in the source region. It appears as negative shifts in threshold voltage, which invokes additional drain currents by FET operation. The phototransistor internal gain of InP HEMT at turn-on state is mainly attributed to this photovoltaic effect. The other is photoconductive effect which dominates photodetection process in InP HEMT under turn-off condition. Because it only includes the photoconductor gain, it is possible to estimate primary photodetected power corresponding to actually absorbed optical power in InP HEMT. The identification of these two photoeffects is experimentally verified by fitting measured data into the dependence of photocurrents on optical power due to each mechanism.

Phototransistor internal gain and optical current gain cutoff frequency indicating the device performance of a phototransistor are determined by taking difference between photodetected power measured at turn-on state and primary photodetected power, and finding interception point between them, respectively. The fabricated InP pHEMT offers G_{int} of 45dB at 100MHz and optical f_T of 102GHz, which are comparable to the phototransistors reported by other research groups.

As initiative studies on the applications of InP HEMT to fiber-optic/millimeter-wave systems, 60GHz photodetection is first demonstrated. Optimum bias conditions for high photodetection efficiency are also investigated. The dependence of photodetection power on the bias conditions exhibits explicit similarities with the dependence of G_m

on bias conditions which partially indicates the phototransistor operation of InP HEMT is governed by FET operation. Finally, a 622Mbps baseband digital data transmission over 20km single mode fiber is accomplished in order to investigate its feasibility to receive broadband optical data signals. Chapter 3 will present more detailed results of their applications to fiber-optic/millimeter-wave data transmission systems.

References

[1] R. Dingle, H. L. Stormer, A. C. Gossard and W. Wiegmann, "Electron mobilities in modulation-doped semiconductor heterojunction superlattices," *Appl. Phys. Lett.*, vol. 33, no. 7, pp. 665, Oct. 1995.

[2] T. Mimura, S. Hiyamizu, T. Fujii and K. Nanbu, "A new field-effect transistor with selectively doped GaAs/n-$Al_xGa_{1-x}As$ heterojunctions," *Jpn. J. Appl. Phys.*, vol. 19, no. 5, pp. L225, 1980.

[3] F. Ali and A. Gupta, *HEMTs and HBTs: devices, fabrication and circuits*, Artech House, 1991.

[4] Y. Takanashi, K. Takahata and Y. Muramoto, "Characteristics of InAlAs/InGaAs high electron mobility transistors under 1.3μm laser illumination," *IEEE Electron Devices Lett.*, vol. 19, no. 12, pp. 472, Dec. 1998.

[5] Technology Modeling Associates, MEDICI version 4.0, *User's manual*, 1997

[6] A. M. Kusters, R. Wuller, H. J. Geelen, A. Kohl and K. Heime, "Sub-half-micrometer pseudomorphic InP/$In_xGa_{1-x}As$/InP HEMT's ($0.74 \le x \le 0.81$) with very high f_T values," *IEEE Electron Devices Lett.*, vol. 16, no. 9, pp. 396, Sep. 1995.

[7] Y. Yamashita, A. Endoh, K. Shinihara, K. Hikosaka, T. Matsui, S. Hiyamizu and T. Mimura, "Pseudomorphic $In_{0.52}Al_{0.48}As/In_{0.7}Ga_{0.3}As$ HEMTs with an ultrahigh f_T of 562GHz," *IEEE Electron Devices Lett.*, vol. 23, no. 10, pp. 573, Oct. 2002.

[8] Dae-Hyun Kim, "A study on fabrication and characterization of $In_xGaAs/In_{0.52}AlAs$ nano-HEMT's and their impact on high-speed IC's," *Ph.D. dissertation*, Graduate school of electrical engineering, Seoul National University, Seoul, Korea, 2004.

[9] M. H. Somerville, A. Ernst and J. A. del Alamo, "A physical model for the kink effect in InAlAs/InGaAs HEMT's," *IEEE Trans. Electron Devices*, vol. 47, no. 5, pp. 922, May 2000.

[10] L. M. de Barros, A. Paolella, M. Y. Frankel, M. A. Romero and P. R. Herczfeld, "Photoresponse of microwave transistors to high-frequency modulated lightwave carrier signal," *IEEE Trans. Microwave Theory Tech.*, vol. 45, no. 8, pp. 1368, Aug. 1997.

[11] R. N. Simons and K. B. Bhasin, "Analysis of optically controlled microwave/millimeter-wave device structures," *IEEE Trans. Microwave Theory Tech.*, vol.

34, no. 12, pp. 1349, Dec. 1986.

[12] Y. Takanashi, K. Takahata and Y. Muramoto, "Characteristics of InAlAs/InGaAs high-electron-mobility transistors under illumination with modulated light," *IEEE Trans. Electron Devices*, vol. 46, no. 12, pp. 2271, Dec. 1999

[13] A. A. de Salles, "Optical control of GaAs MESFET's," *IEEE Trans. Microwave Theory Tech*., vol. 31, no. 10, pp. 812, Oct. 1983

[14] R. B. Darling and J. P. Uyemura, "Optical gain and large-signal characteristics of illuminated GaAs MESFET's," *IEEE J. Quantum Eletron*., vol. 23, no. 7, pp.1160, Jul. 1987

[15] A. Madjar, P. R. Herczfeld and A. Paolella, "Analytical model for optically generated currents in GaAs MESFETs," *IEEE Trans. Microwave Theory Tech*. vol. 40, no. 8, pp. 1681, Aug. 1992

[16] C. Y. Chen, A. Y. Choi, C. G. Bethea, P. A. Garbinski, Y. M. Pang and B. F. Levine, "Ultrahigh speed modulation-doped heterostructure field-effect photodetectors," *Appl. Phys. Lett*., vol. 42, no. 15, pp. 1040, Jun. 1983.

[17] M. A. Romero, M. A. G. Martinez and P. R. Herczfeld, "An analytical model for the photodetection mechanisms in high-electron mobility transistors," *IEEE Trans. Microwave Theory Tech.,* vol. 44, no. 12, pp. 2279, Dec. 1996.

[18] C. Navarro, J.-M. Zamanillo, A. M. Sanchez, A. T. Puente, J. L. Garcia, M. Lomer and J. M. Lopez-Higuera, "An accurate photonic capacitance model for GaAs MESFETs," *IEEE Trans. Microwave Theory Tech*., vol. 50, no. 4, pp. 1193, Apr. 2002.

[19] M. Marso, P. Gersdorf, A. Fox, A. Forster, U. Hodel, R. Lambertini and P. Kordos, "InAlAs-InGaAs OPFET with responsivity above 200A/W at 1.3μm wavelength," *IEEE Photon. Technol. Lett*., vol. 11, no. 1, pp. 117, Jan. 1999

[20] C. Rauscher and K. J. Williams, "Heterdyne reception of millimeter-wave modulated optical signals with an InP-based transistor," *IEEE Trans. Microwave Theory and Tech.*, vol. 42, no. 11, pp. 2027, Nov. 1994.

[21] J. I. Pankove, *Optical processes in semiconductors*, Dover Publications, Inc. 1971

[22] C.-S. Choi, H.-S. Kang, W.-Y. Choi, H.-J. Kim, W.-J. Choi, D.-H. Kim, K.-C. Jang and K.-S. Seo, "High optical responsivity of InAlAs/InGaAs metamorphic high-electron mobility transistor on GaAs substrate with composite channels," *IEEE Photon. Technol. Lett,* vol. 15, no. 6, pp. 846, Jun. 2003.

[23] J. C. Gammel, H. Ohno and J. M. Ballantyne, "High-speed photoconductive

detectors using GaInAs," *IEEE J. Quantum Electron.*, vol. 17, no. 2, pp. 269, Feb. 1981.

[24] K. Brennan, "Theory of the steady-state hole drift velocity in InGaAs," *Appl. Phys. Lett.*, vol. 51, no. 13, pp. 995, Sep. 1987.

[25] J. L. Thobel, L. Baudry, A. Cappy, P. Bourei and R. Fauquembergue, "Electron transport properties of strained $In_xGa_{1-x}As$," *Appl. Phys. Lett.*, vol. 56, no. 4, pp. 346, Jan. 1990.

[26] Hyo-Soon Kang, Chang-Soon Choi, Woo-Young Choi, Dae-Hyun Kim and Kwang-Seok Seo, "Characterization of phototransistor internal gain in metamorphic high-electron-mobility transistors," *Appl. Phys. Lett.*, vol. 84, no. 19, pp. 3780, May 2004.

Chapter 3

Fiber-optic/millimeter-wave data transmission systems based on InP HEMTs

3-1. Introduction

3-1-1. Direct optical control of microwave devices and circuits for fiber-optic/millimeter-wave systems

Chapter 2 discussed the utilization of InP HEMT as a phototransistor which converts the optically modulated signals into corresponding electrical RF signals with the amplification. Considering their traditional applications, InP HEMTs are microwave devices performing microwave signal processing including amplification, frequency generation and frequency mixing. In these conventional usages, an optical signal injected to the device is regarded as an additional input port or control port, which makes an InP HEMT virtually four terminal-device. These direct optical controls of microwave devices and circuits have many structural advantages such as the availability of wide bandwidth input and control signals, the perfect isolation from RF

signals, and the suitability for the implementation with fiber-optic/millimeter-wave systems [1]. Furthermore, the technological advances of high-speed optical signal processing whose frequency range is much higher than RF signal processing have accelerated these research activities in direct optical control techniques [2]. The low size and low weight of optical fiber are another important reason for their uses, which are particularly attractive in phase-array antenna applications where a lot of control and reference signals distributions to antenna array elements are required. Owing to these attractive features, several works have been done for the applications of these optically controlled microwave devices and circuits to fiber-optic/millimeter-wave data transmission systems. Following sections briefly review them.

3-1-2. Optically controlled amplifiers

The gain of amplifier can be tuned by varying incident optical power which changes the transconductance of three-terminal devices. Figure 3-1-(A) schematically illustrates the optical control of amplifier gain by external optical illumination. A. Paolella et al. reported the amplifier gain control with tuning range of about 15dB in GaAs MMIC transmit/receive modules [3]. R. Simons observed that the S_{21} in GaAs MESFET increases as incident optical power increases [4]. The fabricated InP HEMTs exhibit the similar behaviors that the S_{21} can be changed by varying incident optical power to the device. Figure 3-1-(B) shows the experimental results indicating the changes in S_{21} under different incident optical power. It can be observed that the S_{21} increases with increasing optical power, thus the intrinsic gain control of optically sensitive microwave devices is possible by optical illumination.

3-1-3. Optoelectronic mixers

If the optically modulated IF signals (f_{IF}) and electrical LO signals (f_{LO}) are simultaneously applied to the devices, the frequency mixing components ($f_{LO} \pm f_{IF}$) between them can be observed at the output drain port as illustrated in figure 3-2-(A). The three-terminal devices given by an additional optical input port operates as optoelectronic mixers performing dual functions of photodetection and frequency mixing in a single device. Since the efforts to open another electrical port for frequency mixing are not required, the consequent matching and parasitic problems happened in design of microwave mixers can be alleviated with optoelectronic mixers. This simplicity is major attraction in utilization of optoelectronic mixers. C. Raucher made pioneering works on this type of optoelectronic receiver [5]. With their compatibility to MMIC process, optoelectronic up-converters based on GaAs-based HEMTs were demonstrated by H. Kamitsuna [6]. Because these optoelectronic mixers have found many applications in fiber-optic/millimeter-wave systems, many works have continuously reported until now [7-9]. Figure 3-2-(B) shows the output spectrum of InP HEMT optoelectronic mixer under applying 25GHz LO to gate port and illuminating optical 100MHz IF signal to the device. It can be seen that the output includes the optoelectronic mixing components, $f_{LO} \pm f_{IF}$ and LO component.

3-1-4. Optical control of oscillators

By applying optical signals into active devices served to microwave oscillator,

useful functions to control microwave oscillators can be attained. A. J. Seeds categorized three types of optically controlled oscillators [1]. Optical switching can be achieved by pulsed optical illumination as shown in figure 3-3-(A). It has been investigated for optically controlled transmit/receive modules in phase-array antenna applications. It is also possible to realize tuning of oscillator output frequency by changing optical illumination power shown in figure 3-3-(B). It was demonstrated by several research groups and 3% tuning range of the oscillation frequency was reported [10]. Figure 3-3-(C) gives the schematic illustration of direct optical injection-locking of oscillators. The modulation frequency (f_{master}) to optical signal is set to be close to the frequency of free-running oscillator (f_{osc}). Under optical injection, the oscillation frequency is free from free-running state and synchronized at that of modulated optical signals, which makes f_{osc} equal to be f_{master}. Therefore, the frequency and the phase of oscillator are locked to those of injected optical signals. They give many attracting features to phase-array applications where phase-locking of many remotely located microwave oscillator by single microwave source is required [11]. In the same manner, they are also useful in fiber-optic/millimeter-wave that require many low-phase local oscillators in remote antenna base station enough to support millimeter-wave wireless cellular networks.

The remains of this chapter mainly concern about the optoelectronic mixers and optical injection-locked oscillators based on InP HEMT and their applications to fiber-optic/millimeter-wave data transmission systems. After investigating their operation characteristics, new system configurations that can offer simple antenna base station architectures are proposed and experimentally demonstrated in the constructed fiber-optic/millimeter-wave data transmission systems.

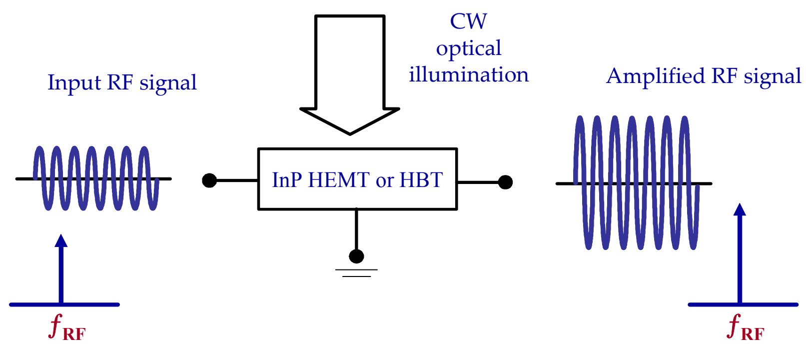

(A)

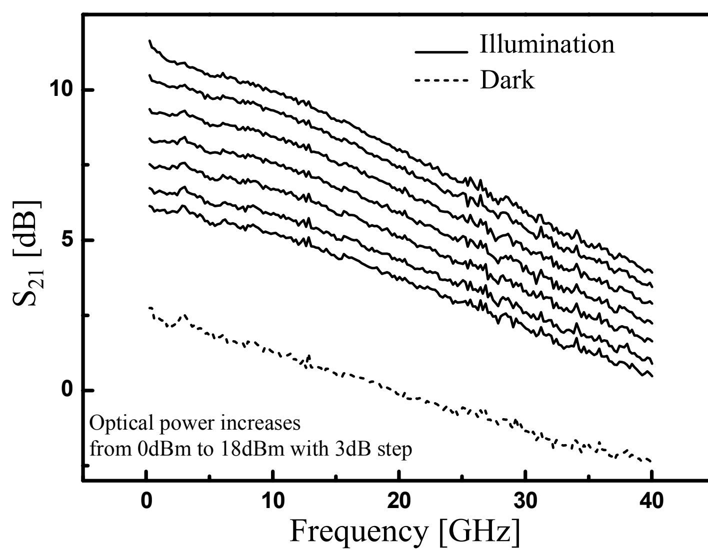

(B)

Figure 3-1. optically controlled intrinsic gain of microwave transistors (B) Experimental S_{21} variation of InP HEMT with increasing optical power

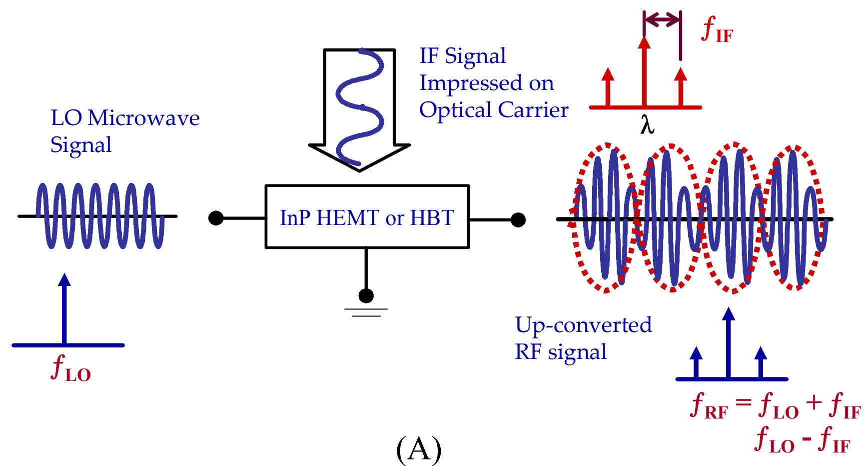

(A)

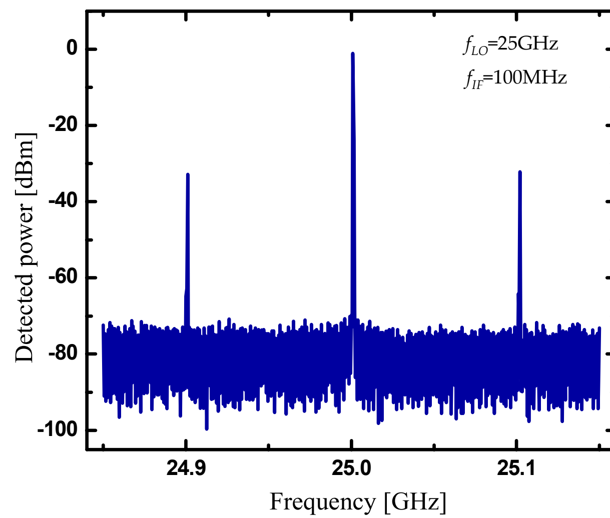

(B)

Figure 3-2. (A) Optoelectronic mixing in microwave devices (B) Experimental output spectrum of InP HEMT under applying 25GHz LO signal to the gate port and illuminating 100MHz optical signal.

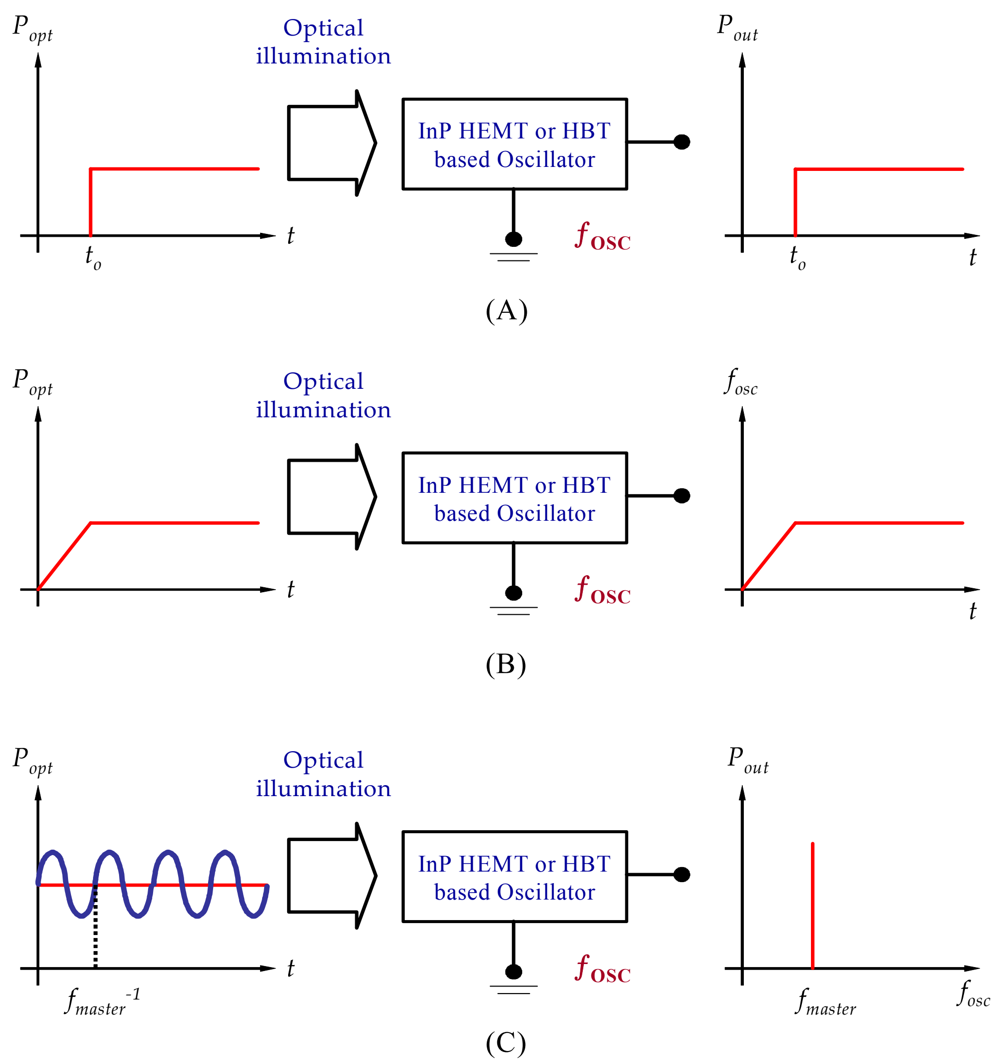

Figure 3-3. Optical control of oscillators (A) optical switching, (B) optical tuning and (C) optical injection-locking. Adapted from [1]

3-2. Subharmonic optoelectronic mixer

3-2-1. Motivation

In remote up-conversion systems described in figure 1-5-(B), the required components for antenna base stations are photodetectors, millimeter-wave frequency mixers, local oscillators (LO), power amplifiers, radiation antennas and the other passive components such as filters. These complex base station architectures can be simplified by introducing optoelectronic mixers as shown in figure 3-2. Since they unify the functions of photodetection and frequency mixing in a single device, it is possible to eliminate high-frequency electrical mixers in antenna base stations.

A number of different optoelectronic devices have been investigated to realize optoelectronic mixing for fiber-optic/millimeter-wave system applications, for example, electro-absorption modulators [12], photodiodes [13], phototransistors based on microwave transistors [7-9]. It was previously explained in chapter 1 that three-terminal phototransistors are attractive for optoelectronic MMICs because of their fabrication process compatibility. Furthermore, since they inherently have two input ports (electrical and optical), it is not necessary to use additional RF components such as RF circulators or diplexer required for external RF signal injection into two-terminal devices to achieve optoelectronic mixing. High conversion gain and perfect isolation between two input signals are additional benefits for utilizing these phototransistors as optoelectronic mixers.

Unfortunately, these approaches essentially need millimeter-wave LOs for the frequency up-conversion into millimeter-wave frequency bands, which burdens the design and cost of antenna base stations. In this section, InP HEMTs are utilized as

subharmonic optoelectronic mixers having the potential to use low LO frequency which is some integer fraction (1/n) of the fundamental LO frequency. Optimum bias conditions for InP HEMT subharmonic optoelectronic mixers are first determined. Such optoelectronic mixer performance characteristics as internal conversion gain, usable LO ranges and nonlinear distortion characteristics are also experimentally evaluated.

3-2-2. Features of InP HEMT subharmonic optoelectronic mixers

Incorporating the photodetection characteristics described in chapter 2 with the device intrinsic nonlinearities, InP HEMTs can be used as optoelectronic mixers by applying LO to the gate port. For the purposes mentioned before, LO frequency multiplication function is added, which allows less stringent use of high frequency LO, resulting in subharmonic optoelectronic mixer. Figure 3-4 gives the schematic diagram for utilizing the InP HEMT as a subharmonic optoelectronic mixer and its frequency up-converted output spectrum at 60GHz band. It can be seen that there are harmonic optoelectronic mixing products $2f_{LO}+f_{IF}$ (60.1GHz), $2f_{LO}-f_{IF}$ (59.9GHz) and 2nd harmonic of applied LO at $2f_{LO}$ (60GHz) under applying 30GHz LO to the gate port and illuminating 100MHz optical signal.

Operation principle of an InP HEMT subharmonic optoelectronic mixer is identified as follows. As described in chapter 2, the dominant photodetection mechanism to contribute the phototransistor internal gain in InP HEMT is the photovoltaic effect which is exposed as the threshold voltage shift of I_{DS}-V_{GS} characteristics. When low power optical signals are illuminated to InP HEMT, the photovoltage (V_{ph}) which is

linearly proportional to the absorbed optical power (P_{opt}) is given as,

$$V_{ph} \approx a_1 P_{opt} . \qquad (3\text{-}1)$$

When the LO signal is applied to the gate port, frequency mixing between LO and optical signal occurs by device intrinsic nonlinearity. Although a HEMT has many nonlinear parameters, the predominant one for optoelectronic mixing is considered to be nonlinear characteristics of I_{DS}-V_{GS} relationship because the input optical signal can be regarded as another voltage input signal to the gate port [14].

The I_{DS} of a HEMT can be written as

$$I_{DS} = I_S + b_1 V_{GS} + b_2 V_{GS}^2 + b_3 V_{GS}^3 + \cdots, \qquad (3\text{-}2)$$

where $b_{1\cdots n}$ are the Taylor series coefficients and I_S is the static drain-to-source current. The optical power of IF modulated lightwave is described by

$$P_{opt} = P_0 [1 + m\cos(2\pi f_{IF} t)], \qquad (3\text{-}3)$$

where P_0 is the average optical power and m is the optical modulation index. Considering LO signal applied to the gate port and optical signal which is converted to photovoltage (V_{ph}), V_{GS} in equation (3-2) can be modified as

$$V_{GS} = V_{GB} + V_S \cos(2\pi f_{LO} t) + V_{ph} \cos(2\pi f_{IF} t), \qquad (3\text{-}4)$$

where V_{GB} is the DC gate bias voltage and V_S and f_{LO} are the amplitude and frequency of LO, respectively. By substituting equations (3-3) and (3-4) into equation (3-2), the optoelectronic mixing products at $f_{LO} + f_{IF}$ and $2 f_{LO} + f_{IF}$ can be obtained as

$$I_{DS}(f_{LO}+f_{IF}) \propto a_1 m P_0 \cdot b_2 V_S, \tag{3-5}$$

$$I_{DS}(2f_{LO}+f_{IF}) \propto a_1 m P_0 \cdot b_3 V_S. \tag{3-6}$$

Since b_2 and b_3 are strongly dependent on applied DC gate bias voltage, V_{GB}, the mixing efficiencies of the desired frequency components can be controlled by changing the gate bias condition.

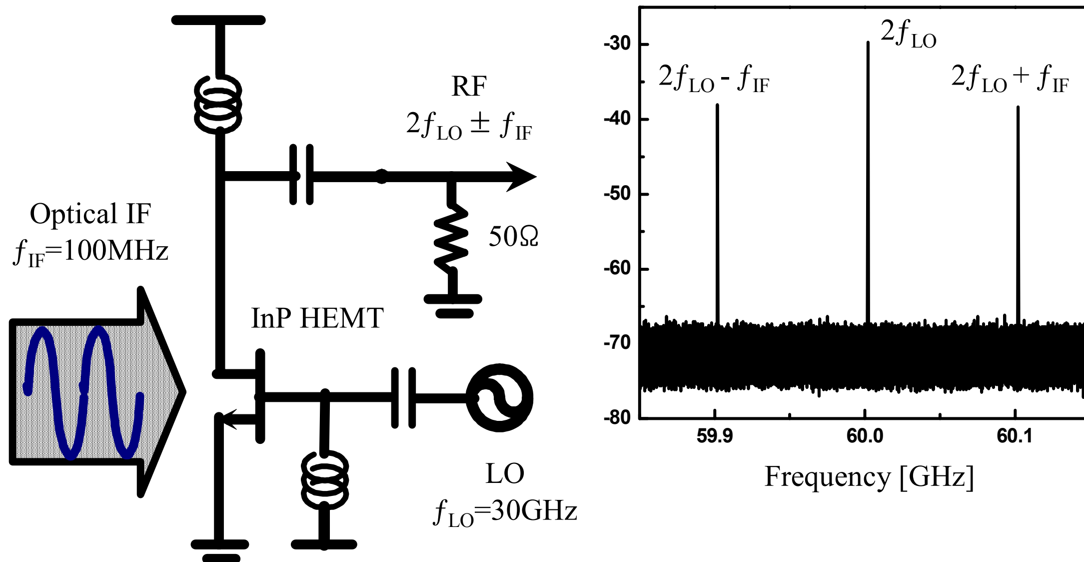

Figure 3-4. InP HEMT subharmonic optoelectronic mixer and its output spectrum at 60GHz band.

3-2-3. *Optimum bias conditions and internal conversion gain*

In order to obtain maximum performance of the InP HEMT subharmonic optoelectronic mixer, DC bias conditions are optimized considering conversion efficiency. In the case of a microwave mixer, the conversion gain which is the ratio of input IF signal power to output RF power is used as an important parameter representing mixer performance. Unfortunately, the same definition cannot be used in optoelectronic mixers based on HEMT and HBT since the actually absorbed optical IF power is not accurately known. Instead, the internal conversion gain is defined as the power ratio of the optoelectronic mixing signal to the primary photodetected signal without any internal gain, which can be estimated from the measured data at turn-off condition as mentioned in chapter 2. Figure 3-5 shows the optoelectronic mixing products at $f_{LO} + f_{IF}$ and $2f_{LO} + f_{IF}$ and their internal conversion gains as a function of V_{GS}. For its characterization, 30GHz LO with 0dBm power was connected to the gate port and the output signals from the drain port were measured by an RF spectrum analyzer incorporated with external A-band (Agilent 11970A) and V-band (Agilent 11974V) harmonic mixers. Optical 100MHz IF signal was illuminated to the device. The primary photodetected f_{IF} signal power of -55dBm was extracted from the photodetected power measured at V_{GS} of -2V. It should be noted in this figure that the mixing products at $2f_{LO} + f_{IF}$ can be selectively enhanced at V_{GS} of -0.9V while suppressing undesired mixing components at $f_{LO} + f_{IF}$. This feature is advantageous for InP HEMT subharmonic optoelectronic mixer in which $2f_{LO} + f_{IF}$ is utilized. In these experiments, 17dB internal conversion gain is obtained for 60GHz harmonic optoelectronic frequency up-conversion by setting the optimum V_{GS} of -0.9V.

For further investigation of the bias condition, we measured the dependence of mixing products at $f_{LO} + f_{IF}$ and $2f_{LO} + f_{IF}$ on V_{DS} as shown in figure 3-6. In the linear mode where V_{DS} is low, the harmonic optoelectronic mixing products at $2f_{LO} + f_{IF}$ are enhanced. However, in the saturation mode, it begins to decreases as increasing V_{DS}. The experimental results correspond to the characteristics of microwave mixer in which even-order harmonics of LO become strong under the linear mode of FET [15]. From these measurements, optimum bias conditions of V_{GS} of -0.9V and V_{DS} of 0.5V were obtained. In these conditions, the output spectrum of InP HEMT when 10GHz LO is applied to the InP HEMT is shown in figure 3-7. The reason for applying 10GHz LO is to simultaneously observe the output spectrum in RF spectrum analyzer whose frequency ranges are below 26.5GHz. It can be seen that the output power of $2f_{LO} + f_{IF}$ is much larger than that of $f_{LO} + f_{IF}$. The determined optimum bias conditions have been used in following experiments including broadband data transmission in fiber-optic/60GHz downlink systems.

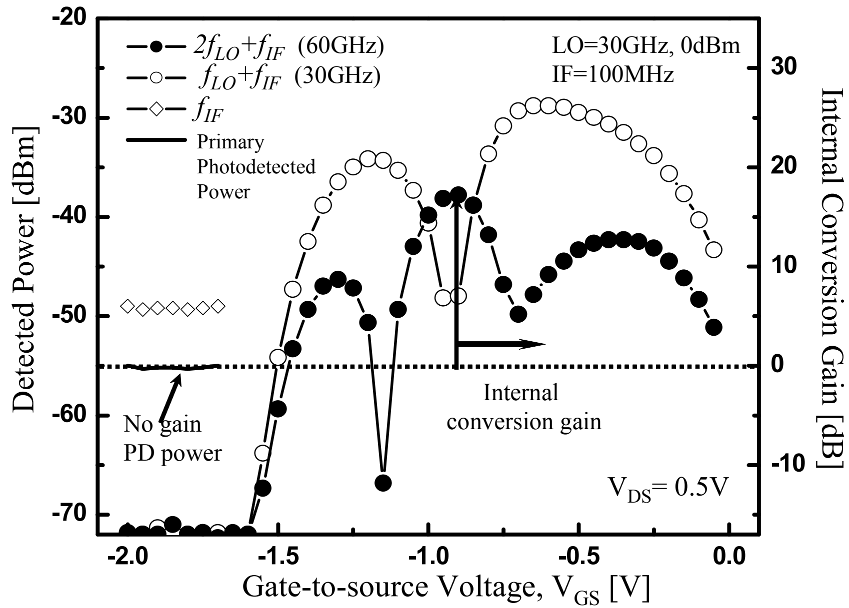

Figure 3-5. The dependence of optoelectronic mixing products at $f_{LO} + f_{IF}$ and $2f_{LO} + f_{IF}$ on V_{GS} under applying 30GHz, 0dBm LO to the gate port and 100MHz optical IF signal at V_{DS} of 0.5V. The solid line indicates the primary photodetected power (f_{IF}) extracted from measured data at turn-off state. The internal conversion gain defined as the ratio of output frequency up-converted signal powers to the primary photodetected power is included and displayed to the right axis.

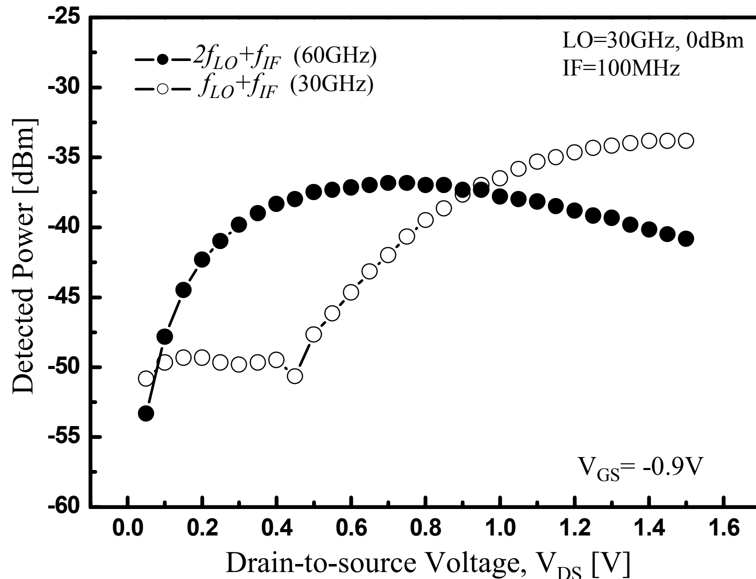

Figure 3-6. The dependence of optoelectronic mixing products at $f_{LO} + f_{IF}$ and $2f_{LO} + f_{IF}$ on V_{DS} under applying 30GHz, 0dBm LO to the gate port and 100MHz optical IF signal at V_{GS} of -0.9V.

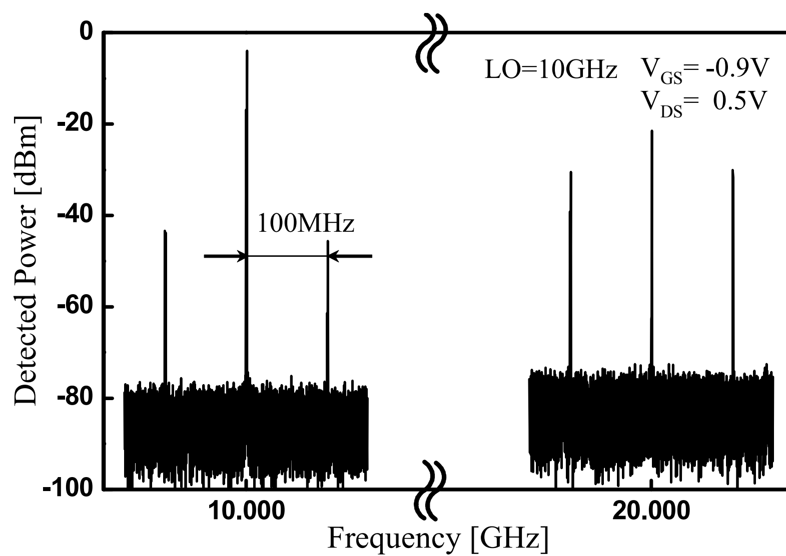

Figure 3-7. The output RF spectrum of InP HEMT subharmonic optoelectronic mixer with optimum bias conditions, V_{GS}=-0.9V and V_{DS}=-0.5V. It should be noted that LO frequency was set to be 10GHz in order to simultaneously view both fundamental and second harmonic optoelectronic mixing products.

3-2-4. Usable LO ranges

LO pumping power determines the conversion efficiency in a frequency mixer. Figure 3-8-(A) indicates the internal conversion gain of harmonic optoelectronic mixing products at $2f_{LO} + f_{IF}$ as a function of LO pumping power under optimum conditions. The required LO power to achieve positive internal conversion gain is about -7dBm. When the LO power is higher than 6dBm, it was observed that the internal conversion gain begins to saturate. LO frequency range of subharmonic optoelectronic mixer is also investigated for its uses at V-band. However, measurements were only taken from 50GHz to 60GHz because the millimeter-wave components in the experimental setup were not guaranteed above 60GHz. As observed in figure 3-8-(B), the InP HEMT subharmonic optoelectronic mixer exhibits wide LO frequency ranges while maintaining high internal conversion gain, which are expected to be sufficient for millimeter-wave operation.

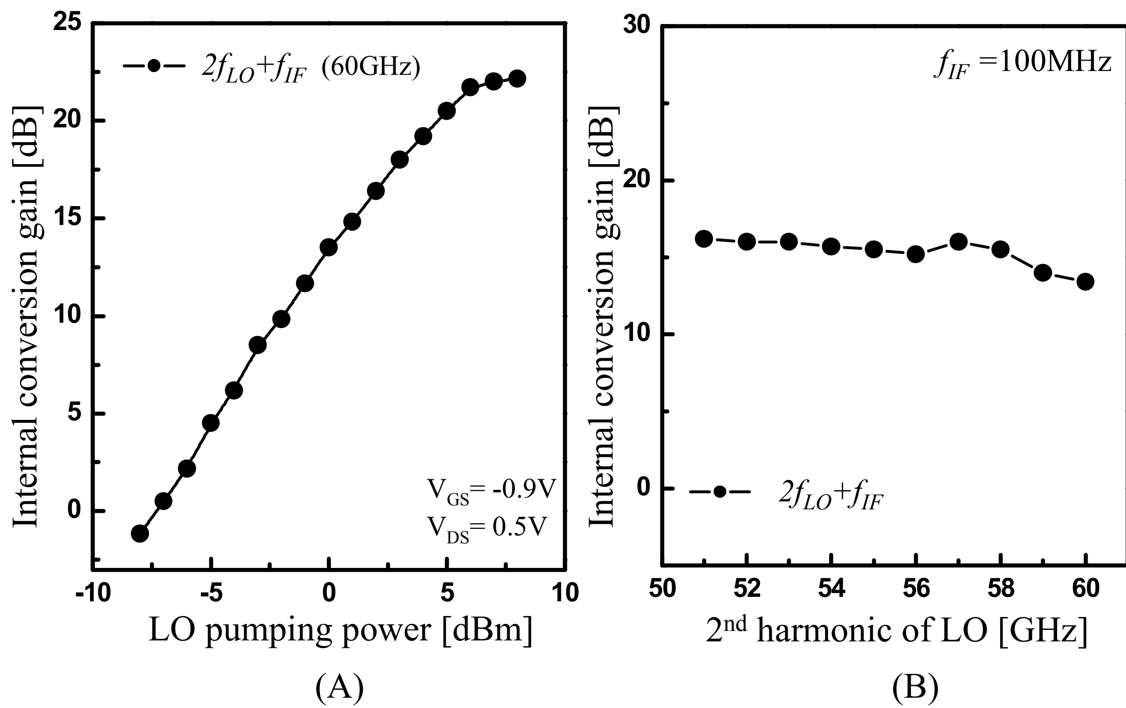

Figure 3-8. The dependence of internal conversion gain for InP HEMT subharmonic optoelectronic mixer on (A) LO pumping power and applied LO frequency

3-2-5. Nonlinear distortion characteristics

Fiber-optic/millimeter-wave wireless systems are currently finding the convergence with the previously deployed fiber-optic networks. Introducing subcarrier multiplexing (SCM) to these systems is one possible candidate because it gives an efficiency way to provide many diverse services to each subscriber, as well as make it possible to realize adaptive array antennas in wireless applications [16]. In addition, it has been reported that SCM is useful in the frequency sectorization schemes used for wireless cellular communication systems [17]. In employing SCM in fiber-optic/millimeter-wave systems, multi-channel IF signals are transmitted over optical fiber and simultaneously frequency up-converted to desired frequency bands. Since the frequency up-conversion process is done by the device intrinsic nonlinearities, intermodulation products (IMPs) between these two IF signals cannot be avoided. Especially, the third order IMP (IMP3) signals can be located in adjacent IF bands, which seriously degrade the system performance. For these reasons, nonlinear distortion characteristics of an InP subharmonic optoelectronic mixer are investigated utilizing the experimental setup illustrated in figure 3-9. In order to eliminate the nonlinearity of optical source, two DFB laser diodes with different wavelength were directly modulated with 99MHz and 101MHz, independently. In this configuration, the nonlinear distortion products are generated by a subharmonic optoelectronic mixer itself, but not the laser diodes. Because of high background noise levels in an external V-band harmonic mixer, the experiments were carried out in 20GHz band with 10GHz LO under the optimum bias conditions. Figure 3-10 shows the RF spectrum for frequency up-converted upper sideband signals using InP HEMT subharmonic optoelectronic mixer without low-noise amplification. It can be observed the IMP3

signals at $2f_{LO}+(2f_{IF1}-f_{IF2})$ and $2f_{LO}+(2f_{IF2}-f_{IF1})$ which are generated during harmonic optoelectronic mixing process. In order to determine spurious free dynamic range (SFDR) indicating power ranges where IMP3 are suppressed below noise level, the measurements were performed for the signal powers of $2f_{LO}+f_{IF2}$ and $2f_{LO}+(2f_{IF2}-f_{IF1})$, and noise levels under different IF powers. Because the RF spectrum analyzer gives the display noise level lower limit of -130dBm/Hz at 20GHz band, the low noise amplifier having the 17dB gain and 4dB noise figure was inserted after the output drain port to increase noise floor intentionally [18]. The noise level for InP HEMT subharmonic optoelectronic mixer was determined by subtracting the sum of amplifier gain and noise figure from the measured noise floor at RF spectrum analyzer. It is about -150dBm/Hz at 20GHz band. The experimental results for the SFDR measurements are shown in figure 3-11. It was obtained the SFDR of 94.5dB·$Hz^{2/3}$, which is high enough for the requirements of SCM links and wireless LAN systems.

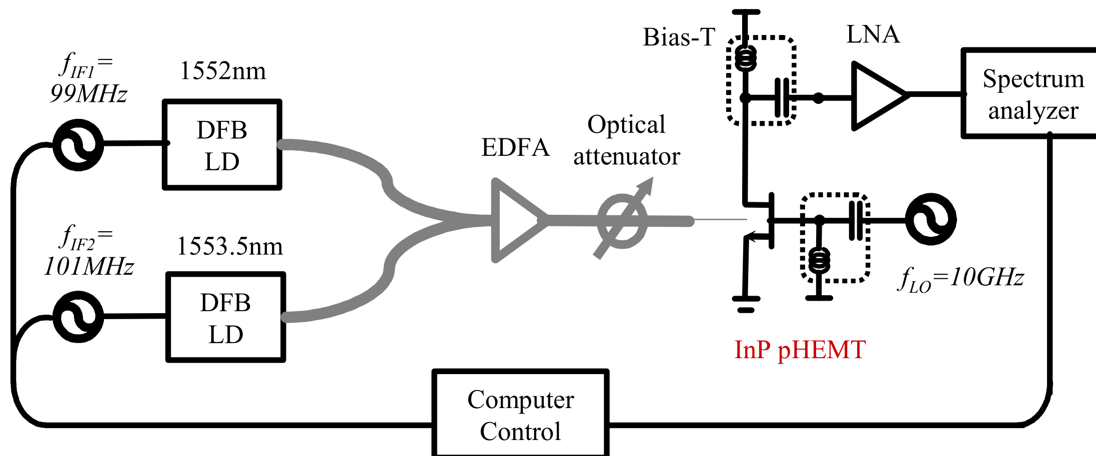

Figure 3-9. Experimental setup for the measurement of SFDR.

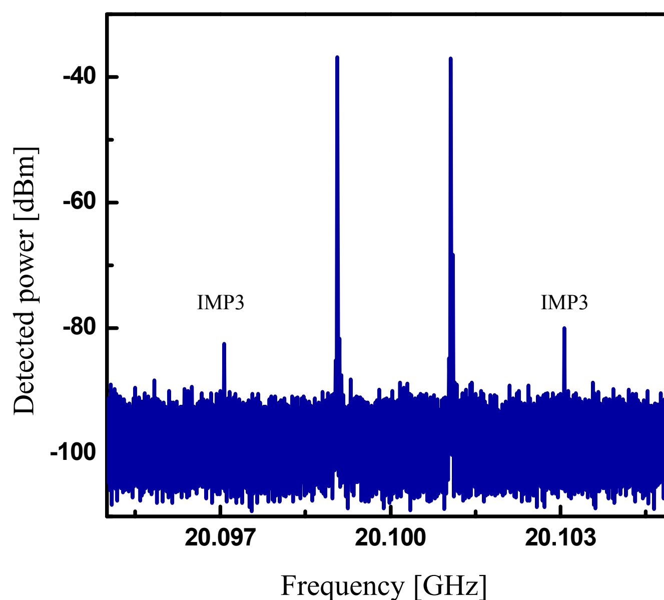

Figure 3-10. The measured output RF spectrum of InP HEMT subharmonic optoelectronic mixer. LO frequency and power are 10GHz and 0dBm. IMP3 indicates the third-order intermodulation product generated at harmonic optoelectronic mixing process

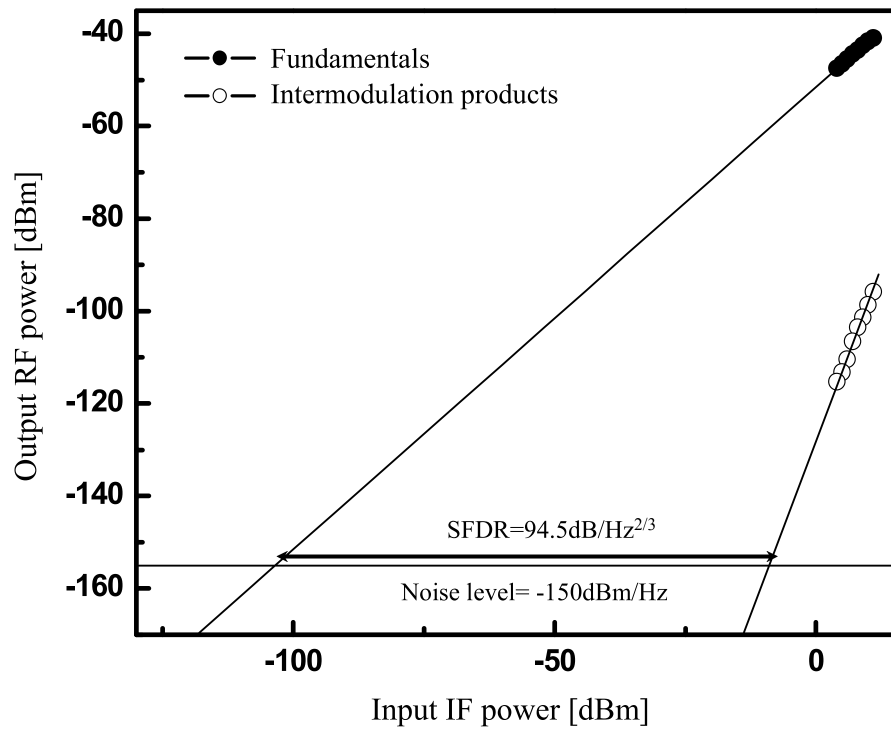

Figure 3-11. Spurious Free Dynamic Range (SFDR) measurements for InP HEMT subharmonic optoelectronic mixer at 20GHz band under V_{GS} of -0.9V and V_{DS} of 0.5V. LO frequency and power are 10GHz and 0dBm, optical IF frequencies are 99MHz (fIF1) and 101MHz (fIF2).

3-3. Fiber-optic/60GHz data transmission systems based on InP HEMT subharmonic optoelectronic mixers

In order to investigate the feasibility of using InP HEMT subharmonic optoelectronic mixer, broadband data transmission is demonstrated in fiber-optic/millimeter-wave system. Figure 3-12 describes the constructed remote up-conversion fiber-optic/60GHz broadband data transmission systems using InP HEMT subharmonic optoelectronic mixer. The DFB laser diode having the wavelength of 1552nm was directly modulated with 622Mbps nonreturn-to-zero (NRZ) pseudo-random bit sequence having the pattern length of 2^{15}-1. The baseband optical data signals were transmitted from central office to antenna base station over 30km single-mode fiber followed by EDFA amplification. At antenna base station, the optically transmitted data signals were frequency up-converted to 60GHz band using InP HEMT subharmonic optoelectronic mixer with the optimum bias conditions and 30GHz, 1dBm LO. The output signal at the drain port was amplified by a 17dB post-amplifier and radiated from a 60GHz horn antenna with 20dB gain. Figure 3-13 shows the 60GHz spectrum of frequency up-converted 622Mbps data measured at the output of the amplifier. After 3m transmission in 60GHz wireless link, the received signals are demodulated using direct detection technique with a Schottky diode at mobile terminal. After low-pass filtering, the recovered baseband signals were connected to the sampling oscilloscope or the error detector.

Clear eye opening for recovered 622Mbps data is observed as show in figure 3-14–(A). The fiber-optic/60GHz link performance was evaluated by measuring bit-error-rate (BER) as a function of incident optical power. Figure 3-14-(B) gives the experimental

results for BER characteristics of the constructed fiber-optic/60GHz data transmission systems. Error-free transmission (BER < 10^{-9}) was achieved when incident optical power is higher than 9dBm. The high required power for error-free transmission is mainly attributed to poor quantum efficiency in InP HEMT as mentioned previously. Comparing the BER characteristics of 30km fiber-optic links with those of back-to-back, there is no significant transmission penalty at identical incident optical power. The results advocate the fact that remote up-conversion systems are free from the dispersion induced transmission penalty because low frequency optical data/IF signals propagate through optical fiber. It would be possible to increase wireless transmission distance if higher power amplifier is utilized. The experimental demonstration gives me a proof that InP HEMT subharmonic optoelectronic mixer can be utilized in fiber-optic/60GHz downlink data transmission systems.

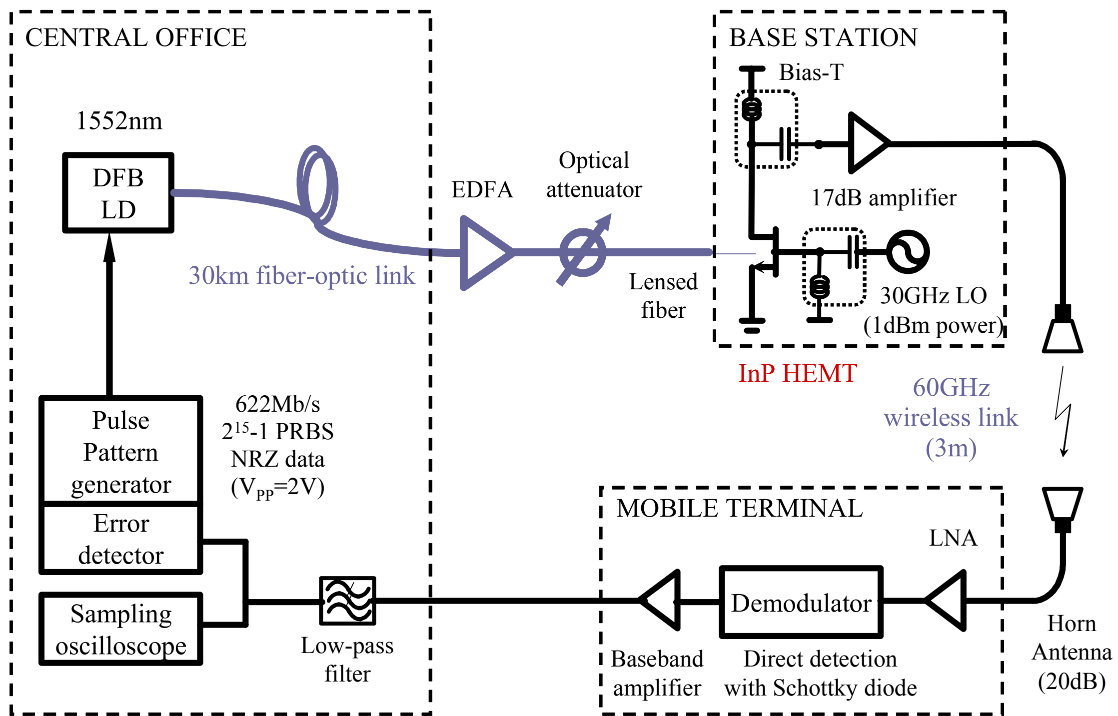

Figure 3-12. Fiber-optic/60GHz broadband data transmission system utilizing InP HEMT as a subharmonic optoelectronic mixer.

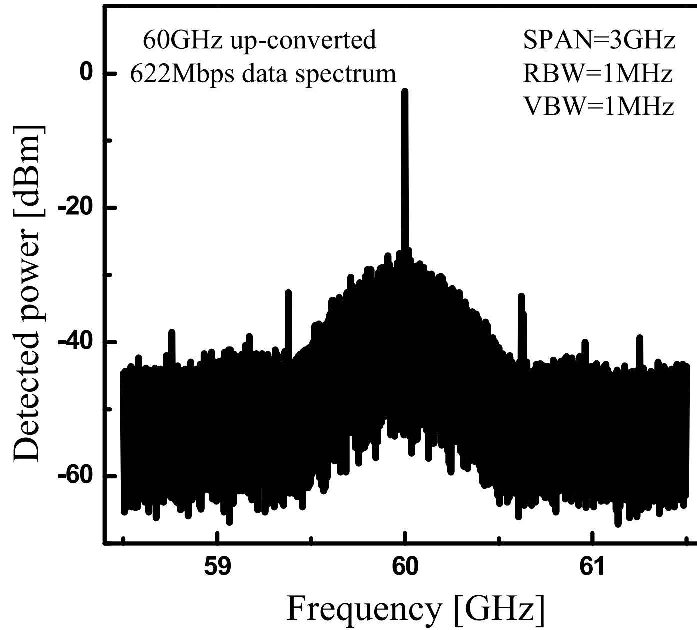

Figure 3-13. The measured 60GHz spectrum of frequency up-converted 622Mbps signal by InP HEMT subharmonic optoelectronic mixer.

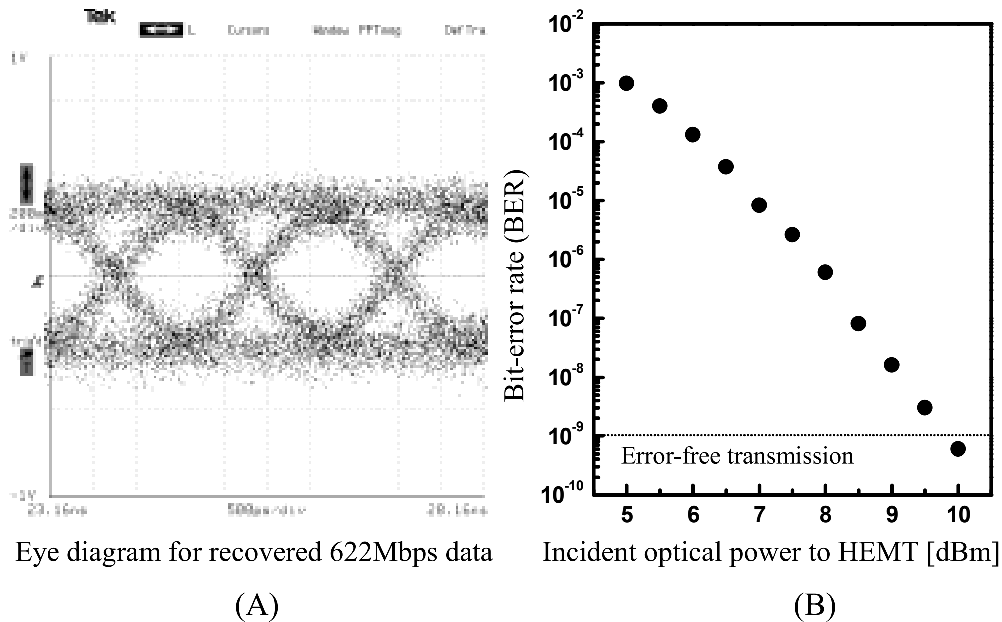

Figure 3-14. (A) Eye diagram for recovered 622Mbps data after transmission over 30km single-mode fiber and 3m free-space at 60GHz band. (B) Bit-error rate (BER) characteristics as a function of incident optical power to the InP HEMT. The actually absorbed optical power is estimated to be less than 2% of incident optical power.

3-4. Direct optical injection-locked oscillator

3-4-1. Motivation

As investigated in previous section in 3-3, optoelectronic mixers are useful devices for simplification of antenna base station architecture since they unify the functions of the photodetection and the frequency up-conversion in a single device. However, they essentially require phase-locked oscillators for the wireless data transmission adopting phase-modulation schemes such as phase-shift-keying (PSK) and quadrature amplitude modulations (QAM). As required LO frequency gets closer to millimeter-wave frequency bands, it impose many problems on antenna base station architecture in terms of cost and design complexity.

These requirements can be relaxed by introducing optically generated LO signals which are distributed to each antenna base station [19-21]. Optical data/IF signals having the different wavelength from optical LO signals are transmitted and remotely frequency up-converted into desired frequency bands with the help of optical LO signals arrived at antenna base stations. Nonlinear photodetection in photodiode [20] and cross-gain modulation in SOA [21] have been proposed for this frequency mixing function. These schemes provide many structural advantages including the elimination of high-frequency phase-locked oscillators in antenna base stations and the flexibility to previously deployed WDM networks [22]. Figure 3-15 shows the schematic illustration of the proposed WDM/radio-on-fiber (RoF) convergence networks using optically delivered LO separated from optical IF signals.

The major drawback in this approach is the low output power of LO signals limited by maximum output power of photodiode that converts received optical LO signals

into corresponding electrical LO signals. Although high levels of output power are typically required for efficient frequency mixing and RF radiation, the optically delivered LO schemes cannot afford to support them, to make matters worse, their output power strongly depends on optical transmission distance. To overcome this limitation, one proposed that photodetected optical LO signals are amplified and frequency-mixed with the photodetected data/IF signals using electrical mixers [22]. However, many RF components including amplifier, filter and frequency mixer are indispensable for this microwave signal processing, as a result, it increases the complexities of antenna base station architecture.

In order to utilize the optical LO signals with maintaining high output power, this dissertation work proposes the use of direct optical injection-locked oscillators for fiber-optic/millimeter-wave system application, which is briefly explained in section 3-1-4. They make the frequency and phase of free-running oscillator to be synchronized to those of modulated optical signal. Therefore, they greatly simplify the antenna base station architecture because any difficult phase-locking schemes such as phase-locked loop are not required. In addition, their output powers depend not on input optical signal power but on the free-running oscillator itself. With the help of them, it is possible to realize high-power and phase-locked oscillators with a simple architecture. In this section, the detailed characteristics of direct optical injection-locked oscillator based on InP HEMT are investigated. Useful features for fiber-optic/millimeter-wave system applications as well as the locking ranges of optical injection-locked oscillator are also presented. A fiber-optic/millimeter-wave phase-modulated data transmission system utilizing them incorporated with harmonic optoelectronic mixing is proposed and experimentally demonstrated in the section 3-5.

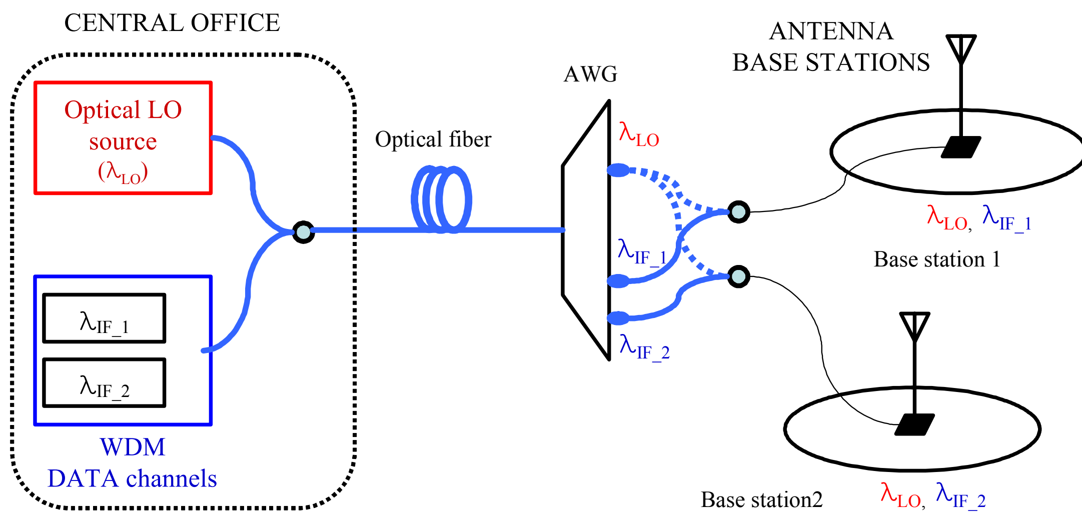

Figure 3-15. Proposed WDM/RoF link configuration using optical LO distribution separated from WDM data channels.

3-4-2. Characteristics of direct optical injection-locked oscillators

A 10GHz-band free-running oscillator based on single InP HEMT is schematically illustrated in figure 3-16. The drain signals were fed back to the gate electrode through narrow bandpass filter centered at 10.24GHz. The bias conditions were V_{GS} of -0.7V and V_{DS} of 1.2V. The output spectrum of free-running oscillator is given in figure 3-17-(A). It was found that the oscillation frequency of the free-running oscillator was very unstable and sensitive to environmental conditions. For direct optical injection-locking, high purity microwave signals from a frequency synthesizer directly modulated a DFB laser diode and the optical signals were illuminated to InP HEMT using lensed fiber. As the modulation frequency becomes closer to the oscillation frequency, a free-running oscillator is synchronized and phase-locked to optically modulated signals. In this condition, the oscillator exhibits suppressed phase-noise characteristics as well as high purity and stabilized oscillation, resulting in optical injection-locked oscillator as shown in figure 3-17-(B). The long-term stability of the optical injection-locked oscillator was found to be also very good. Further increasing optical modulation frequency makes the oscillator to be unlocked and the resulting spectrum is shown in figure 3-17-(C). Under this unlocked condition, many sidebands can be observed due to the frequency mixing of free-running oscillator signals and optically injected signals.

The locking range where a frequency deviation allows the locking process is an important parameter of optical injection-locked oscillators. If the phase-locking is broken, it is impossible to achieve stable and low-phase LO output signal, which deteriorates the phase-modulation data transmission quality. For this purpose, the locking ranges as a function of incident optical power to InP HEMT were measured for

fundamental oscillation frequency of 10.24GHz. According to Adler's equation [23], the locking range (Δf) for electrical injection-locked oscillator, is expressed as

$$\Delta f = \frac{f_{osc}}{Q_{ext}}\left(\frac{P_{inj}}{P_{osc}}\right)^{\frac{1}{2}} \tag{3-6}$$

where f_{osc} is the oscillation frequency, Q_{ext} is the external quality factor, P_{inj} is the injected power and P_{osc} is the oscillation power.

In the case of a direct optical injection-locked oscillator, P_{inj} corresponds to the photodetected power of optically-modulated signals. According to the equation (3-6), the locking range depends on the incident optical power to InP HEMT. As can be seen in the experimental results in figure 3-18, the locking range increases as incident optical power, which corresponds to the equation (3-6).

The phase-noise of optically injection-locked oscillator is much smaller than that of free-running oscillator as one can intuitively see the RF spectra shown in figure 3-17. In the free-running oscillator, the phase-noise is determined by the Q factor of bandpass filter and feedback loss. The experiment showed its phase-noise of -77.6dBc/Hz at 10kHz offset carrier, which is rather high and not suitable for phase-modulated data transmission. When an optical injection locking is applied, the phase-noise is suppressed to be about -98dBc/Hz at 10KHz offset carriers. These phase-noise characteristics are strong function of incident optical powers to the InP HEMT as described in the equation (3-6) and the results are given in figure 3-19. They increases as decreasing incident optical power, nevertheless, -82.33dBc/Hz at 10KHz offset can be obtained at 10dBm optical power. Compared to other reports about heterojunction phototransistors (HPTs), the phase-noise characteristics of optically injection-locked

oscillator versus incident optical power are relatively high. It is because that the actually absorbed optical power in InP HEMT is much lower than incident one.

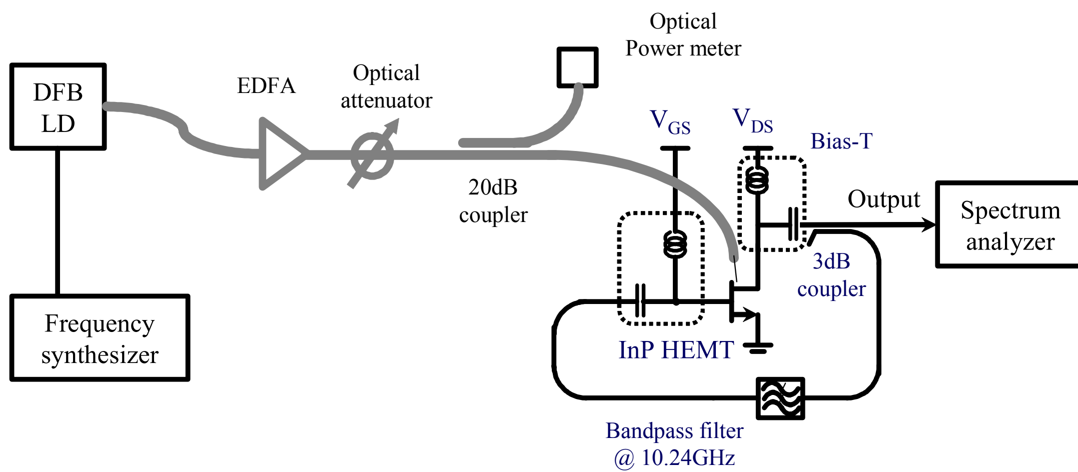

Figure 3-16. Experimental setup for direct optical injection-locking to 10GHz InP HEMT-based oscillator.

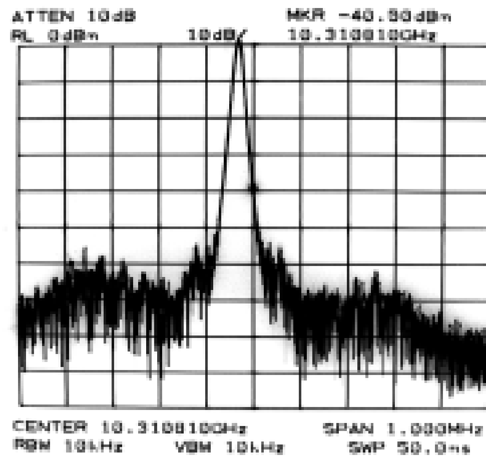

(A)

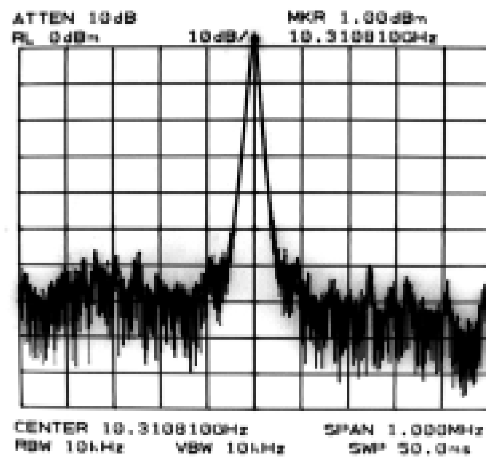

(B)

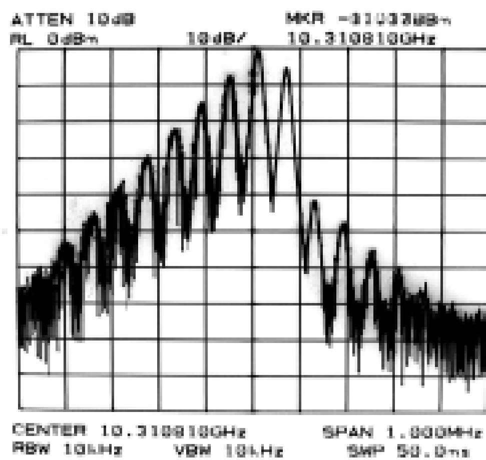

(C)

Figure 3-17. RF spectra of direct optical injection-locked oscillator based on InP HEMT (A) free-running (B) injection-locked (C) unlocked states.

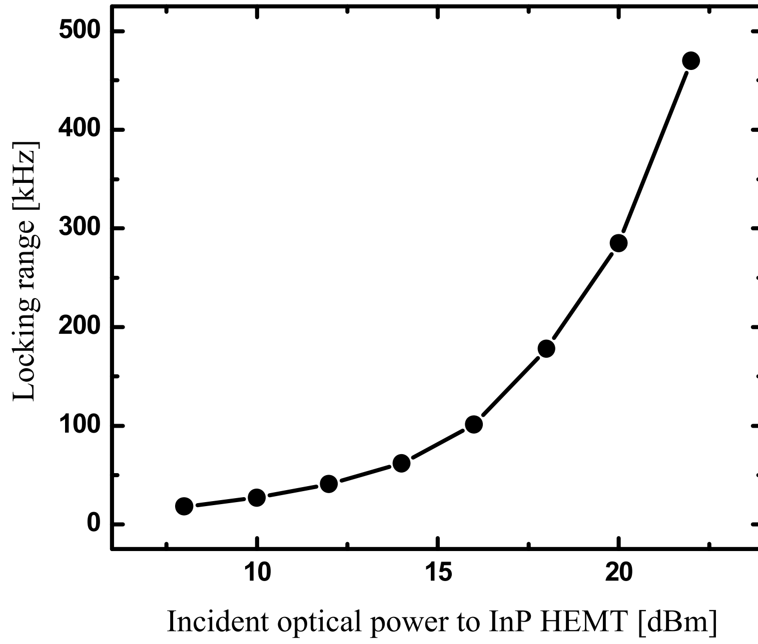

Figure 3-18. Locking ranges as a function of incident optical power.

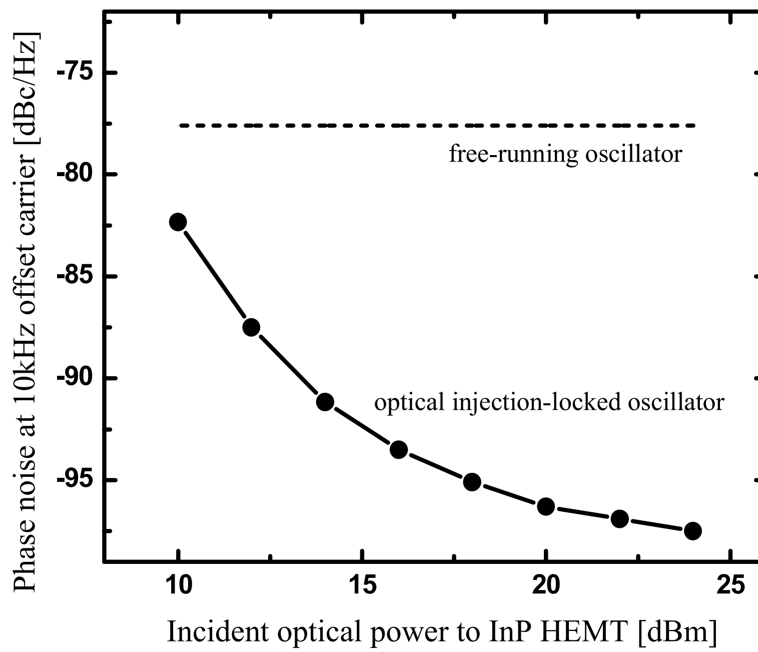

Figure 3-19. Phase-noise at 10kHz offset carrier as a function of incident optical power.

3-5. Fiber-optic/millimeter-wave data transmission systems based on optically controlled InP HEMT oscillators

3-5-1. Proposed scheme

As demonstrated in previous section, direct optically injection-locked oscillators are attractive in realizing high power and high-frequency phase-locked oscillators which are indispensable for phase-modulated data transmission in fiber-optic/millimeter-wave systems. If we desire to construct 30GHz wireless links, these approaches need 30GHz band free-running oscillators and 30GHz optical LO signals. Setting aside the difficulties in design of high-frequency oscillators, another serious limitation arises from the generation and transmission of high-frequency optical LO signals. As described in chapter 1, optical generations of high-frequency signals are not mature yet and their optical transmissions are severely affected by dispersion-induced carrier suppression and phase-noise degradation. These problems get worse if high-frequency optical LO signals are required in fiber-optic/millimeter-wave systems.

Furthermore, these schemes displayed in figure 3-15 require an additional optoelectronic mixer for the frequency mixing of optically transmitted data (IF) with the electrical output of injection-locked LO. In these configurations, the optical data signals are illuminated to optoelectronic mixers, while optical LO signals are injected to free-running oscillators. This spatial segregation between two optical signals increases the structural complexity in antenna base station architecture although one reported the use of WDM couplers [7].

In this section, a novel antenna base station architecture which is expected to solve

above-mentioned problems is proposed and experimentally demonstrated. It consists of a single InP HEMT and other passive components, nevertheless, it simultaneously performs the optical injection-locked oscillation and harmonic optoelectronic mixing functions. Utilizing it, 20Mbps 16QAM data transmission in fiber-optic/30GHz downlink system is successfully achieved.

Figure 3-20 schematically illustrates the proposed simple antenna base station architecture for fiber-optic/30GHz data transmission systems. A 10GHz free-running oscillator is first realized using simple feedback method described above and injection-locked by the optically delivered 10GHz LO signals transmitted from a central office. At the same time, optically transmitted data/IF signals with different wavelength are illuminated to the same InP HEMT and, as a results, harmonic frequency up-conversion to 30GHz band is achieved. The resulting RF spectrum measured at the output of oscillator is shown in the inset of figure 3-20. In this proposed scheme, the InP HEMT operates as an optically injection-locked oscillator and a harmonic optoelectronic mixer investigated in section 3-2. This phase-locked LO source makes it possible to achieve phase-modulated data transmission in wireless links. The output LO power depends not on the incident optical power but on the free-running oscillator itself as mentioned in previous section, therefore it allows to achieve high LO power independent of optical transmission distance. In addition, this scheme is fully compatible to WDM/RoF convergence networks shown in figure 3-15. Although, discrete components and hybrid connection are used for verifying the proposed scheme, an integrated approach based on InP MMIC technology should be equally applicable, providing one-chip integration (except radiation antenna) for simple antenna base station architecture.

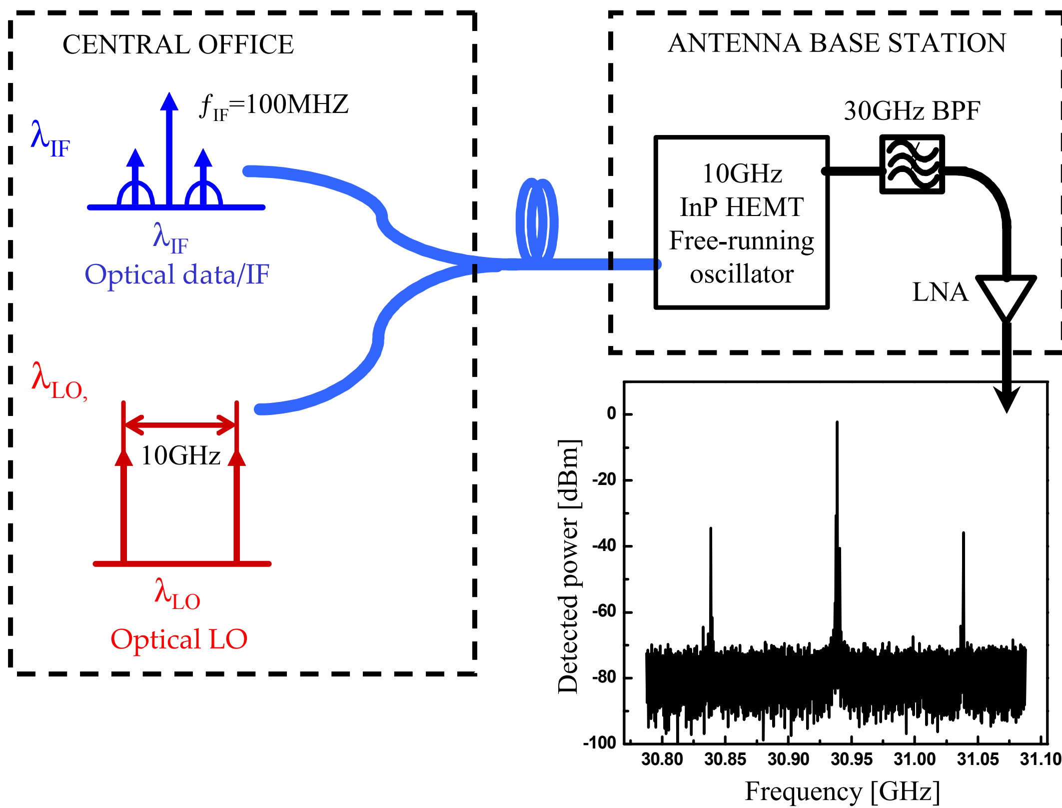

Figure 3-20. Proposed antenna base station architecture based on optically controlled InP HEMT oscillator.

3-5-2. Fiber-optic/30GHz data transmission demonstration

With extending the previous works described in section 3-4, the third harmonic characteristics of 10GHz optically injection-locked oscillator were utilized for 30GHz wireless applications. After optical injection-locking to 10GHz free-running oscillator using experimental setup shown in figure 3-16, 30GHz band signals from oscillator are observed after bandpass filtering. Figure 3-21 shows 30GHz band output RF spectra (3rd harmonic of oscillator) for (A) free-running, (B) optically injection-locked and (c) unlocked conditions. As observed fundamental locking RF spectra shown in figure 3-17, 3rd harmonic output of oscillator exhibit the similar characteristics excepting relatively low output LO power. The locking range and output LO power for 3rd harmonic of injection-locked oscillator is also investigated with varying incident optical powers shown in figure 3-22. The locking range for 3rd harmonics resembles that of fundamental oscillation frequency. The output power is independent of incident optical power to HEMT, which maintains the constant high output LO power even if the incident optical power is small.

For the phase-modulated data transmission in this radio-on-fiber links, the phase-noise characteristics for 3rd harmonic of optical injection-locked oscillator were measured and the results are shown in figure 3-23. It exhibits the phase noise of -83dBc/Hz at 10KHz offset and -101dBc/Hz at 100KHz offset, which is sufficient for phase-modulation scheme. With the help of these excellent low phase-noise characteristics in optically injection-locked oscillator, 20Mbps 16QAM data transmission is successfully demonstrated. Figure 3-24 shows the constructed fiber-optic/30GHz downlink data transmission systems based on the proposed antenna base

station architecture. The optical generations of LO signal were achieved by the directly modulated laser diode due to its simplicity. The 20Mbps 16QAM data with 100MHz IF from the output of HP E4432B signal generator was directly modulated to the other DFB-LD having 1553.5nm wavelength to produce optical data/IF signals. Under the optically injection-locked condition, these optical data/IF signals were simultaneously illuminated to the InP HEMT which performs the harmonic optoelectronic mixing of these data signals with the 3rd harmonics of injection-locked LO signal. And then, the frequency up-converted signals were filtered and amplified. The resulting RF spectrum including lower sideband 16QAM signals and 3rd harmonic of LO signal is shown in figure 3-25-(A). In practical wireless communication systems, these signals would be radiated to free space through the antenna.

In order to evaluate the link performance of the constructed fiber-optic/millimeter-wave system, these resulting signals are frequency down-converted to IF band whose spectrum is given in figure 3-25-(B). After additional low-pass filtering, error vector magnitudes (EVM) were measured using a HP 89441A vector signal analyzer. The EVM is defined as the ratio of average error magnitude to the normalized peak signal magnitude. Under the incident optical power of 9dBm, EVM is about 4.7% which corresponds to 24dB signal-to-noise ration (SNR). In this condition, the eye diagram and the constellation for recovered 16QAM data is shown in the inset of figure 3-26. Assuming these QAM signals are demodulated using an optimum receiver in Additive White Gaussian Noise (AWGN) channel, the 24dB SNR indicates the BER of 4.8×10^{-14} [24]. The BER characteristics as a function of SNR which can be varied with incident optical power is given in figure 3-27. During the experiments, it was found that the unlocked condition of InP HEMT oscillator induces the SNR below 17dB, which results

in severe distortion for recovering QAM data signals. Therefore, it can be said that the proposed scheme effectively advocates the phase-modulation data transmission, as well as simplifies antenna base station architecture in fiber-optic/millimeter-wave data transmission systems.

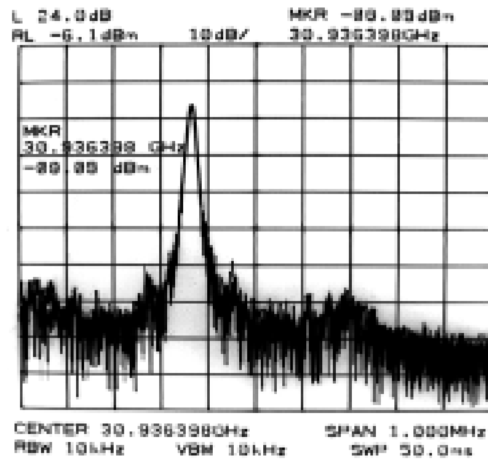

(A)

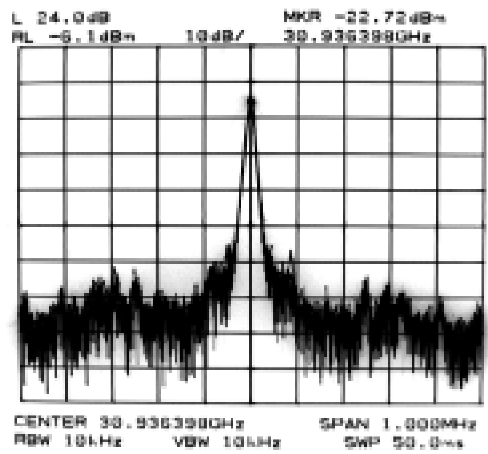

(B)

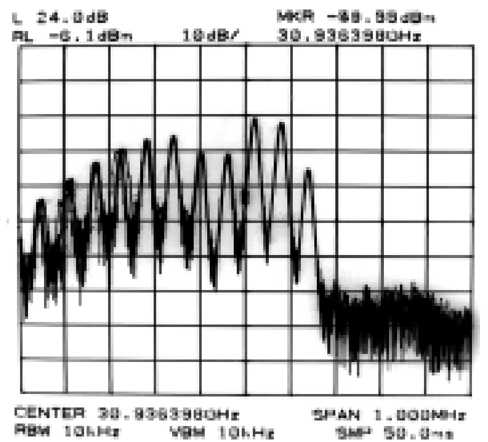

(C)

Figure 3-21. RF spectra of the third harmonic of 10GHz direct optical injection-locked oscillator based on InP HEMT (A) free-running (B) injection-locked (C) unlocked states.

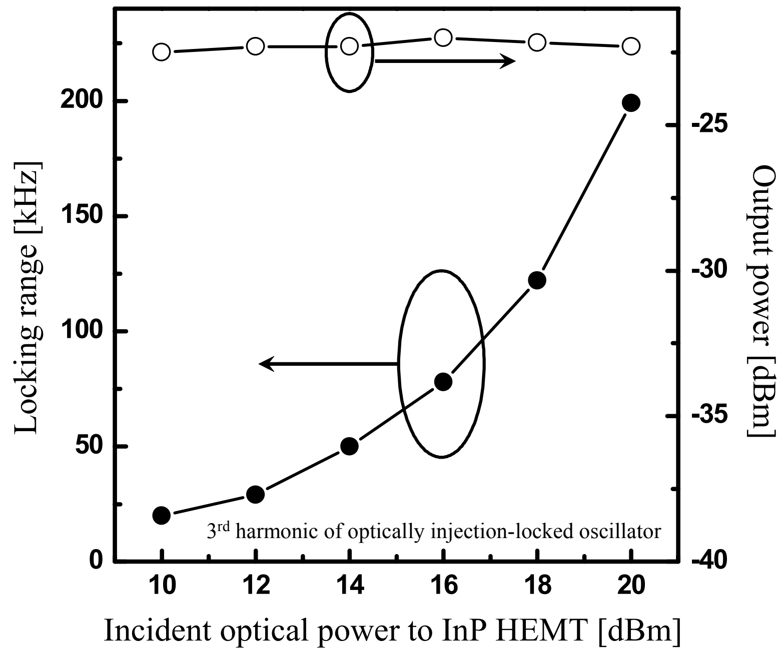

Figure 3-22. Measured locking ranges and output power for 3rd harmonic of optically injection-locked oscillator as a function of incident optical power.

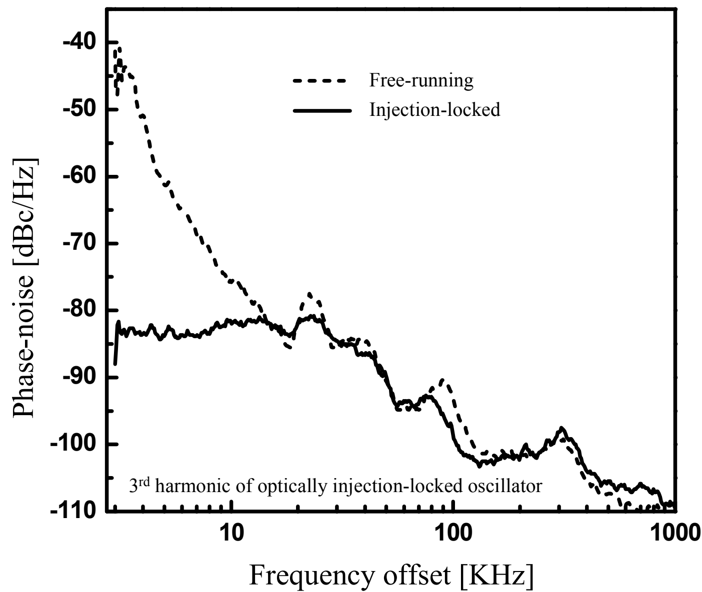

Figure 3-23. Phase-noise characteristics for 3rd harmonic of LO under free-running and injection-locked conditions.

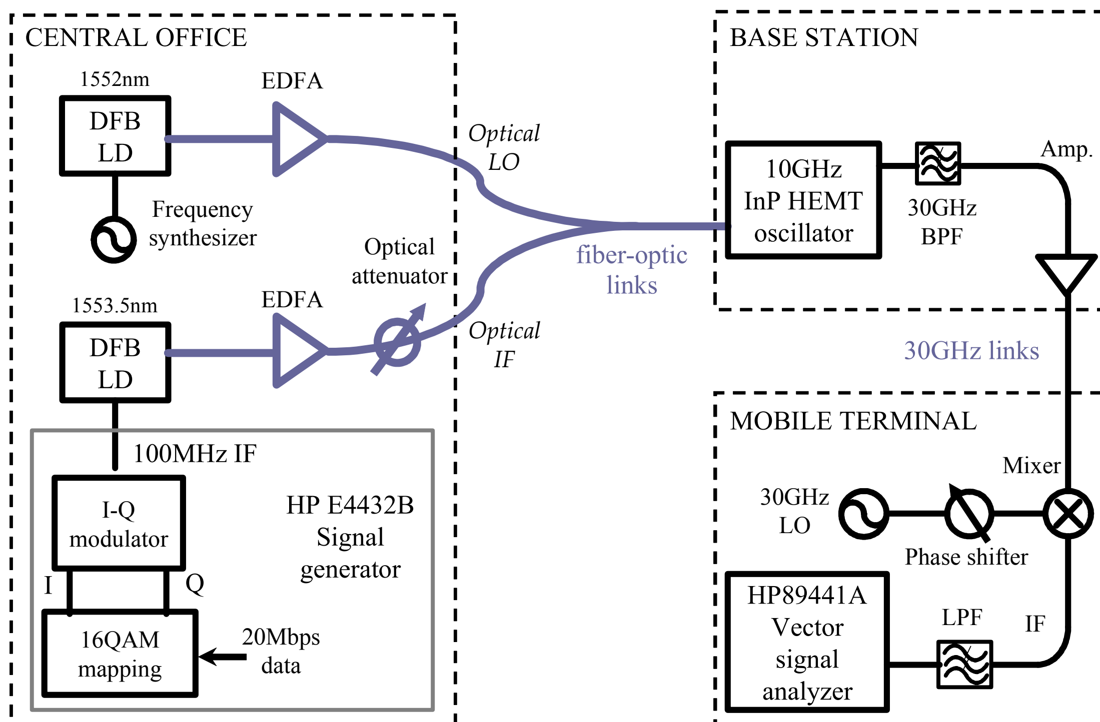

Figure 3-24. Proposed fiber-optic/millimeter-wave data transmission system based on optically controlled InP HEMT oscillator.

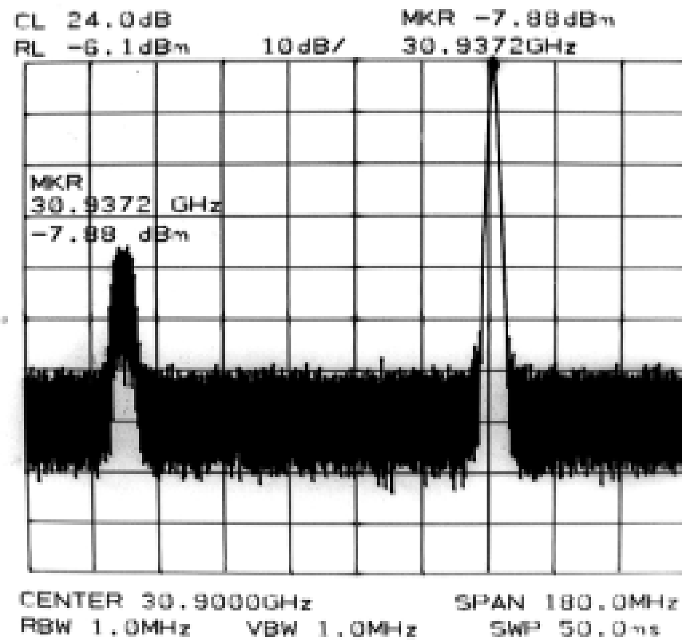

(A)

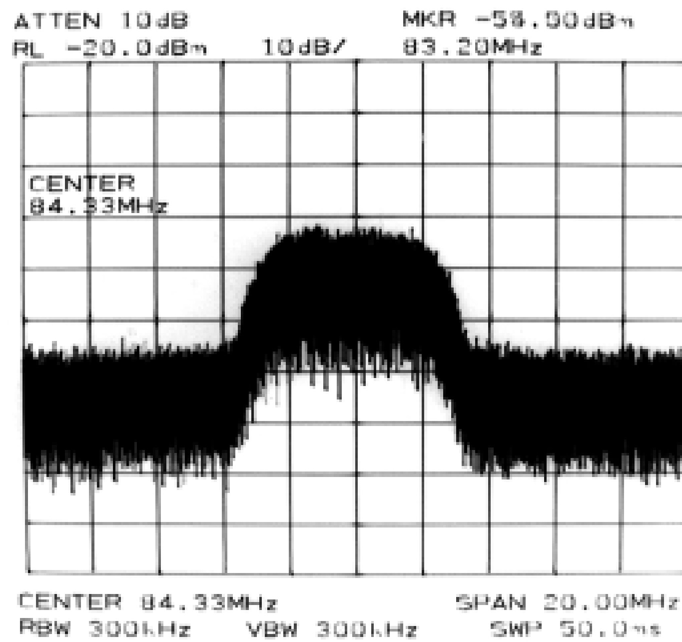

(B)

Figure 3-25. (A) 30GHz band RF spectrum including 3rd harmonic of injection-locked LO and frequency up-converted 16QAM data signal. (B) RF spectrum for frequency down-converted 16QAM signal at IF band.

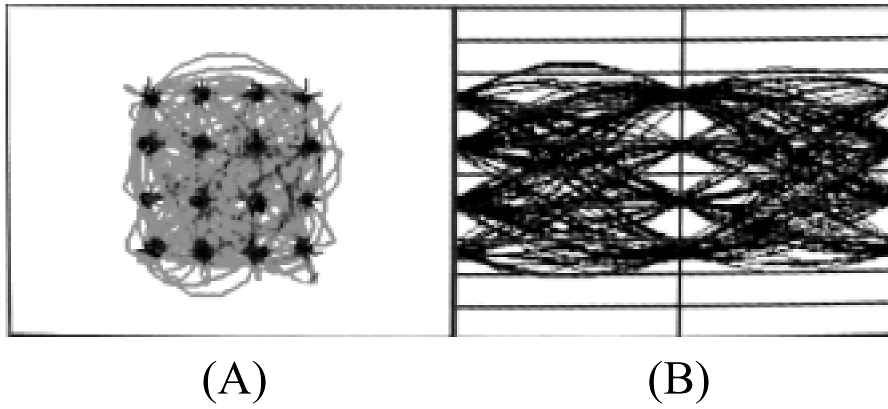

Figure 3-26. (A) constellation and (B) eye diagram for recovered 16QAM data signals

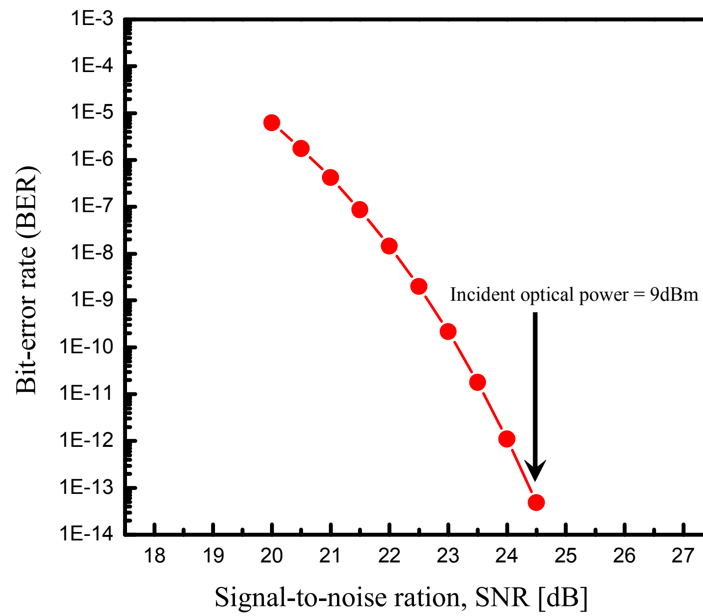

Figure 3-27. BERs as a function of signal-to-noise ratio for 16QAM data signal assuming optimum receiver and AWGN channel.

3-6. Conclusion

In this section, two possible applications of optically controlled InP HEMTs to fiber-optic/millimeter-wave systems were investigated. First, it was demonstrated that the phototransistors based on InP HEMT can be used as subharmonic optoelectronic mixers which offer the possibility to lower frequency LO for 60GHz frequency up-conversion. The performance was evaluated by introducing internal conversion gain which directly indicates the conversion efficiency of an optoelectronic mixer. The InP HEMT subharmonic optoelectronic mixers provide 17dB internal conversion gain at 60GHz band. The other important parameters indicating mixer performances, usable LO ranges and nonlinear distortion characteristics are also investigated. In order to demonstrate their feasibility, 622Mbps data transmission was achieved in constructed fiber-optic/60GHz downlink data transmission system.

Direct optical injection-locked oscillators are the other attractive application to fiber-optic/millimeter-wave systems. They provide high power and low phase LO source which are essential for phase-modulated data transmission in these systems. After a 10GHz band oscillator was realized using a single InP HEMT and the other passive components, the optical injection-locking processes were investigated. The phase-noise of about -95dBc at 10KHz offset and the locking range of 220kHz were obtained, which is sufficient to transmit phase-modulated data. Incorporating the optical injection-locked oscillation with the harmonic optoelectronic mixing characteristics, a novel antenna base station architecture was proposed for fiber-optic/millimeter-wave downlink systems. It is possible to simultaneously achieve the optically injection-locked oscillation and harmonic optoelectronic mixing in the

optically controlled InP HEMT oscillator. For its practical implementation, 20Mbps 16QAM data transmission in the constructed fiber-optic/30GHz downlink data transmission systems was demonstrated. This proposed single InP HEMT approach are expected to provide simple antenna base station architecture in fiber-optic/millimeter-wave systems that allow phase-modulated data transmission.

References

[1] A. J. Seeds and A. A. de Salles, "Optical control of microwave semiconductor devices," *IEEE Trans. Microwave Theory Tech.*, vol. 38, no. 5, pp. 577, May 1990.

[2] Yan Han and B. Jalali, "Photonic time-stretched analog-to-digital converter: fundamental concepts and practical considerations," *J. Lightwave Technol.*, vol. 21, no. 12, pp. 3085, Dec. 2003.

[3] A. Paolella and P. R. Herczfeld, "Optical control of a GaAs MMIC transmitt/receive module," *IEEE MTT-S Int. Microwave. Symp. Tech. Digest*, pp.959, May 1988.

[4] R. N. Simons, "Microwave performance of an optically controlled AlGaAs/GaAs high electron mobility transistor and GaAs MESFET," *IEEE Trans. Microwave Theory Tech.*, vol. 35, no. 12, pp. 1444, Dec. 1987.

[5] C. Rauscher, L. Goldberg and S. Yurek, "GaAs FET demodulator and down-converter for optical-microwave links," *Electronic Letters*, vol. 22, no. 13, pp. 705, Jun. 1986.

[6] H. Kamitsuna and H. Ogawa, "Monolithic image-rejection optoelectronic up-converters that employ the MMIC process," *IEEE Trans. Microwave Theory Tech.*, vol. 41, no. 12, pp. 2323, Dec. 1993.

[7] J. Lasri, A. Bilenca, G. Eisenstein and D. Ritter, "Optoelectronic mixing, modulation and injection-locking in millimeter-wave self-oscillating InP/InGaAs heterojunction bipolar photo transistors – single and dual transistor configurations," *IEEE Trans. Microwave Theory Tech.*, vol. 49, no. 10, pp. 1934, Oct. 2001.

[8] M. Muller, S. Withitsoonthorn, M. Roet, J.-L. Benchimol and C. Gonzales, "Millimeter-wave InP/InGaAs photo-HBT and its applications to optoelectronic integrated circuits," *IEICE Trans. Electron.*, vol.E86-C, no. 7, pp. 1299, Jul. 2003.

[9] C.-S. Choi, H.-S. Kang, W.-Y. Choi, D.-H. Kim and K.-S. Seo, "Phototransistors based on InP HEMTs and their applications to millimeter-wave radio-on-fiber systems," *IEEE Trans. Microwave Theory Tech.*, vol. 53, no. 1, Jan. 2004.

[10] H. J. Sun, R. J. Gutmann and J. M. Borrego, "Optical tuning in GaAs MESFET oscillators," *IEEE MTT-S Int. Microwave. Symp. Tech. Digest*, pp.40, Jun. 1981

[11] D. Yang, P. Bhattacharya, R. Lai, T. Brock and A. Paolella, "Optical control and injection locking of monolithically integrated InGaAs/InAlAs MODFET oscillators,"

IEEE Trans. Electron Devices, vol. 42, no. 1, pp. 31, Jan. 1995.

[12] D. S. Shin, G. L. Li, C. K. Sun, S. A. Pappert, K. K. Loi, W. S. C. Chang and P. K. L. Yu, "Optoelectronic RF signal mixing using an electroabsorption waveguide as an integrated photodetector/mixer," *IEEE Photon. Technol. Lett.*, vol. 12, no. 2, pp. 193, Feb. 2000.

[13] G. Jaro and T. Berceli, "A new high-efficiency optical-microwave mixing approach," *J. Lightwave Technol.*, vol. 21, no. 12, pp. 3078, Dec. 2003

[14] A. Paelella, S. Malone, T. Berceli and P. R. Herczfeld, "MMIC compatible lightwave-microwave mixing technique," *IEEE Trans. Microwave Theory Tech.*, vol. 43, no. 3, pp. 518, Mar. 1995.

[15] S. A. Mass, *Microwave Mixers*, Artech House, 1993.

[16] O. Shibata, I. Seto, S. Obayashi and H. Shoki, "Optical SCM transmission multiplexing IF and locak signals for adaptive array," *IEEE Antenna Propagat. Symp*. P. 218, Jul. 2001.

[17] R. B. Waterhouse, D. Novak, A. Nirmalathas and C. Lim, "Broadband printed sectorized coverage antennas for millimeter-wave wireless applications," *IEEE Trans. Antenna Propagat.*, vol. 50, no. 1, pp. 12, Jan. 2002.

[18] Jun-Hyuk Seo, Young-Kwang Seo and Woo-Young Choi, "Spurious-free dynamic range characteristics of the photonic up-converter based on semiconductor optical amplifier," *IEEE Photon. Technol. Lett.*, vol. 15, no. 11, pp. 1591, Nov. 2003.

[19] X. Wang, N. J. Gomes, L. Gomez-Rojas, P. A. Davies and D. Wake, "Indirect optically injection-locked oscillator for millimeter-wave communication system," *IEEE Trans. Microwave Theory Tech.*, vol. 48, no. 12, pp. 2596, Dec. 2000.

[20] M. Tsuchiya and T. Hoshida, "Nonlinear photodetection scheme and its system applications to fiber-optic millimeter-wave downlinks," *IEEE Trans. Microwave Theory Tech.*, vol. 47, no. 7, pp. 1342, Jul. 1999.

[21] Young-Kwang Seo, Chang-Soon Choi and Woo-Young Choi, "All-optical signal up-conversion for radio-on-fiber applications using cross-gain modulation in semiconductor optical amplifier," *IEEE Photon. Technol. Lett.*, vol. 14, no. 10, pp. 1448, Oct. 2002.

[22] C. Lim, A. Nirmalathas, M. Attygalle, D. Novak and R. Waterhouse, "On the merging of millimeter-wave fiber-radio backbone with 25GHz WDM ring networks," *J.*

Lightwave Techonl., vol. 21, no. 10, pp. 2203, Oct. 2003.

[23] R. Adler, "A study of locking phenomena in oscillators," *Proc. IEEE*, vol. 61, no. 10, pp. 1380, 1973.

[24] J. G. Proakis, *Digital communications*, McGraw-hill, 2001

Chapter 4

Phototransistors based on InP HBTs and their applications to gigabit data transmission links

4-1. Introduction

4-1-1. InP HBT for optoelectronic MMIC

The Heterojunction Bipolar Transistor (HBT) is basically a bipolar junction transistor (BJT) with the exception that emitter material has larger bandgap than base material. Introducing this heterojunction concept to BJT allows the design of device to be free from conventional BJT design limitations. The maximum DC current gain of HBT is given by [1]

$$\beta_{\max} = \frac{N_{de}}{N_{ab}} \cdot \frac{v_{nb}}{v_{pe}} \exp\left(\frac{\Delta E_V}{kT}\right), \quad (4\text{-}1)$$

where N_{de} is the donor concentration in emitter, N_{ab} is the acceptor concentration in base, v_{nb} is mean velocity of electrons in base, v_{pe} is the mean velocity of holes in emitter and ΔE_V is the valence band discontinuity between emitter and base.

In homojunction BJT where ΔE_V is zero, the only way to obtain high current gain is to increase the ratio of emitter doping concentration to base doping. This lightly doped thin base layer exhibits high base resistance and highly doped emitter region increases emitter-base junction capacitance, both severely limits the high frequency performance. On the other hands, the heterojunction between emitter and base layers provides the high ΔE_V. For example, InP/InGaAs heterojunction used in this work gives the ΔE_V of about 0.34eV which is many times of kT. As a result, high current gain can be achieved almost regardless of the doping ratio. Without adversely affecting HBT performance, low doped emitter and highly doped base could be realized to reduce base-emitter junction capacitance and base resistance, respectively, leading to high frequency performance. In addition to this merit, HBT has a number of structural advantages over BJT: (1) higher Early voltage due to high base doping; (2) high electron mobility in base layer; (3) reduced parasitic capacitance owing to semi-insulating substrate.

The first type of HBT utilized AlGaAs/GaAs material system. A number of different circuit applications have been demonstrated using these GaAs-based HBT technologies, presently they are most mature HBT technologies and fabricated in large volume for commercial RF applications. For the low power and high-speed applications, InP-based HBT technologies have emerged as a viable alternative to GaAs-based HBT. Lower bandgap of InGaAs decreases turn-on voltage thus lessens power dissipations and higher carrier velocity in InGaAs base layer gives the shorter transit time in base-collector space-charge layer, which gives rise to high frequency performance. They also offer the phototransistor operation to 1.55μm lightwave, which is attributed to the photoabsorption in InGaAs layers and amplification by BJT operation. Compared to

phototransistors based on InP HEMT, an InP HBT has thicker photoabsorption layer, which offers high optical responsivity. Owing to their excellent photonic and RF characteristics, a lot of works have devoted to the developments of optoelectronic MMIC using InP HBTs [2-4]. This dissertation work shows that InP HBTs have their own structural advantages over InP HEMT as phototransistors and gives the possible applications to fiber-optic/millimeter-wave data transmission systems. After briefly introducing the photodetection mechanism in InP HBT, the experimental results on the photodetection and optoelectronic mixing characteristics will be provided. With the help of their wide photonic bandwidth that cannot be obtained in InP HEMTs, gigabit transmission in both fiber-optic link and 60GHz link is experimentally demonstrated.

4-1-2. InP/InGaAs HBT used in this work

Figure 4-1 schematically illustrates the InP/$In_{0.53}Ga_{0.47}As$ HBT[3] used in this work. The epitaxial layers consist of, from top to bottom, 100nm n+ $In_{0.53}Ga_{0.47}As$ emitter capping layer, 50nm n+ InP emitter grading layer, 150nm n emitter layer, 5nm undoped $In_{0.53}Ga_{0.47}As$ spacer layer, 50nm p+ $In_{0.53}Ga_{0.47}As$ base layer, 450nm n- $In_{0.53}Ga_{0.47}As$ collector layer and 500nm n+ subcollector layer. Figure 4-2 shows the simulated band diagram for the InP/InGaAs HBT under applying the collector-to-emitter voltage (V_{CE}) of 1V.

It can be seen that the HBT has the large valence band discontinuity at InP/ $In_{0.53}Ga_{0.47}As$ heterointerface, which is the most distinct feature of HBT compared with BJT. It effectively suppresses the hole injection from base layer to emitter region, resulting in improved the current gain of HBT as described in the equation (4-1). The emitter layer can be either InP material or InAlAs material, both are lattice-matched to $In_{0.53}Ga_{0.47}As$ base layer. In contrast with the InP HEMT utilizing $In_{0.52}Al_{0.48}As$ as large bandgap material, InP material is generally preferred to emitter material of the HBT. It is because the large valence band discontinuity (ΔE_V) is required in InP HBT to block hole diffusion from base to emitter, therefore, InP with ΔE_V=0.34eV is more suitable than $In_{0.52}Al_{0.48}As$ with ΔE_V=0.19eV for emitter material for HBT. On the contrary, InP HEMT needs large conduction band discontinuity to obtain high density 2DEG as explained in chapter 2. Therefore, InP material was used as emitter material of the fabricated InP HBT.

Undoped spacer layer was used as "setback layer" in order to suppress undesirable

[3] The InP HBTs were fabricated by Dr. Hong-Seung Kim and Dr. Eun-Soo Nam in Basic Research Lab, Electronics and Telecommunications Research Institute (ETRI), Daejun, Korea.

device operation caused by conduction band spike at emitter-base heterointerface. It cannot fully eliminate the conduction band spike but makes it electrically less active. Reference [5] gives the influence of conduction band spike on the device characteristics and the epitaxial layer design for reducing it.

According to base-collector junctions, InP-based HBTs are classified into two groups. Single heterojuction bipolar transistor (SHBT) refers to those where only base-emitter junction is heterojunction. If both base-emitter and base-collector junctions are heterojunction, it is double heterojunction bipolar transistor (DHBT). To decide whether a homojunction or a heterojunction is used in base-collector layer accompanies with its structural advantages on electrical and photonic characteristics. SHBT provides not only simple fabrication process and but also higher frequency performance than DHBT. However, small Early voltage due to the low bandgap of collector layer is a crucial problem, which causes large output conductance and low breakdown voltage. It can be overcome by introducing DHBT structure, thus DHBTs are preferred to high-voltage applications. From the standpoint of photonic characteristics, the main advantage of SHBT is high optical responsivity attributed to thick $In_{0.53}Ga_{0.47}As$ absorption layers. Unfortunately, this thick photoabsorption layers extended from base to collector allows the photogenerated holes to drift toward collector layer, leading to speed limitation in photodetection process. DHBT is the best alternative because the photogenerated holes are blocked by high bandgap InP collector layer. However, it inherently has low optical responsivity because optical absorption only occurs in thin base layer. In this work, InP/InGaAs HBT having single heterojunction is utilized as a phototransistor to obtain high responsivity.

Because collector layer is lightly doped to obtain high Early voltage, highly doped

n+ $In_{0.53}Ga_{0.47}As$ subcollector layer is positioned between the collector and the contact metal for suppressing parasitic collector resistance and ensuring low contact resistance. If one desire to apply backside illumination to avoid making optical window onto HBT, optically transparent large bandgap InP subcollector should be used, which efficiently delivers optical signals into base-collector depletion region without optical absorption loss. Unfortunately, it deteriorates the high frequency performance because of high contact resistance at InP subcollector layer, therefore, n+ $In_{0.53}Ga_{0.47}As$ subcollector was employed in the HBT and top-side illumination onto base layer was used.

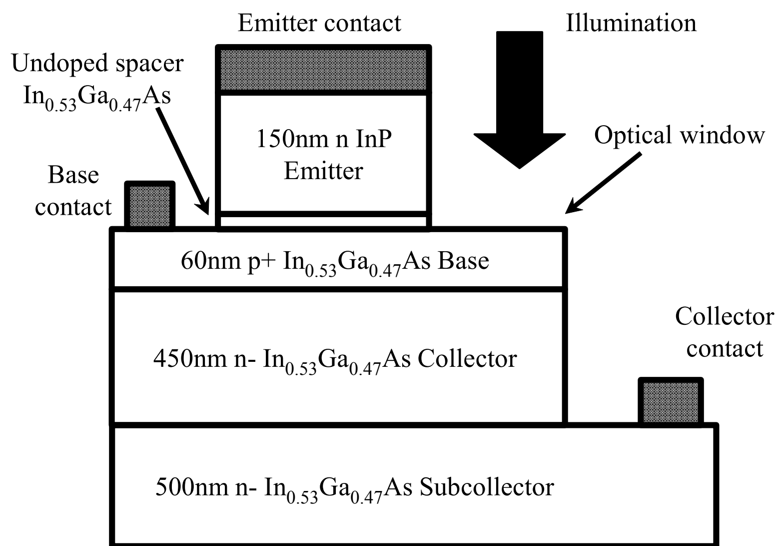

Figure 4-1. The schematic cross-section of fabricated InP/InGaAs SHBT. The optical window exists on the base layer.

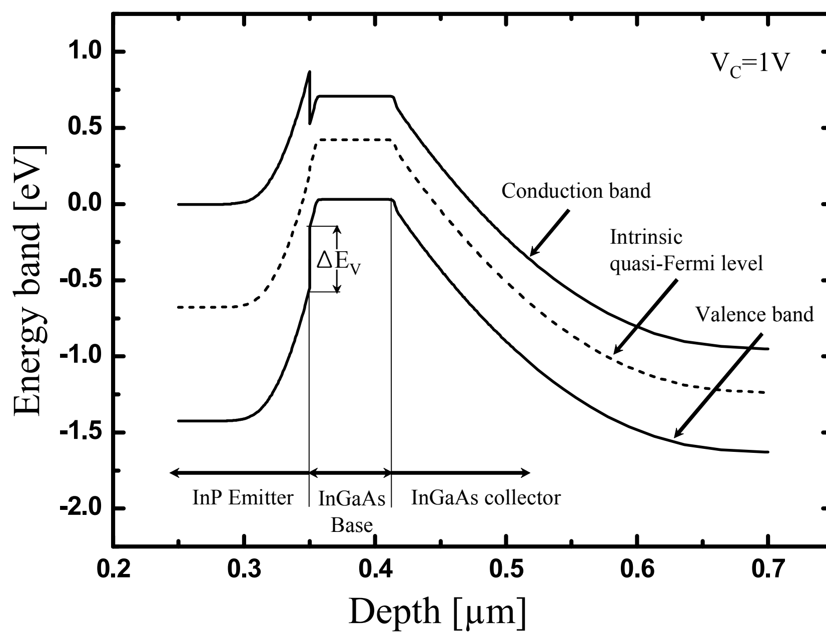

Figure 4-2. Simulated energy band diagram for the $InP/In_{0.53}Ga_{0.47}As$ HBT at the collector-to-emitter voltage (V_{CE}) of 1V.

4-1-3. Device characteristics of InP/InGaAs HBT

The fabricated InP/InGaAs HBT has the emitter size of 2×10μm^2. Figure 4-3 shows the dependence of collector-current (I_C) and base-current (I_B) on the base-emitter voltage (V_{BE}) indicating the gummel plot of the fabricated InP HBT. Current gains as high as 134 were obtained at particularly high I_B. After the I_C-V_{BE} characteristic was numerically fitted, it was obtained that the ideality factor (n_C) of I_C is equal to 1.18. The reason that n_C is slightly higher than 1 is the thermionic field emission of electrons tunneling from emitter to base [6]. The ideality factor (n_B) for I_B is 1.71 which is higher than n_C. Considering emitter geometry, both surface recombination currents and space-charge recombination current are thought to contribute the overall base current of HBT [6].

Figure 4-4 shows the common-emitter I_C-V_{CE} characteristics of the InP HBT with increasing I_B from 0μA to 150μA with the step of 50μA. The fabricated InP HBT has the low offset voltage of 0.3V and the common emitter breakdown voltage of about 1.8V. This low breakdown voltage is a severe problem in SHBT as described in section 4-1.

Microwave characteristics of the fabricated InP HBT are also investigated by measuring f_T and f_{max} as did in section 2-2-2. Figure 4-5 shows the dependence of f_T and f_{max} on I_C. The maximum f_T and f_{max} are 90GHz and 75GHz, respectively. The slightly decreased f_T at high I_C can be explained by emitter-crowding effect [6]. It should be noted that the maximum operation frequencies of HBT is lower than those of InP HEMT, which is so unfortunate for millimeter-wave applications investigated in this work.

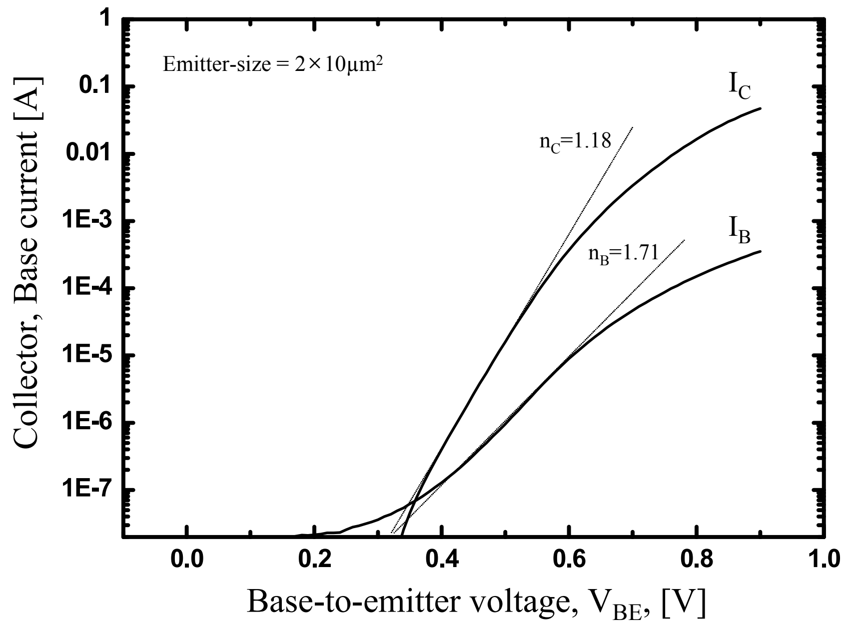

Figure 4-3. Gummel plots for the fabricated InP HBT

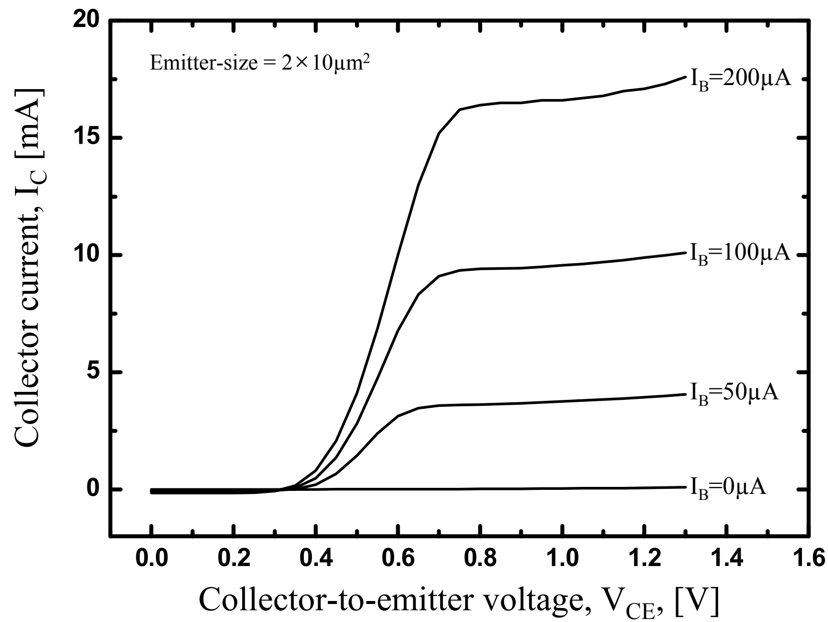

Figure 4-4. Common-emitter I_C-V_{CE} characteristics of the InP HBT with increasing I_B from 0μA to 150μA with the step of 50μA.

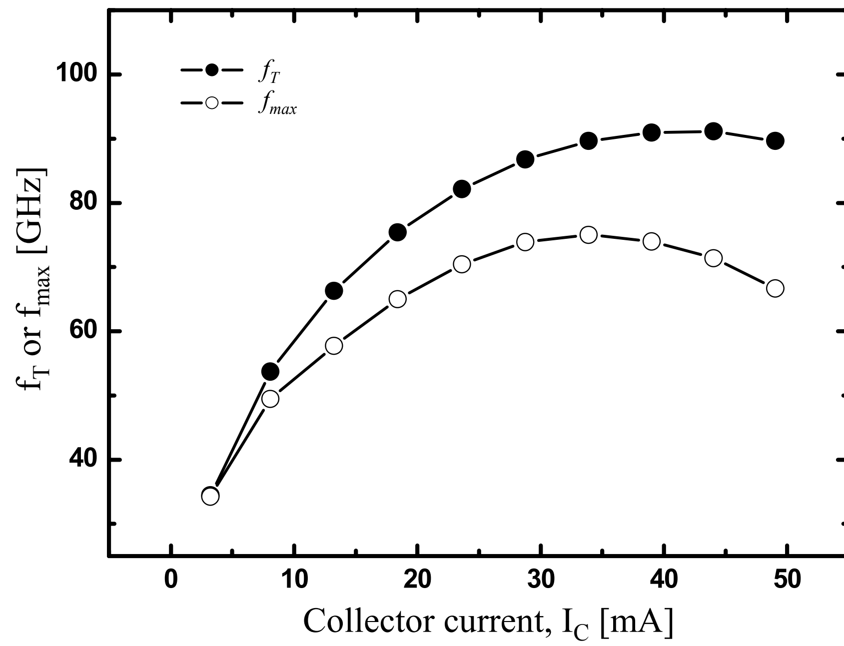

Figure 4-5. The dependence of f_C and f_{max} of the InP HBT on the collector current (I_C). V_{CE} is set to be 1V.

4-2. Experimental setup

The experimental setup for InP HBT is similar to that of InP HEMT depicted in figure 2-3 excepting illumination method. Because of thick InGaAs subcollector layer as described previously, top-side illumination onto the HBT was applied. The layout of the fabricated HBT is given in figure 4-6. It allows only 2μm diameter optical window where base layer is not blocked by contact and pad metals. For efficient optical coupling, a lensed fiber with minimum beam diameter of 2.5μm was used.

The absorption coefficient for InGaAs is about $10^4 cm^{-1}$ at 1.55μm lightwave. It implies that the thickness of photoabsorption layer in HBT (1.01μm) gives the maximum quantum efficiency of 65%. The misalignment of lensed fiber and the surface reflection are major origin for an optical coupling loss in HBT.

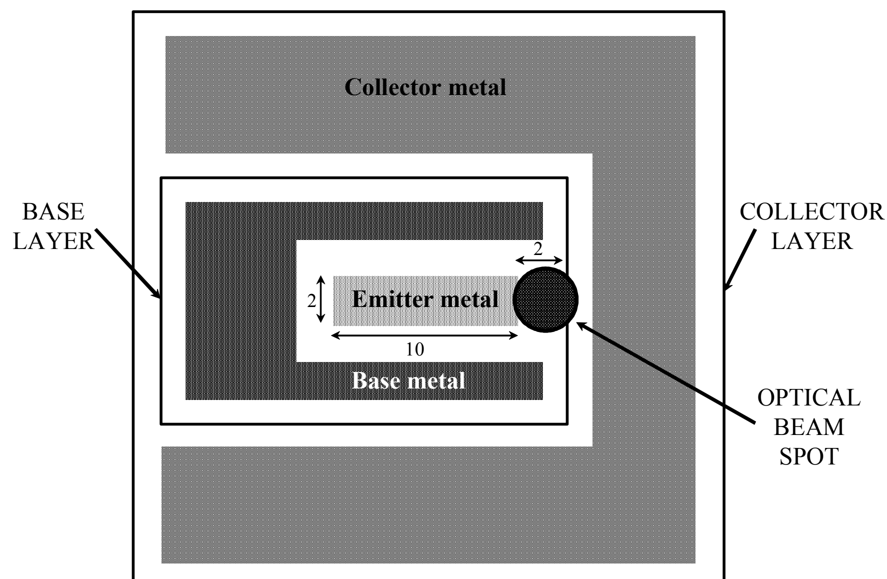

Figure 4-6. The top view of the fabricated InP HBT. Optical beam is located between emitter metal and collector metal.

4-3. Photodetection characteristics of InP HBT

4-3-1. Photodetection mechanism in InP HBT

The theories for photodetection process in InP HBT are well established since the phototransistor internal gain mechanism is identical to the electrical current gain of InP HBT itself [7]. Figure 4-7 illustrates the band diagram explaining phototransistor operation of InP HBT. When 1.55μm optical illumination is applied to the topside of InP HBT, it passes through wide bandgap InP emitter without the absorption. In an $In_{0.53}Ga_{0.47}As$ base-collector junction where depletion field exists, photoabsorption takes place creating electron-hole pairs. The photogenerated electrons drift into the collector region, which contributes to the photocurrent (I_{PD}) by photodiode operation. On the contrary, the holes move to opposite direction and accumulate in the base region. This raises the base-emitter potential, leading to increased electron injection rate from emitter into base. If the lifetime of the injected electrons in the base is longer than their transit time, the electrons are able to reach the collector region, which contributes to photocurrent (I_{PT}) provided by phototransistor operation of InP HBT. The total photocurrent (I_{PH}) measured at collector port is the sum of these two components, given by

$$I_{PH} = I_{PD} + I_{PT} . \quad (4\text{-}2)$$

The time constant which governs the optical modulation response of InP HBT is the sum of emitter-base charging time, base transit time, base-collector charging time and collector transit time [5]. Since it is similar to the time constant which determines its current gain cutoff frequency (f_T), the optical modulation response follows the microwave response of InP HBT, thus it is expected to be faster than that of InP HEMT

whose optical modulation response depends not on its microwave response but on the lifetime of photogenerated holes. Next section presents the experimental results on the photodetection characteristics of InP HBT as a high-speed phototransistor.

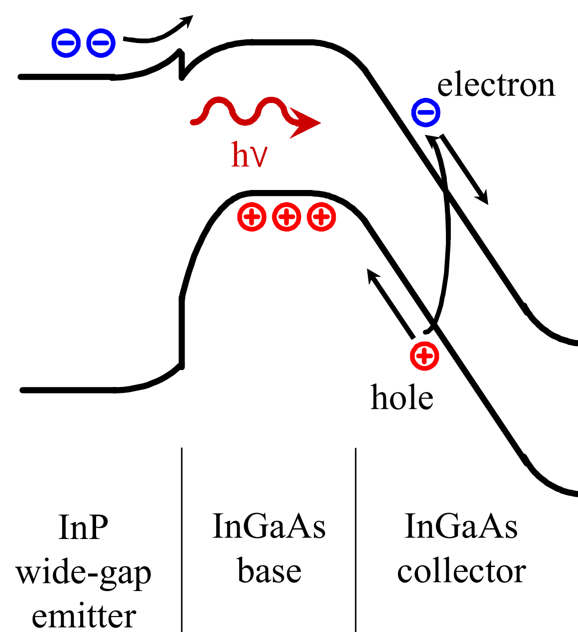

Figure 4-7. Energy band diagram of InP HBT under optical illumination.

4-3-2. DC photodetection characteristics of InP HBT

Setting V_{BE} to 0V makes the HBT to be under cut-off condition where HBT cannot provide the intrinsic gain by transistor operation. In the case of phototransistor operation, this cut-off condition is referred to photodiode mode (PD-mode) performing only photodetection without offering intrinsic gain. Figure 4-8 shows the I_C as a function of V_{CE} at PD-mode (V_{BE}=0V) under dark and illuminated (P_{opt}=0dBm) conditions, indicating photodiode characteristics of base-collector junction. The responsivity of 0.25A/W was obtained for base-collector junction photodiode. It indicates the quantum efficiency of 31.25%.

By applying small currents into base port, the HBT operates at active condition and provides a phototransistor internal gain. Figure 4-9 shows the common-emitter I_C-V_{CE} characteristics at I_B of 50μA with increasing optical powers from -12dBm to 0dBm. The maximum DC responsivity of 40A/W was obtained at I_B of 50μA and V_{CE} of 1V, which is much higher than that of InP HEMT. In order to clarify which photoeffect is dominant in InP HBT, the photocurrents as a function of incident optical power were measured. As can be seen in figure 4-10, the photocurrents show linear dependence on incident optical power. It indicates that the photoconductive effect is major photodetection mechanism in InP HBT as described in equation 2-6. Figure 4-11 shows the measured DC responsivities as a function of incident optical power for I_B=50μA and V_{CE}=1V. Unlike the InP HEMTs shown in figure 2-17, the InP HBTs exhibits uniform responsivity over wide ranges of input optical power with maintaining high responsivity. On the other hands, InP HEMT shows large responsivity at low optical power but it rapidly decreases as optical power increases. Therefore, InP HBTs are

suitable for the applications requiring a high power photodetector.

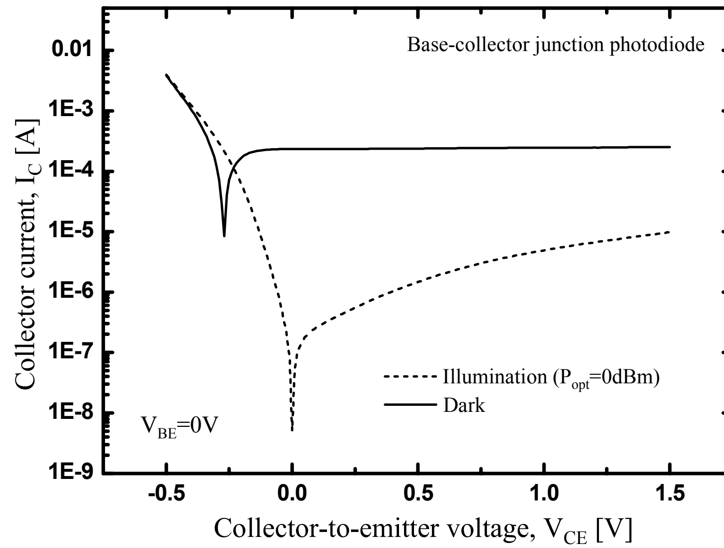

Figure 4-8. I_C of the InP HBT with V_{BE}=0V (cut-off condition) as a function of V_{CE} under dark and illuminated conditions, which indicates the base-collector junction photodiode characteristics

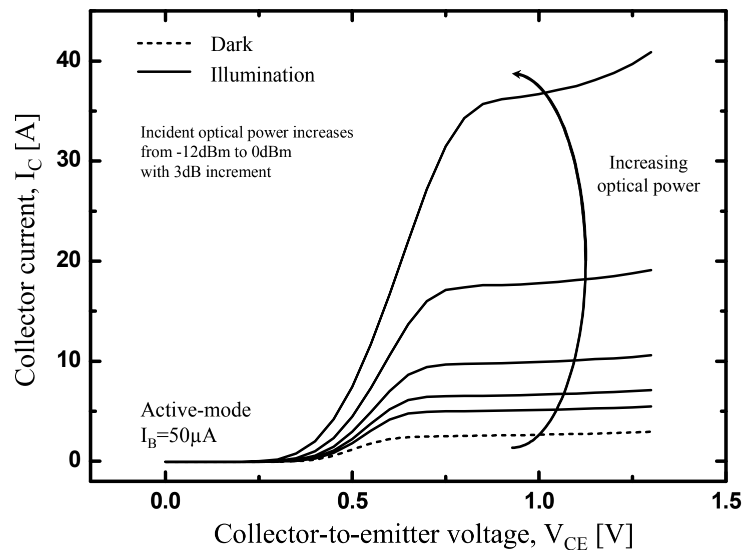

Figure 4-9. Common-emitter I_C-V_{CE} characteristics of the InP HBT under dark and optical illumination. Optical power increases from -12dBm to 0dBm with 3dB increment

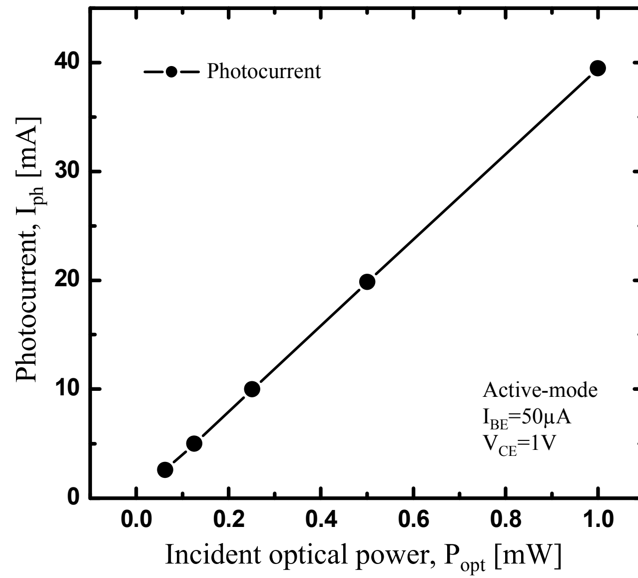

Figure 4-10. Photocurrents as a function of incident optical power to InP HEMT under active condition (I_{BE}=50μA, V_{CE}=1V).

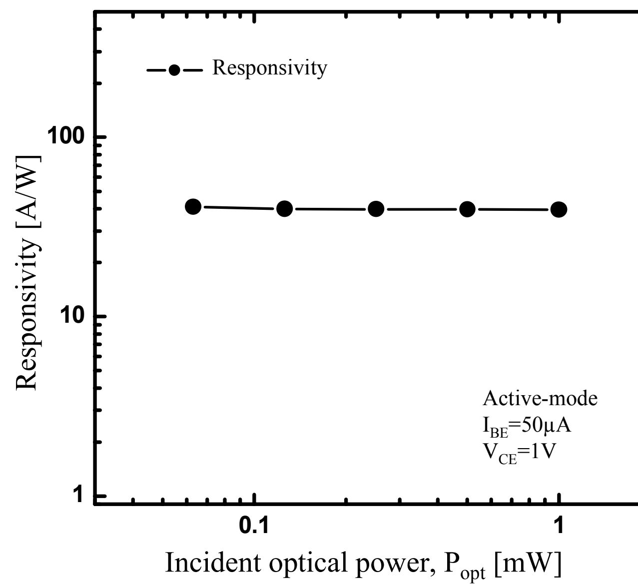

Figure 4-11. Optical responsivities of InP HBT as a function of incident optical power under I_{BE}=50μA, V_{CE}=1V

4-3-3. Optical modulation response of InP HBT

Figure 4-12 shows the optical modulation responses of InP HBT under active condition (Tr-mode) and cut-off condition (PD-mode). Under Tr-mode where I_B is 100μA, the InP HBT provides the phototransistor internal gain, thus shows very large photoresponse. The optical 3dB bandwidth is 1.4GHz which is governed by the summation of time constants for InP HBT. The predominant one to determine optical modulation response is thought to be the base-emitter charging time related to base-emitter capacitance (C_{BE}). It can be seen that the optical 3dB bandwidth of InP HBT is much larger than that of InP HEMT (figure 2-18) although its RF characteristics are inferior to those of InP HEMT. It is because the optical modulation response of InP HBT strongly depends on its microwave response, while InP HEMT exhibits the optical modulation response irrespective of its microwave response. PD-mode represents the InP HBT operates as a photodiode without providing phototransistor gain. In this condition, optical 3dB bandwidth is dominated by base-collector transit time relating to base-collector capacitance (C_{BC}).

Phototransistor internal gain (G_{int}) of InP HBT is the photoresponse difference between Tr-mode and PD-mode. The fabricated InP HBT has the 23.6dB phototransistor internal gain at 100MHz optical modulation frequency. The figure 4-12 also includes the optical gain cutoff frequency (optical f_T) where phototransistor internal gain is zero. The InP HBT exhibits relatively low optical f_T of 10GHz. In contrast with the high optical responsivity and large optical 3dB bandwidth obtained from InP HBT, the G_{int} and optical f_T are much lower than those of InP HEMT. It is attributed to the relatively poor transconductance and RF characteristics of InP HBT comparing with InP HEMT. It can be concluded that the fabricated InP HBT is suitable

to receive broadband optical signal, however high frequency optical signal is not acceptable. Since the optical modulation response is directly related to the microwave response in InP HBT, there is a room for their improvements according to the developments of InP HBT device technologies.

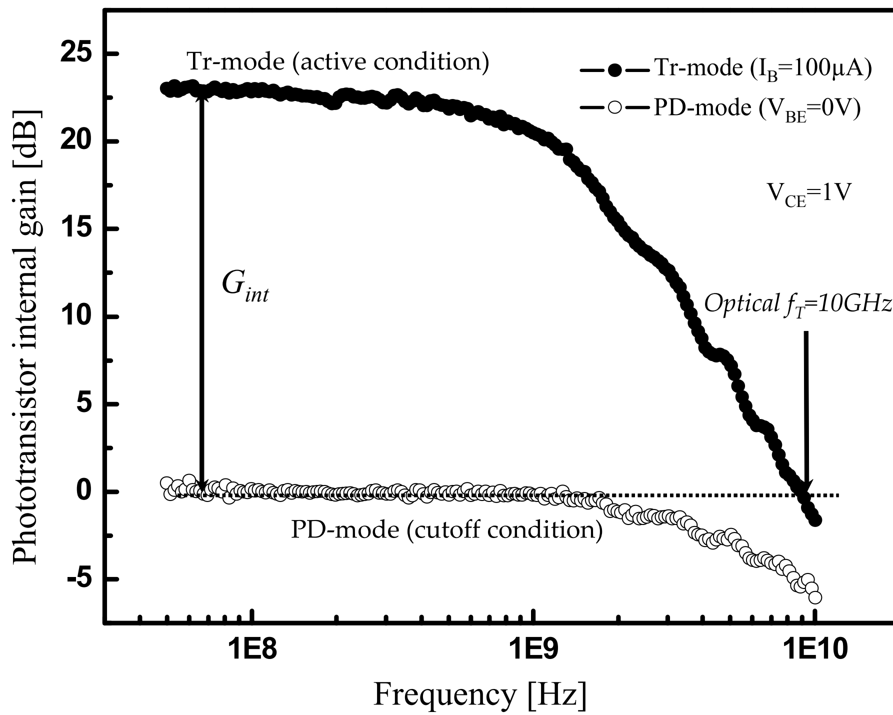

Figure 4-12. The measured optical modulation responses of InP HBT under I_B of 100μA (active condition) and V_{BE} of 0V (cutoff condition) at fixed V_{CE} of 1V. G_{int} represents phototransistor internal gain of InP HBT. Optical gain cutoff frequency (optical f_T) is the frequency where phototransistor internal gain is 0dB. The InP HBT exhibit the optical f_T of about 10GHz

4-4. Optoelectronic mixer

4-4-1. Features of InP HBT optoelectronic mixer

The InP HBT can be also used as an optoelectronic mixer, taking advantage of its device intrinsic nonlinearities. By simultaneously applying electrical LO signals to the base port and illuminating optical IF signals, the frequency up-conversion of optical IF signals into RF band ($f_{LO} \pm f_{IF}$) is possible. Figure 4-13 shows the output spectrum of InP HBT optoelectronic mixer by applying 10GHz LO and optical 100MHz IF signals.

Like InP HEMT optoelectronic mixers presented in chapter 2, the internal conversion gain of InP HBT is defined as the output power ratio of frequency up-converted signal ($f_{LO} + f_{IF}$) to the primary photodetected signal (f_{IF}) measured at PD-mode where no phototransistor gain is provided. Figure 4-14 shows the optoelectronic mixing products at $f_{LO} + f_{IF}$ and and photodetected signals at f_{IF} as a function of V_{BE}. When V_{BE} is 0V, the output photodetected power at f_{IF} is the primary photodetected power that is about -24.5dBm. The photoresponse difference between it and the measured power at V_{BE} of 0.8V is the maximum phototransistor internal gain (G_{int}) which is about 23.6dB. For optoelectronic mixing experiments, 10GHz LO signal with 0dBm power is connected to base port and 100MHz optical signal with 0dBm optical power is illuminated onto the device, simultaneously. The best optoelectronic mixing efficiency was obtained at V_{BE} of 0.8V. In this condition, the InP HBT optoelectronic mixer provides 7.2dB internal conversion gain (G_{conv}).

Figure 4-15 shows the dependence of optoelectronic mixing products on V_{CE} for I_B= 100μA and LO power of 0dBm. Under saturation mode where V_{CE} is low, the power of mixing product increases as V_{CE} increases. As V_{CE} increases over 0.9V indicating the

active mode, it begins to decrease because the device nonlinearities cannot be altered with high V_{CE} condition [8].

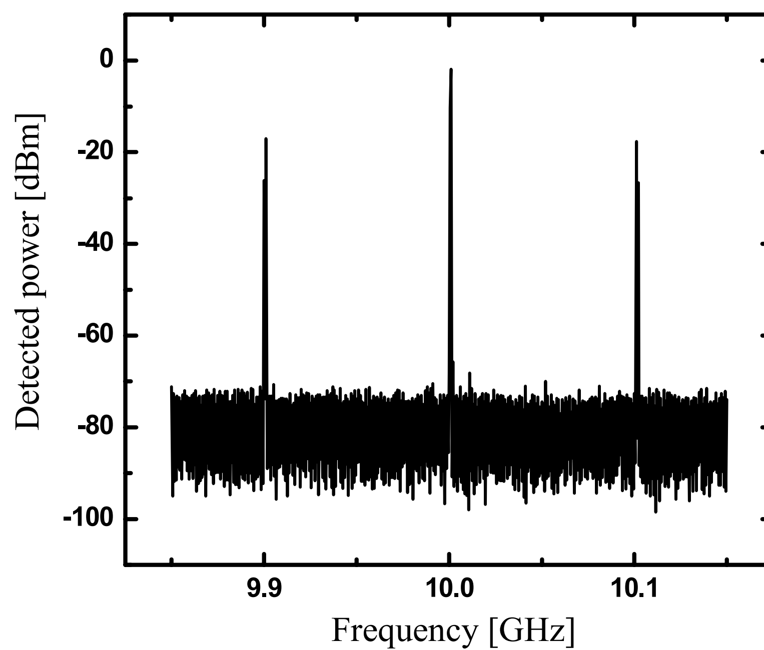

Figure 4-13. The RF spectrum of InP HBT optoelectronic mixer under applying 10GHz LO and optical 100MHz signals.

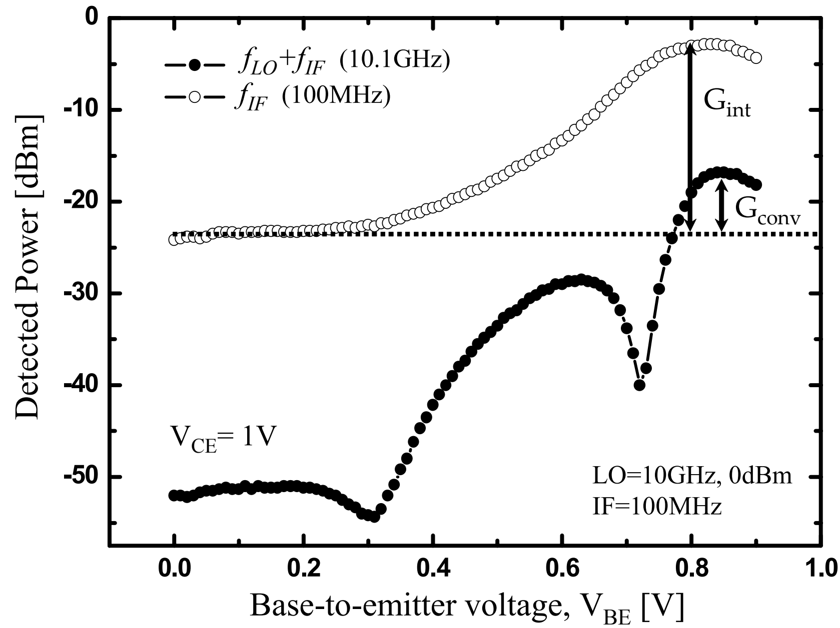

Figure 4-14. The dependence of optoelectronic mixing products at $f_{LO}+f_{IF}$ and photodetected signal at f_{IF} on V_{BE} under applying 10GHz, 0dBm LO to the base port and 100MHz optical IF signal at V_{CE} of 1V. Gint is the phototransistor internal gain and Gconv is the internal conversion gain of InP HBT optoelectronic mixer.

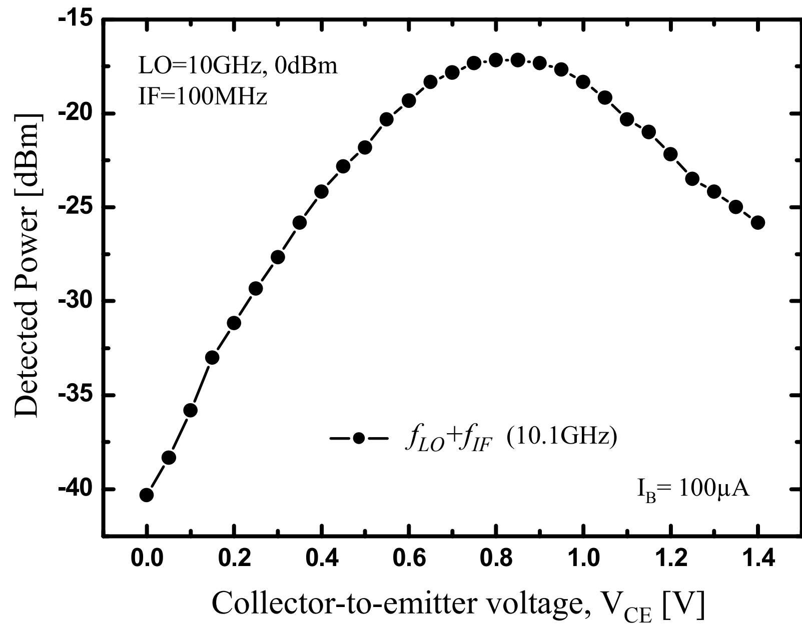

Figure 4-15 The dependence of optoelectronic mixing products at $f_{LO}+f_{IF}$ and photodetected signal at f_{IF} on V_{CE}.

4-4-2. Usable LO frequency ranges

Figure 4-16 shows the internal conversion gain (-○-) as a function of applied LO frequencies. It decreases with increasing LO frequencies, following S_{21} characteristics (solid line) included in this figure and displayed to right axis. When LO frequency is higher than 25GHz, the InP HBT optoelectronic mixer cannot provide positive internal conversion gain any longer. Compared with InP HEMT optoelectronic mixers, maximum LO frequency to obtain positive internal conversion gain in InP HBT is relatively low. It is attributed to both phototransistor internal gain and RF characteristics of InP HBT, which are inferior to those of InP HEMT. Therefore, the efforts for their improvements are necessary to obtain wide LO frequency range of optoelectronic mixer.

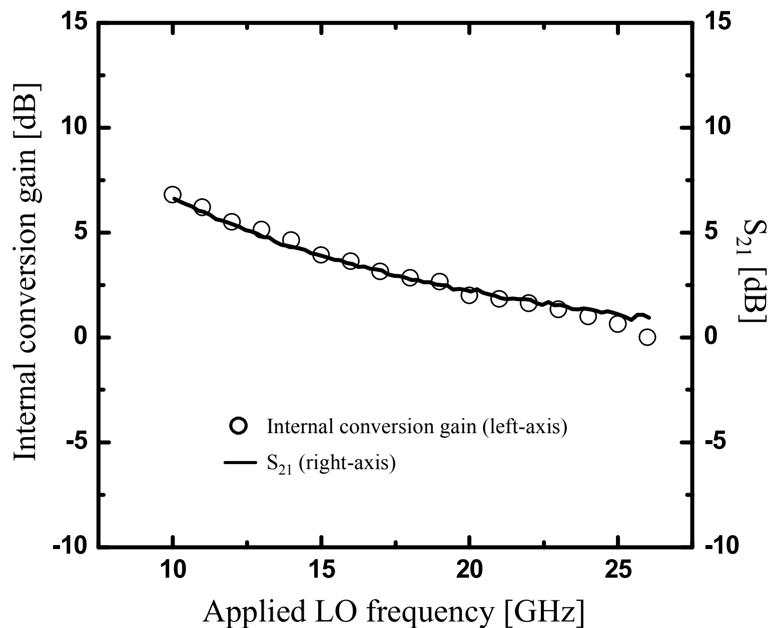

Figure 4-16. Internal conversion gain as a function of applied LO frequency to InP HBT optoelectronic mixer. S_{21} (solid line) of InP HBT is also included and displayed to right axis for comparison. The bias conditions are I_B of 100uA and V_{CE} of 1V.

4-5. Gigabit data transmission in fiber-optic wireline and 60GHz wireless links

4-5-1. Motivation

Gigabit data transmissions in wireline access networks have made a great progress in last decade with the help of fiber-optic technologies. In parallel, the markets for wireless access networks is also rapidly growing, which gives rise to much attention in wireless gigabit data transmission. In most cases, since subscribers may desire to access either wireline or wireless links according to their network environments, it is important to merge these two wireline and wireless access networks together.

Remote up-conversion systems based on phototransistors are attractive for realizing these broadband convergence networks. Figure 4-17 illustrates the remote up-conversion fiber-optic/millimeter-wave data transmission systems based on phototransistors to provide broadband data services by wireline and wireless, simultaneously. In this scheme, baseband data signals are optically transmitted through optical fibers. If subscribers wish to receive these data by wireless access, it is only required that LO signals are applied to the input port of a phototransistor, making optoelectronic mixer. If not, the phototransistor just recovers the optically transmitted data into corresponding electrical data with amplification. Therefore, these dual-functionalities of phototransistors are expected to facilitate the incorporation of fiber-optic networks with wireless networks.

Previously, in chapter 3, 622Mbps data transmissions in both baseband and 60GHz wireless links were demonstrated utilizing InP HEMT. In order to extend them to

gigabit transmission, wide photodetection bandwidth more than GHz range is essential for optoelectronic mixer. Unfortunately, InP HEMT used in this work cannot satisfy this requirement because the photodetection bandwidth of InP HEMT follows not its excellent microwave characteristics but slow photovoltaic effects. Therefore, it gives maximum optical 3dB bandwidth less than 600MHz.

The InP HBT has an ability to provide high responsivity as well as wide photonic bandwidth up to GHz range. Although InP HBT used in this work has the optical 3dB bandwidth (f_{3dB}) of about 1.4GHz, the other research groups have reported the higher speed InP HBTs having optical f_{3dB} of 3.8GHz [2], 7.5GHz [4] and 12GHz [9]. Therefore, it is concluded that phototransistor based on InP HBT is one of the best candidates to these applications. In this section, the applicability of the fabricated InP HBT to gigabit transmission in fiber-optic wireline and 60GHz wireless links is experimentally verified.

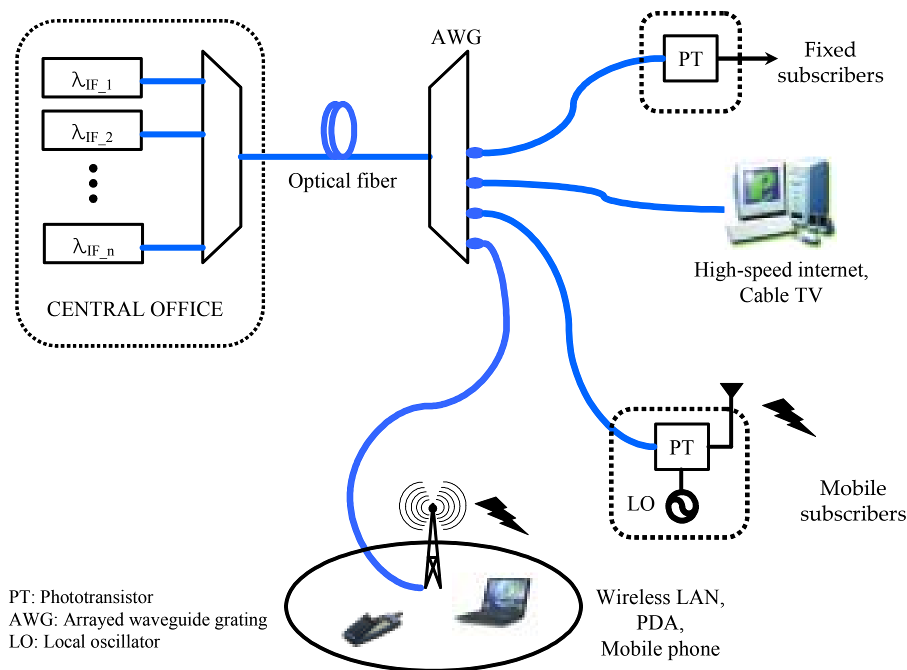

Figure 4-17. Merging broadband fiber-optic wireline links and millimeter-wave wireless links by using phototransistors

4-5-2. Gigabit data transmission in fiber-optic and 60GHz links

As can be seen in figure 4-12, the optical f_{3dB} for the fabricated InP HBT is about 1.4GHz, which is sufficient for receiving 1.25Gbps optical data signals in this investigation. For its validation, 10Km fiber-optic transmission of 1.25Gbps NRZ data signals is demonstrated and the results are shown in figure 4-18. Clear eye opening for photodetected 1.25Gbps signal can be observed. The link BER characteristics are shown in figure 4-18-(B). The error-free transmission was achieved at incident optical power of -2.5dBm which is much lower than that of InP HEMT (figure 2-24). It is mainly due to high optical responsivity as well as high quantum efficiency of InP HBT.

The InP HBT can be used as an optoelectronic mixer presented in section 4-3. Figure 4-19 shows the 63GHz band output spectrum of InP HBT optoelectronic mixer under applying 63GHz LO and 100MHz IF signals. The fiber-optic/60GHz data transmission systems based on InP HBT optoelectronic mixer was constructed and depicted in figure 4-20. At central office, 1.25Gbps NRZ data with the amplitude of 2Vpp was directly modulated to DFB laser diode. The optically transmitted data signals over 10km single mode fiber were frequency up-converted to 63GHz band in InP HBT optoelectronic mixer with optimum bias conditions of I_B=250μA and V_{CE}=0.7V. For this frequency up-conversion, 63GHz oscillator in conjunction with RF attenuator was applied to the base port. The frequency up-converted signals would be actually radiated into free-space by an antenna, it was skipped in this experiments. After bandpass filtering, the 60GHz band output signals were amplified by LNA and demodulated using direct detection technique with a Schottky diode in a mobile terminal. The recovered signals are low-pass filtered and connected to a sampling oscilloscope and an error detector.

The figure 4-21-(A) shows the eye-diagram for the recovered 1.25Gbps data having the pattern length of 2^{15}-1. There are inconsiderable errors which are further evaluated by BER measurements shown in figure 4-21-(B). The error-free transmission was achieved at incident optical power of 7dBm which is rather high comparing with the error-free condition (P_{opt}=-2dBm) in fiber-optic baseband data transmission. The origin for relatively high required optical power in 60GHz link is the high conversion loss of InP HBT optoelectronic mixer at 60GHz band, which can be also seen in figure 4-16. When LO frequency is over than 25GHz, the InP HBT optoelectronic mixer tends to lose conversion gain but gives just conversion loss. Although increasing LO power alleviated this problem, it was inevitable to have a conversion loss of about 18dB in 60GHz band. Therefore, it can be said that microwave characteristics of InP HBT should be improved in order to fully utilize its excellent photonic characteristics.

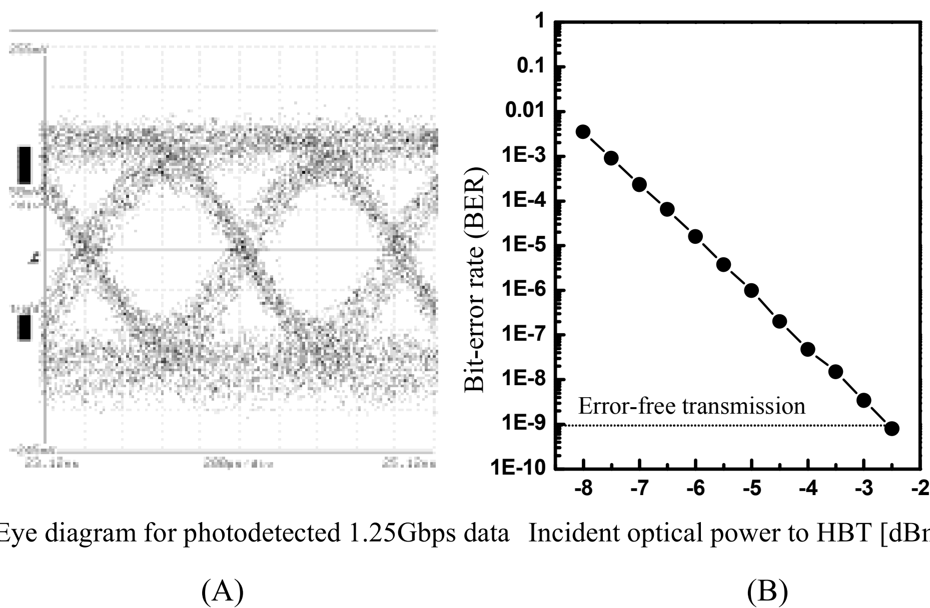

Figure 4-18. (A) Eye diagram for photodetected 1.25Gbps data signals (B) BER characteristics as a function of incident optical power to HBT.

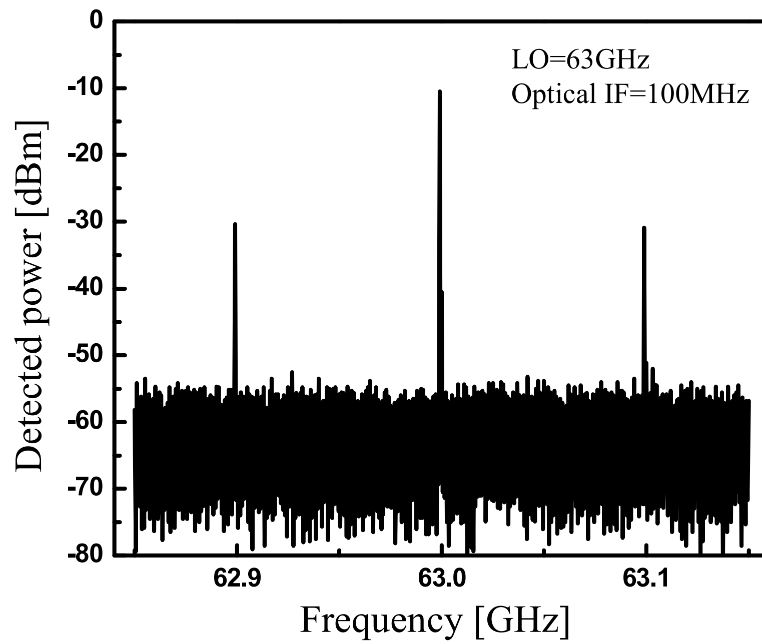

Figure 4-19. 63GHz band spectrum of frequency up-converted 100MHz optical IF signal by InP HBT optoelectronic mixer.

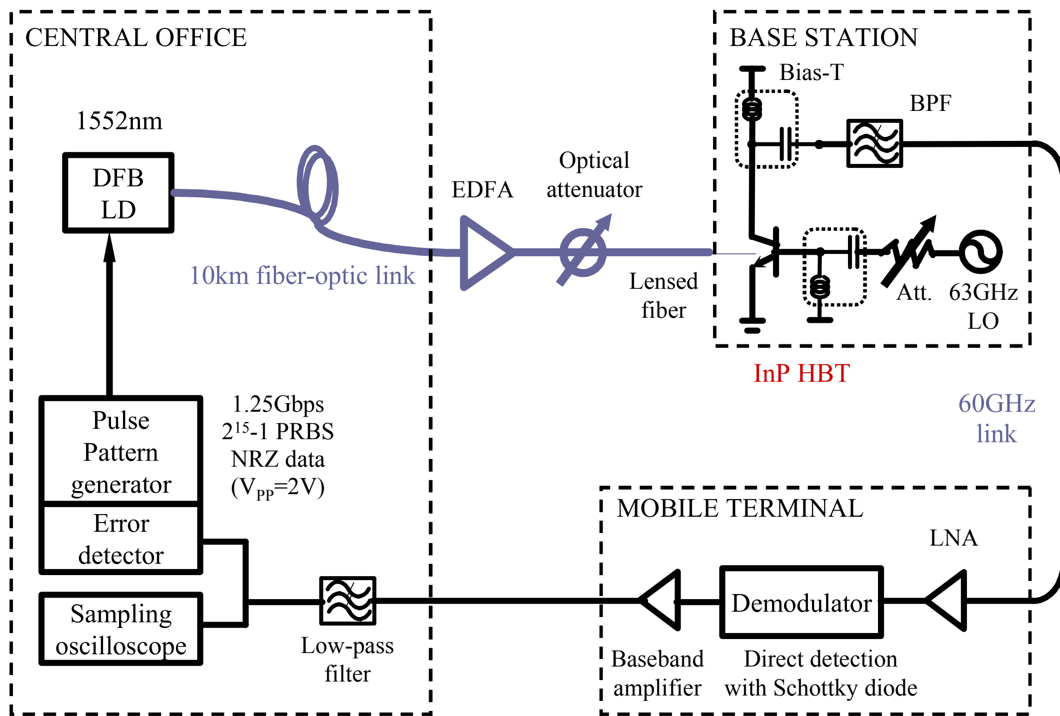

Figure 4-20. Fiber-optic/60GHz gigabit data transmission systems utilizing InP HBT as an optoelectronic mixer.

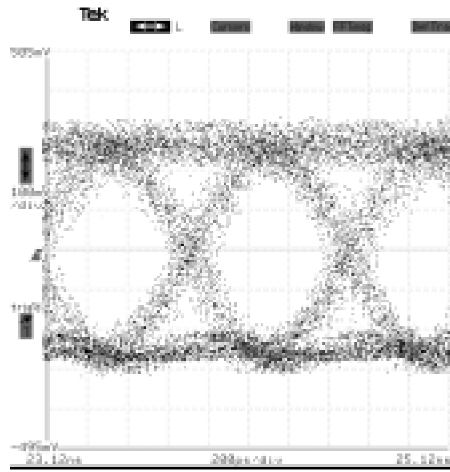

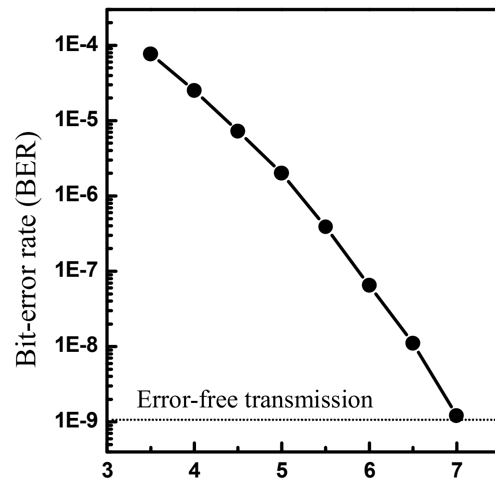

Eye diagram for recovered 1.25Gbps data   Incident optical power to HBT [dBm]

(A)   (B)

Figure 4-21. (A) Eye diagram for recovered 1.25Gbps data after transmission over 30km fiber-optic link and 60GHz link. (B) BER characteristics of constructed fiber-optic/60GHz data transmission systems as a function of incident optical power to HBT.

4-6. Conclusion

This chapter presents the photodetection characteristics of InP HBTs and how to implement them into fiber-optic/millimeter-wave gigabit data transmission systems. The photodetection mechanism in InP HBT is a photoconductive effect in which the optical responsivity is linearly proportional to input optical power. This feature is very attractive in the applications handling high optical power, whereas InP HEMT showing low responsivity at high optical power cannot afford it. It exhibit high optical responsivity of 40A/W and wide optical 3dB bandwidth of 1.4GHz. The phototransistor internal gain and the optical gain cutoff frequency of the fabricated InP HBT are 23.6dB at 100MHz optical modulation frequency and 10GHz, respectively. Because the optical modulation response of InP HBT is closely related to its microwave response, it can be further improved if higher speed InP HBT is utilized.

The InP HBT can be also utilized as optoelectronic mixer. It offers high internal conversion gain at low LO frequency, however, it severely worsens as LO frequency increases. The maximum LO frequency to achieve conversion gain in InP HBT is about 25GHz which is much lower than that of InP HEMT. It is due to relatively poor RF characteristics of InP HBT. The main advantage of InP HBT optoelectronic mixer is the wide photonic bandwidth of about 1.4GHz. Utilizing this merit, 1.25Gbps data transmission was successfully achieved in both fiber-optic wireline and 60GHz wireless links.

References

[1] H. Kroemer, "Heterostructure bipolar transistors and integrated circuits," *Proc. IEEE*, vol. 70, no. 1, pp. 13, 1982

[2] H. Kamitsuna, Y. Matsuoka, S. Yamahata and N. Shigekawa, "Ultrahigh-speed InP/InGaAs DHPT for OEMMICs," *IEEE Trans. Microwave Theory Tech.*, vol. 49, no. 10, Oct. 2001.

[3] H. Kamitsuna, T. Shibata, K. Kurishima and M. Ida, "Direct optical injection locking of InP/InGaAs HPT oscillator ICs for microwave photonics and 40Gbps-class optoelectronic clock recovery," *IEEE Trans. Microwave Theory Tech.*, vol. 50, no. 12, Dec. 2002.

[4] M. Muller, S. Withitsoonthorn, M. Roet, J.-L. Benchimol and C. Gonzales, "Millimeter-wave InP/InGaAs photo-HBT and its applications to optoelectronic integrated circuits," *IEICE Trans. Electron.*, vol.E86-C, no. 7, pp. 1299, Jul. 2003.

[5] F. Schwierz and J. J. Liou, *Modern Microwave Transistors*, Wiley Interscience, 2003.

[6] W. Liu, "Handbook of III-V heterojunction bipolar transistors," Wiley Interscience, 1998.

[7] J. C. Campbel, *Phototransistors for lightwave communication* in Semiconductor and Semimetal, vol 22, part. D, Academic Press, 1985

[8] Y. Betser, D. Ritter, C. P. Liu, A. J. Seeds and A. Madjar, "A single-stage three-terminal heterojunction bipolar transistor optoelectronic mixer," *J. Lightwave Technol.*, vol. 16, no. 4, pp. 605, Apr. 1998.

[9] H. Kamitsuna, "Ultra-wideband monolithic photoreceivers using HBT-compatible HPT's with novel base circuits, and simultaneously integrated with an HBT amplifier," *J. Lightwave Technol.*, vol. 13, no. 12, pp. 2301, Dec. 1995.

Chapter 5

Summary and future works

5-1. Summary

Recent years have seen the growing interest in fiber-optic/millimeter-wave data transmission systems for wireless link applications since they offer low-loss and wide-bandwidth transmission medium that accommodates the deliveries of broadband data and high frequency signals. To push these systems into daily lives, the realization of cost-effective antenna base station architecture is a crucial issue. Phototransistors which were conventionally recognized as just photodetector have received much attention for their potential to perform high-speed optical signal processing functions. Their compatibility to MMIC fabrication process is another attractive incentive, which gives the possibility of one-chip integration between photonic and microwave components on a single substrate. All these features are expected to make these fiber-optic/millimeter-wave systems to be simplified and practically implemented.

This dissertation work has aimed to characterization of three-terminal phototransistors and development of fiber-optic/millimeter-wave data transmission systems utilizing them. The InP HEMTs, most distinctive transistors in high frequency operation, were first examined for phototransistor applications. Comprehensive

studies were devoted to clarify physical origins for the photodetection in InP HEMT, the experimental results gave me a proof that photovoltaic effect is dominant under turn-on condition while photoconductive effect under turn-off condition. The former provides the InP HEMT with phototransistor internal gain, the latter makes it possible to estimate actually absorbed optical power in InP HEMT. Utilizing their dependences on bias conditions, two important device parameters, the phototransistor internal gain and optical gain cutoff frequency, were determined for their phototransistor applications.

Incorporating their photodetection characteristics with original device functionalities, two kinds of new optical signal processing functions in InP HEMT were presented and implemented to fiber-optic/millimeter-wave data transmission systems. Proposed one is to utilize it as an InP subharmonic optoelectronic mixer that allows less stringent use of high frequency LO for the frequency up-conversion to millimeter-wave frequency band. It was experimentally characterized at 60GHz band in order to determine optimum bias conditions for obtaining maximum conversion efficiency. The device performance parameters including internal conversion gain, nonlinear distortion characteristics and usable LO ranges were also evaluated. Utilizing it, 622Mbps broadband data transmission was demonstrated in the constructed fiber-optic/60GHz downlink system.

The other is a single InP HEMT approach performing unified functions of optically injection-locked oscillation and harmonic optoelectronic mixing, simultaneously. Remotely delivered optical LO signals make a free-running oscillator to be phase-locked, resulting in phase-locked oscillator. At the same time, optical data/IF signals are frequency up-converted by harmonic optoelectronic mixing functions. Since proposed

scheme employs only a single InP HEMT with the other passive circuitries, it allows the antenna base station architecture in fiber-optic/millimeter-wave system architecture to be very simple and miniaturized. In order to demonstrate its feasibility, 20Mbps 16QAM data transmission was achieved in the constructed fiber-optic/millimeter-wave downlink system.

InP HBTs, renowned phototransistors for a long time, were also investigated to know their structural advantages over InP HEMT in terms of phototransistor characteristics. Experimental results indicated that they has an ability to provide high optical responsivity and wide photonic bandwidth, both are obvious merits of InP HBTs. By utilizing it as an optoelectronic mixer having wider photonic bandwidth in comparison with InP HEMT, 1.25Gbps data transmission in both fiber-optic wireline and 60GHz wireless links was demonstrated.

As emphasized in the introductory chapter, the realization of simple antenna base station architecture is a crucial issue for commercial developments of fiber-optic/millimeter-wave data transmission systems. These experimental results presented in this work confirm the potentials of phototransistors to be integrated in optoelectronic MMIC as well as to provide optical signal processing methodology to contribute the construction of fiber-optic/millimeter-wave data transmission systems. Therefore, continuous efforts should be invested on the development of high performance phototransistors for these fiber-optic/millimeter-wave system applications.

5-2. Comparison between two types of phototransistors, InP HEMTs and HBTs

In this dissertation, two types of phototransistors, InP HEMTs and InP HBTs are investigated. Although it is difficult to determine what phototransistor is optimum for fiber-optic/millimeter-wave system applications, exploratory comparison between them are given with considering their photonic and RF characteristics. The obtained device parameters in this work are compiled in Table 1, and figures of merit in a phototransistor are explained.

Quantum efficiency (η) indicates the probability that incident photons on the device are collected to photocurrent. It can be written as

$$\eta = (1-R)\varsigma[1-\exp(-\alpha d)], \qquad (5\text{-}1)$$

where R is the reflectance, ς is the fraction of electron-hole pairs that contribute successfully to the photocurrent, α is the absorption coefficient and d is the absorption depth.

The $In_{0.53}Ga_{0.47}As$ material that used in photoabsorption layers of InP HEMTs and HBTs has the absorption coefficient of $10^4 cm^{-1}$ for 1.55μm lightwave. The fabricated InP HEMT used in this work has only 20nm thickness $In_{0.53}Ga_{0.47}As$ layers which give maximum external quantum efficiency of 2% if no surface reflection occurs. Therefore, actual quantum efficiency in InP HEMT is known to be much lower than 2%. In the case of InP HBT, the absorption layer has the 1μm thickness corresponding maximum external quantum efficiency of 65%. Therefore, actually absorbed photons in InP HBT active regions are expected to be much higher than InP HEMT.

The responsivity ($\Re$) of a phototransistor can be described as

$$\Re = G_{\text{int}} \eta \frac{\lambda_0}{1.24}, \qquad (5\text{-}2)$$

where G_{int} is the phototransistor internal gain and λ_0 is the wavelength of input optical signal.

Responsivity was characterized by measuring ratio of output photocurrent to incident optical power. The maximum responsivities of InP HEMT and InP HBT acquired in this work are 10A/W and 40A/W, respectively. The most noticeable features are their dependences on incident optical power as shown in figures 2-16 and 4-11. In an InP HEMT, a responsivity decreases as incident optical power increases, which is attributed to photovoltaic effects as shown in figure 2-14. On the other hands, InP HBTs exhibit uniform responsivity over wide range of input optical power with preserving high responsivity. Therefore, an InP HBT would be better for high optical power applications.

The equation 5-2 gives that responsivity is the product of phototransistor internal gain and quantum efficiency. Although InP HBT exhibits higher responsivity than InP HEMT, its ratio is not perfectly matched to that of quantum efficiencies. From these results, it can be anticipated that phototransistor internal gain (G_{int}) of InP HBT may be lower than that of InP HEMT considering their quantum efficiency. The phototransistor internal gain is defined as the ratio of output photocurrent to primary photocurrent without any gain. Experimental results show that InP HEMT has the G_{int} of 45dB, while InP HBT gives G_{int} of 23.6dB at 100MHz optical modulation frequency under identical modulation index and optical power. The reason why the InP HEMT has larger G_{int} is its higher transconductance representing higher device intrinsic gain.

The optical 3dB bandwidths of InP HEMT and InP HBT are 580MHz and 1.4GHz, respectively. Since the optical modulation response of InP HBT is closely related to its microwave response, it can be further improved if higher speed InP HBT is developed. For InP HEMT, it depends not on microwave response but long lifetime of photogenerated holes as explained in section 2-4-3. It implies that the improvement in device speed cannot enlarge the optical 3dB bandwidth, in the other direction, the efforts to reduce the lifetime of photogenerated holes accumulated beneath source area are necessary to improve it in phototransistors based InP HEMTs.

Optical gain cutoff frequency (optical f_T) where phototransistor internal gain is zero is associated with both phototransistor internal gain and optical 3dB bandwidth. Although InP HEMT has relatively low optical 3dB bandwidth, the optical f_T is high due to its high G_{int}. High-frequency modulated optical signals are more acceptable in InP HEMT assuming no optical loss. In the case of InP HBT, the improvements of microwave performances are believed to simultaneously increase both G_{int} and optical f_T.

Optoelectronic mixers can be regarded as optical devices or microwave devices. Therefore, the effort to improve both optical and microwave characteristics results in high performance optoelectronic mixer. In this work, the InP HEMT offers high internal conversion gain at 60GHz band as well as wide LO frequency ranges, supported by its excellent microwave characteristics.

Merit Parameters	InP HEMT	InP HBT	Consideration
Device Feature Size	0.1μm (Gate-length)	$2\times10\mu m^2$ (Emitter size)	InP HEMT requires stringent lithography tech.
f_T	148GHz	90GHz	InP HEMT is higher speed
f_{max}	165GHz	75GHz	
Maximum Quantum efficiency	2%	65%	Assuming no surface reflection (only consider InGaAs thickness)
DC Responsivity	4A/W	40A/W	Input optical power = 0dBm
Phototransistor Internal Gain	45dB	23.6dB	Optical modulation frequency =100MHz
Optical 3dB bandwidth	580MHz	1.4GHz	Turn-on conditions
Optical f_T	105GHz	10GHz	Dependent on G_{int} and 3dB BW
Internal Conversion Gain	26.8dB	7.2dB	Optoelectronic mixer under 10GHz LO with 0dBm
Photodetector Structure	Lateral (photoconductor)	Vertical (photodiode)	HBT has thicker absorption layer
Photodetection Mechanism	Photovoltaic effects	Photoconductor effects	Photoconductive effects are dominant in off-state InP HEMT
Optical Modulation Response	Independent of microwave char.	Dependent on microwave cha.	InP HEMT (hole lifetime) InP HBT (C_{BE} charging time)
Illumination Method	Backside	Top-side	Additional mask design is required for InP HBT

Table 5-1. Comparison between InP HEMT and HBT in terms of phototransistor operation. It gives not absolute but relative comparison because two devices are different microwave characteristics

5-3. Future works

Further studies should be expanded into three ways. First, it is important to develop the device models of phototransistors. It will be utilized in the design of optoelectronic MMICs having the potential to simplify antenna base station architectures. In contrast with InP HBTs, it has been reported that there are many difficulties in building accurate models for InP HEMTs, especially optically controlled InP HEMTs. Therefore, many efforts should be assigned to investigate the device physics and to develop physical and equivalent circuit models for InP HEMTs.

Another one is to optimize phototransistor structures considering their applications. According to previous investigation, poor optical coupling efficiency and low optical 3dB bandwidth in InP HEMTs are severe obstacles for their practical applications. Edge-coupled InP HEMT-based phototransistors are expected to promise high coupling efficiency. To obtain wide optical 3dB bandwidth, body-contacted InP HEMTs can be adopted. Many studies on suppressing kink effects in silicon-on-insulator (SOI) MOSFET are also applicable, providing reduced the lifetime of photogenerated holes. For the case of InP HBT, the improvement of microwave performance is the best way to achieve high performance phototransistor.

The last one is to invent a novel fiber-optic/millimeter-wave data transmission system architecture utilizing these phototransistors. As described in section 3-1, they can perform many types of optical signal processing functions without frequency limitation. Therefore, it is certain that they can substitute for conventional microwave components, which are expected to create new system architectures with reduced cost and construction complexities.

Appendice

A. High-speed photodiode as an optoelectronic mixer for fiber-optic/millimeter-wave uplink data transmission.

A-A-1. Motivation

The fiber-optic/millimeter-wave system demonstrations presented in this work were mainly performed for downlink transmission. Considering their applications such as wireless LANs, the uplink transmission should be considered for achieving bi-directional links. Directly modulated laser diodes are widely used as uplink optical sources for transmitting IF signals from antenna base station to central office because of its low cost and simplicity. In this configuration, frequency mixers and oscillators are indispensable for the frequency down-conversion from millimeter-wave to IF. However, as mentioned before, it fatally increases the complexities of antenna base station architecture.

One attractive solution is to incorporate an optoelectronic mixer with an optical LO for frequency down-conversion. When incoming millimeter-wave signals (f_{RF}) and optical LO signals (f_{LO}) are simultaneously applied to optoelectronic mixers, the

frequency down-conversion into IF signals (f_{IF}) is performed by their nonlinearities, as described in section 3-2. Since the optical LO distribution scheme shifts the expensive millimeter-wave phase-locked oscillator away from many antenna base stations to single central office, it can be expected to realize simplified antenna base station architecture. For optoelectronic mixers, InP HEMTs and HBTs have been attracted because of their simplicity and high conversion gain as emphasized in this work. However, as shown in figures 2-19 and 4-2, they exhibit small optical 3dB bandwidths limiting the use of high frequency optical LO. Therefore, the high speed optical components are more beneficial in optoelectronic mixers performing the frequency down-conversion.

In this section, the use of high-speed photodiode as an optoelectronic mixer is proposed and experimentally demonstrated for the frequency down-conversion. Figure A-1 shows the fiber-optic/millimeter-wave uplink systems under consideration, where optical LO provides reference carrier frequency for each antenna base station, and WDM transceivers are used to transmit and receive IF signals. A photodiode is used as an optoelectronic frequency down-conversion mixer from millimeter-wave to IF with optical LO transmitted from central office. This approach avoids usages of electrical mixer and phase-locked LOs operating at millimeter-wave for the frequency down-conversion.

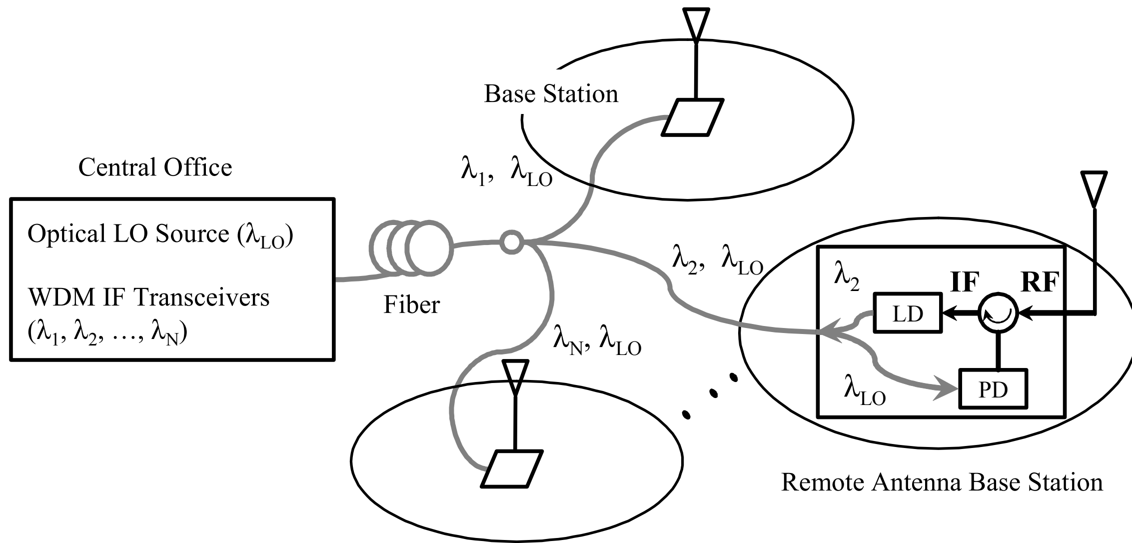

Figure A-1. Proposed fiber-optic/millimeter-wave uplink system.

A-A-2. Experimental Setup

For the reception of high-speed optical signals, high-speed waveguides were utilized as optoelectronic mixer. The photodiode[4] has the epitaxial layers consisting of n-doped InGaAsP layer, 5000Å undoped InGaAs absorption layer and p-doped InP layer from bottom to top. Figure A-2 shows the optical modulation response for the fabricated waveguide photodiode which has 200μm^2 p-n junction area. It can be seen that the waveguide photodiode exhibits the 3dB bandwidth more than 40GHz, which is suitable to detect high frequency optical LO signals. The photodiode exhibits the dark currents lower than -20nA and the maximum input optical saturation power of 10dBm.

The experimental setup for the characterization of photodiode optoelectronic mixer

[4] The high-speed waveguide photodiodes were fabricated by Dr. Yong-Whan Kwon and Dr. Joong-Seon Choe in Basic Research Lab, Electronics and Telecommunications Research Institute (ETRI), Daejun, Korea

is schematically depicted in figure A-3. The power divider was utilized to measure the down-converted IF signals as well as to apply 31GHz RF signal to the photodiode, simultaneously. The optical LO signal at 30GHz was generated by DSB-SC technique using Mach-Zehnder modulator and tunable laser source having the wavelength of 1553nm.

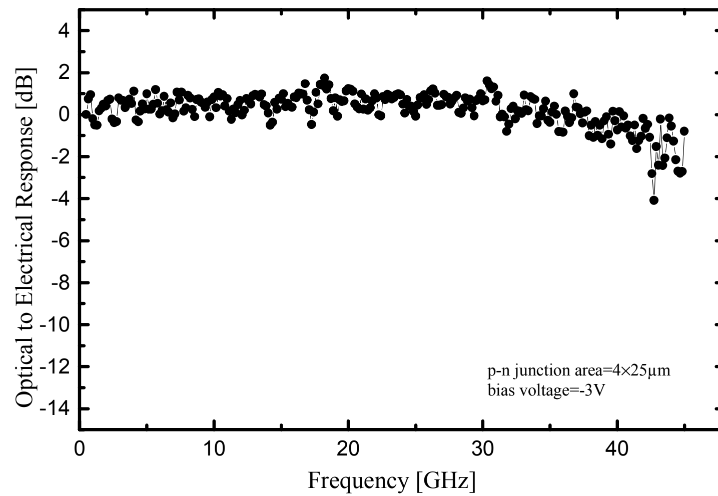

Figure A-2. Optical modulation response for the fabricated waveguide photodiode.

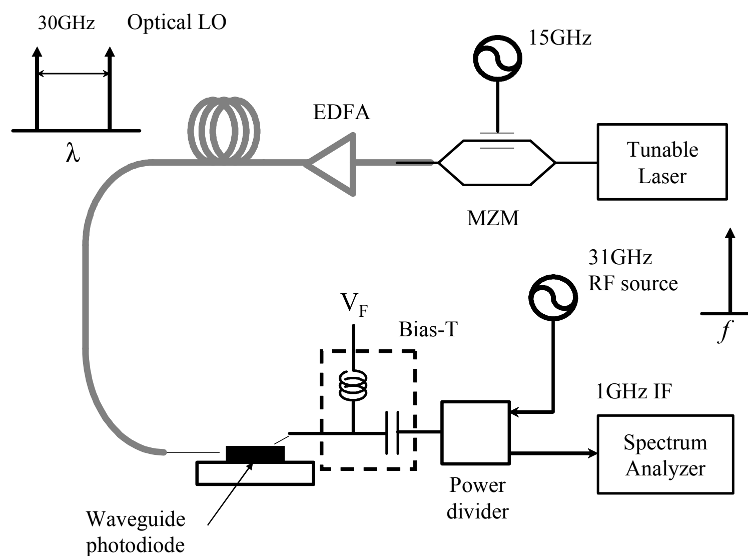

Figure A-3. Experimental setup for optoelectronic frequency down-conversion using high-speed waveguide photodiode.

A-A-3. Experimental results.

In this proposed scheme, the nonlinearities of photodiode are utilized for optoelectronic mixing of RF input with optically delivered LO signals. There are many works for making clear physical origins for its nonlinearities causing frequency mixing. Among them, the nonlinear dependence of optical responsivity on applied bias condition is believed to be major origin for the optoelectronic mixing since the RF input signal effectively alters the voltage across the photodiode. Figure A-4 shows the current-voltage characteristics for the fabricated waveguide photodiode under dark and 1mW optical illumination. It can be seen that the photocurrent is dependent on bias condition and its dependence become more nonlinear as reverse bias gets near to zero bias condition.

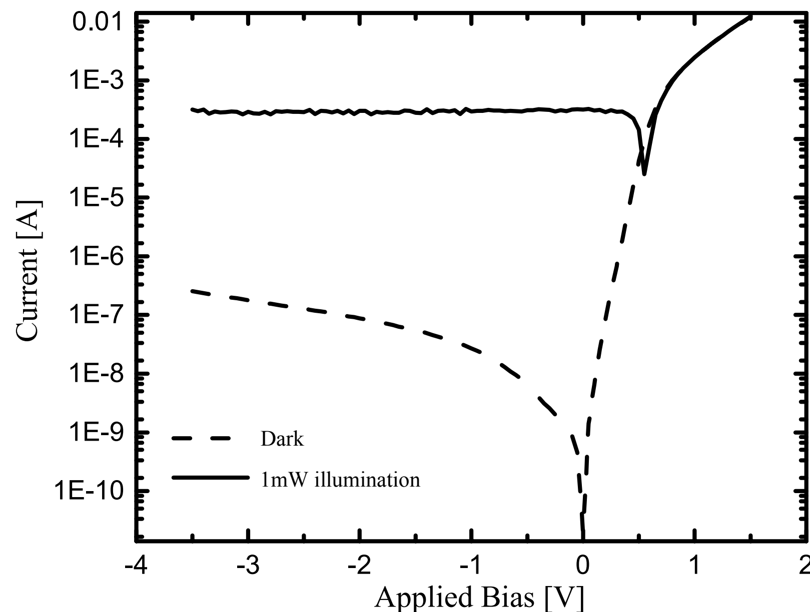

Figure A-4. Current-voltage characteristics for the fabricated photodiode under dark and 1mW optical illumination.

By utilizing its nonlinear characteristics, optoelectronic frequency down-conversion from 31GHz RF input to 1GHz IF is demonstrated by applying 30GHz optical LO into photodiode. Figure A-5-(A) shows the measured spectrum for 1GHz down-converted IF signal. The photodetected 30GHz optical LO signal and 31GHz RF signal applied to the photodiode are also shown in figure A-5-(B). In these spectrums, the asterisked signals are image signals produced by an A-band external harmonic mixer (HP11970A) used for 30GHz band measurements. The optical LO power was 10dBm and the input RF power was 0dBm. During the experiments, it was found that the conversion efficiency was not dependent on the input RF power but limited by optical LO power and the bias condition of photodiode. The measured 1GHz down-converted signal has the power of -57.5dBm under -32dBm photodetected power, which indicates 57.5dB conversion loss. The relatively high conversion loss is mainly limited by the input optical saturation power (10dBm) for waveguide photodiode.

Figure A-6 shows the photodetected signal at 30GHz signals and the 1GHz down-converted signals as a function of photodiode bias conditions. At high reverse bias condition of -3V where the photodiode exhibits very high linearity, the 1GHz down-converted signal power is very small. As decreasing the reverse bias condition, it is enhanced, which corresponds to the fact that the optical responsivity of photodiode becomes more nonlinear as applied voltage decreases as previously mentioned. It can be concluded that the photodiode as an optoelectronic mixer should be operated in zero bias condition for obtaining maximum conversion efficiency. This figure also shows the influence of input optical LO powers on the down-converted IF signal power. It indicates that increasing optical LO power is efficient way to improve conversion efficiency. However, it is limited by optical saturation power for the fabricated

photodiode as mentioned above. If a photodiode with high input optical saturation power is utilized for this purpose, the conversion efficiency can be further improved.

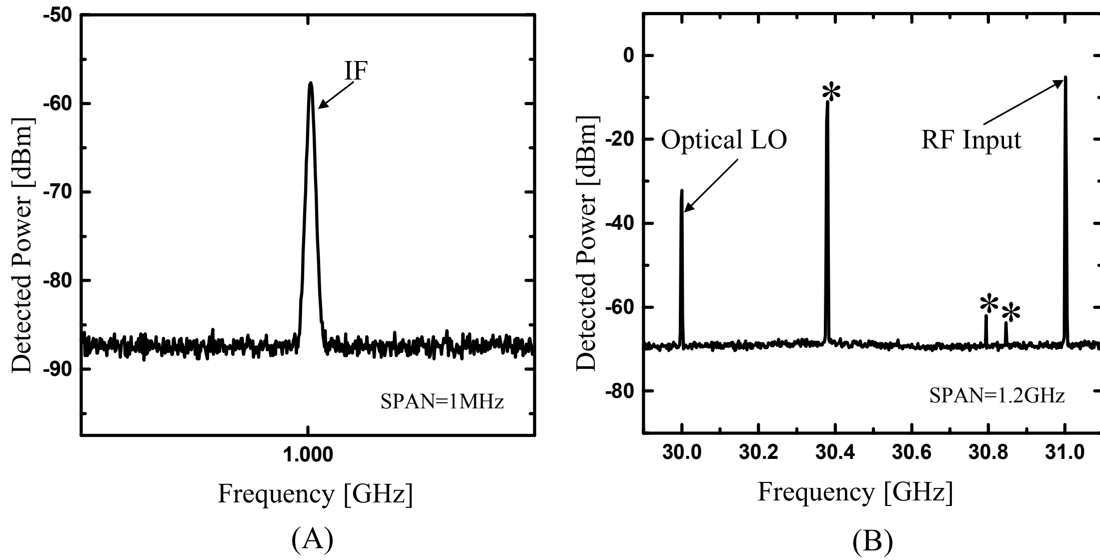

Figure A-5. (A) 1GHz frequency down-converted spectrum (B) photodetected 30GHz LO spectrum and input RF spectrum applied to photodiode. The asterisks indicate image signals caused by external A-band harmonic mixer used for 30GHz measurement.

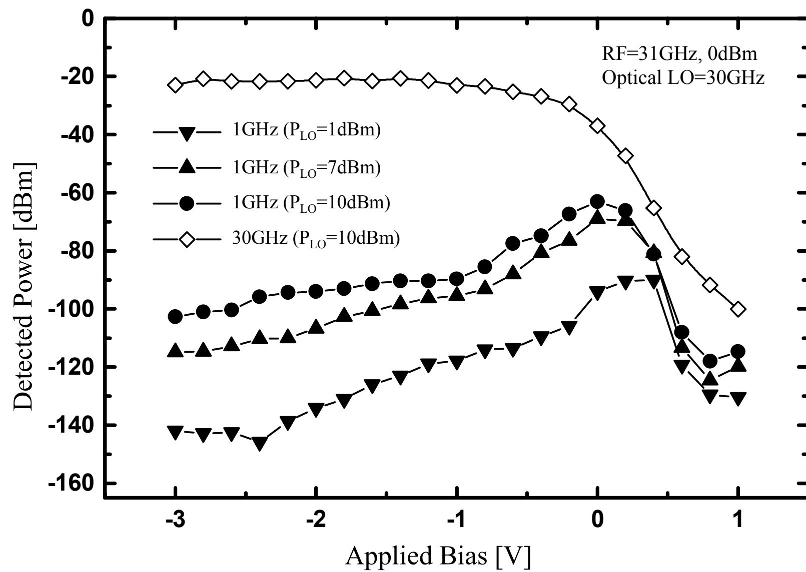

Figure A-6. Dependence of photodetected power at 30GHz LO and frequency down-converted power at 1GHz IF on the bias condition of photodiode.

B. MEDICI simulation code for lattice-matched InP HEMT

These simulation codes were programmed for the two-dimensional analysis of lattice-matched $In_{0.52}Al_{0.48}As/In_{0.53}Ga_{0.47}As/InP$ HEMT.

```
TITLE     Lattice_matched_InP HEMT simulation

COMMENT   Define the mesh
MESH      OUT.FILE=MESH_INPHEMT
X.MESH    WIDTH=0.8     H1=0.1    H2=0.03
X.MESH    WIDTH=0.4     H1=0.03   H2=0.01
X.MESH    WIDTH=1.75    H1=0.01   H2=0.01
X.MESH    WIDTH=0.4     H1=0.01   H2=0.03
X.MESH    WIDTH=0.8     H1=0.03   H2=0.1

Y.MESH    DEPTH=0.04    N.SPACES=3
Y.MESH    DEPTH=0.02    N.SPACES=3
Y.MESH    DEPTH=0.02    N.SPACES=5
Y.MESH    DEPTH=0.0045  N.SPACES=10
Y.MESH    DEPTH=0.02    N.SPACES=20
Y.MESH    DEPTH=0.30    N.SPACES=5
Y.MESH    DEPTH=0.3055  N.SPACES=4

COMMENT   Specify epitaxial layers for InP HEMT
REGION    NAME=PASS NITRIDE
REGION    NAME=BODY INP Y.MIN=0.4045 Y.MAX=2
REGION    NAME=CAPPING1 INGAAS X.MIN=0.0 X.MAX=1.0 Y.MIN=0.04
+         Y.MAX=0.06 X.MOLE=0.47
REGION    NAME=CAPPING2 INGAAS X.MIN=3.15 X.MAX=4.15 Y.MIN=0.04
+         Y.MAX=0.06 X.MOLE=0.47
REGION    NAME=BARRIER ALINAS Y.MIN=0.06 Y.MAX=0.08 X.MOLE=0.48
REGION    NAME=SPACER  ALINAS Y.MIN=0.08 Y.MAX=0.0845 X.MOLE=0.48
REGION    NAME=CHANNEL INGAAS Y.MIN=0.0845 Y.MAX=0.1045 X.MOLE=0.47
REGION    NAME=BUFFER  ALINAS Y.MIN=0.1045 Y.MAX=0.4045 X.MOLE=0.48

COMMENT   Specify electrode
ELECT     NAME=SOURCE     X.MIN=0.0 X.MAX=0.2 Y.MIN=0.0 Y.MAX=0.04
ELECT     NAME=DRAIN      X.MIN=3.95 X.MAX=4.15 Y.MIN=0.0 Y.MAX=0.04
ELECT     NAME=GATE       X.MIN=1.6 X.MAX=1.85 Y.MIN=0.0 Y.MAX=0.06

COMMENT   Specify the doping concentration of each area
PROFILE   REGION=CAPPING1 N.TYPE  CONC=1E18 UNIF
PROFILE   REGION=CAPPING2 N.TYPE  CONC=1E18 UNIF
PROFILE   REGION=BODY     N.TYPE  CONC=1E2  UNIF
```

```
PROFILE     REGION=BARRIER    N.TYPE    CONC=1E2    UNIF
PROFILE     REGION=SPACER     N.TYPE    CONC=1E2    UNIF
PROFILE     REGION=CHANNEL    N.TYPE    CONC=1E2    UNIF
PROFILE     REGION=BUFFER     N.TYPE    CONC=1E2    UNIF
INTERFACE REGION=(BARRIER,SPACER) QF=5.8E12

COMMENT     Specify the gate metal workfunction
CONTACT     NAME=GATE SCHOTTKY WORK=5.17
PLOT.2D     SCALE GRID

COMMENT     Plot InP HEMT structure
PLOT.2D     BOUNDARY FILL Y.MAX=0.45
FILL        REGION=CAPPING1 COLOR=8 ^NP.COL
FILL        REGION=CAPPING2 COLOR=8
FILL        REGION=BARRIER    COLOR=3
FILL        REGION=SPACER     COLOR=4
FILL        REGION=CHANNEL    COLOR=7
FILL        REGION=BUFFER     COLOR=5
FILL        REGION=BODY COLOR=9

COMMENT     Save mesh for InP HEMT
SAVE        MESH     OUT.FILE=MESH_INPHEMT_AFTER

COMMENT     Define the models
MODELS      IMPACT.I CONSRH AUGER ANALYTIC

COMMENT     Initial solution
COMMENT     Turn-on condition simulation
SYMB        NEWT CARR=0
SOLVE       V(DRAIN)=0.05 V(GATE)=0.8 OUT.FILE=HEMT_VG08_NC
LOG         CLOSE

COMMENT     Plot electron and doping profile
PLOT.1D     X.ST=1.8 X.EN=1.8 Y.ST=0.05 Y.EN=0.11 DOPING LOG TOP=1E19
+           OUT.FILE=DOPING_VG08
PLOT.1D     X.ST=1.8 X.EN=1.8 Y.ST=0.05 Y.EN=0.11 ELECTRON LOG UNCH COLOR=2
+           OUT.FILE=ELECTRON_VG08

COMMENT     Energy-band simulation
PLOT.1D     X.ST=1.8 X.EN=1.8 Y.ST=0.05 Y.EN=0.11 COND NEG TOP=1 BOT=-3
+           TITLE="VG04"
+           OUT.FILE=COND_VG08
PLOT.1D     X.ST=1.8 X.EN=1.8 Y.ST=0.05 Y.EN=0.11 VAL UNCH NEG
+           OUT.FILE=VAL_VG08
PLOT.1D     X.ST=1.8 X.EN=1.8 Y.ST=0.05 Y.EN=0.11 QFN UNCH NEG COL=2
+           OUT.FILE=FERMI_VG08

COMMENT     Initial solution
COMMENT         Turn-on condition simulation
SYMB        NEWT CARR=0
```

```
SOLVE      V(DRAIN)=0.05 V(GATE)=0.4 OUT.FILE=HEMT_VG04_NC
LOG          CLOSE

COMMENT     Plot electron and doping profile
PLOT.1D     X.ST=1.8 X.EN=1.8 Y.ST=0.05 Y.EN=0.11 DOPING LOG TOP=1E19
+           OUT.FILE=DOPING_VG04
PLOT.1D     X.ST=1.8 X.EN=1.8 Y.ST=0.05 Y.EN=0.11 ELECTRON LOG UNCH COLOR=2
+           OUT.FILE=ELECTRON_VG04

COMMENT     Energy-band simulation
PLOT.1D     X.ST=1.8 X.EN=1.8 Y.ST=0.05 Y.EN=0.11 COND NEG TOP=1 BOT=-3
+           TITLE="VG04"
+           OUT.FILE=COND_VG04
PLOT.1D     X.ST=1.8 X.EN=1.8 Y.ST=0.05 Y.EN=0.11 VAL UNCH NEG
+           OUT.FILE=VAL_VG04
PLOT.1D     X.ST=1.8 X.EN=1.8 Y.ST=0.05 Y.EN=0.11 QFN UNCH NEG COL=2
+           OUT.FILE=FERMI_VG04

COMMENT     Initial solution
COMMENT            Turn-on condition simulation
SYMB       NEWT CARR=0
SOLVE      V(DRAIN)=0.05 V(GATE)=0.0 OUT.FILE=HEMT_VG00_NC
LOG          CLOSE

COMMENT     Plot electron and doping profile
PLOT.1D     X.ST=1.8 X.EN=1.8 Y.ST=0.05 Y.EN=0.11 DOPING LOG TOP=1E19
+           OUT.FILE=DOPING_VG00
PLOT.1D     X.ST=1.8 X.EN=1.8 Y.ST=0.05 Y.EN=0.11 ELECTRON LOG UNCH COLOR=2
+           OUT.FILE=ELECTRON_VG00

COMMENT     Energy-band simulation
PLOT.1D     X.ST=1.8 X.EN=1.8 Y.ST=0.05 Y.EN=0.11 COND NEG TOP=1 BOT=-3
+           TITLE="VG00"
+           OUT.FILE=COND_VG00
PLOT.1D     X.ST=1.8 X.EN=1.8 Y.ST=0.05 Y.EN=0.11 VAL UNCH NEG
+           OUT.FILE=VAL_VG00
PLOT.1D     X.ST=1.8 X.EN=1.8 Y.ST=0.05 Y.EN=0.11 QFN UNCH NEG COL=2
+           OUT.FILE=FERMI_VG00

COMMENT     Initial solution
COMMENT     Turn-off condition simulation
SYMB       NEWT CARR=0
SOLVE      V(DRAIN)=0.05 V(GATE)=-1.0 OUT.FILE=HEMT_VGm10_NC
LOG          CLOSE

COMMENT     Plot electron and doping profile
PLOT.1D     X.ST=1.8 X.EN=1.8 Y.ST=0.05 Y.EN=0.11 DOPING LOG TOP=1E19
+           OUT.FILE=DOPING_VGm10
PLOT.1D     X.ST=1.8 X.EN=1.8 Y.ST=0.05 Y.EN=0.11 ELECTRON LOG UNCH COLOR=2
+           OUT.FILE=ELECTRON_VGm10
```

```
COMMENT     Energy-band simulation
PLOT.1D     X.ST=1.8 X.EN=1.8 Y.ST=0.05 Y.EN=0.11 COND NEG TOP=1 BOT=-3
+           TITLE="VGm10"
+           OUT.FILE=COND_VGm10
PLOT.1D     X.ST=1.8 X.EN=1.8 Y.ST=0.05 Y.EN=0.11 VAL UNCH NEG
+           OUT.FILE=VAL_VGm10
PLOT.1D     X.ST=1.8 X.EN=1.8 Y.ST=0.05 Y.EN=0.11 QFN UNCH NEG COL=2
+           OUT.FILE=FERMI_VGm10

COMMENT     ID-VG simulation

COMMENT     Initial solution
SYMB        NEWT CARR=0
SOLVE       V(DRAIN)=0.05 V(GATE)=0.4 OUT.FILE=HEMT_VG04_VD005_NC

COMMENT     TWO-carrier simulation
SYMB        NEWT CARR=2
SOLVE       OUT.FILE=HEMT_VG04_VD005_TC

COMMENT     Initial gate voltage sweep
SOLVE       ELEC=GATE VSTEP=-0.1 NSTEP=2   OUT.FILE=HEMT_IDVG_BEFORE

COMMENT     Plot current path for HEMT
PLOT.2D     FILL BOUND Y.MAX=0.15
CONTOUR     FLOW

COMMENT     Plot current path with color
PLOT.2D     BOUNDARY FILL Y.MAX=0.45
FILL        REGION=CAPPING1 COLOR=8 ^NP.COL
FILL        REGION=CAPPING2 COLOR=8
FILL        REGION=BARRIER   COLOR=3
FILL        REGION=SPACER    COLOR=4
FILL        REGION=CHANNEL   COLOR=7
FILL        REGION=BUFFER    COLOR=5
FILL        REGION=BODY COLOR=9

COMMENT          Gate voltage sweep
SOLVE       ELEC=GATE VSTEP=-0.1 NSTEP=25 OUT.FILE=HEMT_IDVG

COMMENT     Plot ID-VG characteristics
PLOT.1D     X.AXIS=V(GATE) Y.AXIS=I(DRAIN) POINTS
+           TITLE="ID-VG characteristics"
+           OUT.FILE=ID_VG_HEMT
LOG         CLOSE

COMMENT     ID-VD simulation

SYMB        NEWT CARR=0
SOLVE       V(GATE)=0.0 V(DRAIN)=0.05 OUT.FILE=HEMT_VG00_VD005_NC
```

```
SYMB        NEWT CARR=2
SOLVE       OUT.FILE=HEMT_VG00_VD005_TC

COMMENT     Initial drain voltage sweep
SOLVE       ELEC=DRAIN VSTEP=0.05 NSTEP=2 OUT.FILE=HEMT_IDVD_BEFORE

COMMENT     Drain voltage sweep
SOLVE       ELEC=DRAIN VSTEP=0.1 NSTEP=10 OUT.FILE=HEMT_IDVD

COMMENT     Plot ID-VD characteristics
PLOT.1D     X.AXIS=V(DRAIN) Y.AXIS=I(DRAIN) POINTS
+           TITLE="ID-VD characteristics"
+           OUT.FILE=ID_VD_HEMT
LOG         CLOSE
```

The device structure of InP HEMT and current conducting path are displayed in figure-A-B-1.

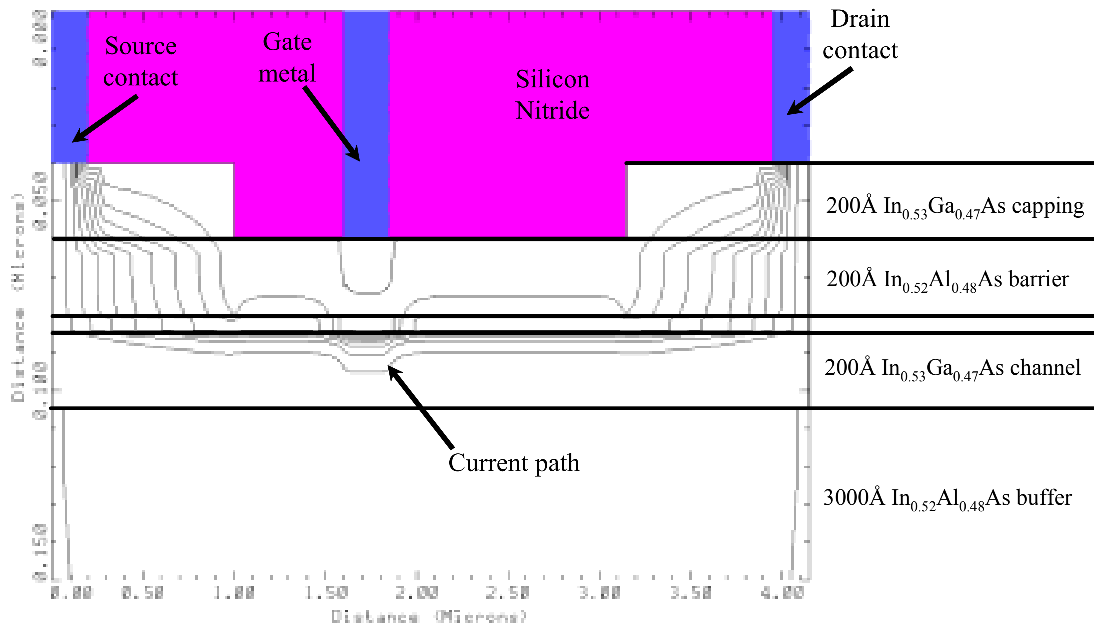

Figure A- 7. Simulated InP HEMT structure and current conducting path.

Publication lists

International Journals

[1] **Chang-Soon Choi**, Hyo-Soon Kang, Woo-Young Choi, Dae-Hyun Kim and Kwang-Seok Seo, "Phototransistors based on InP HEMTs and their applications to millimeter-wave radio-on-fiber systems," *IEEE Trans. Microwave Theory Tech.*, vol. 53, no. 1, Jan. 2005.

[2] Hyo-Soon Kang, **Chang-Soon Choi**, Woo-Young Choi, Dae-Hyun Kim and Kwang-Seok Seo, "Characterization of phototransistor internal gain in metamorphic high-electron mobility transistors," *Appl. Phys. Lett.*, vol. 84, no. 19, pp. 3780, May 2004.

[3] **C.-S. Choi**, H.-S. Kang, W.-Y. Choi, H.-J. Kim, D.-H. Kim. K.-C. Jang and K.-S. Seo, "High optical responsivity of InAlAs/InGaAs metamorphic high-electron mobility transistor on GaAs substrate with composite channel," *IEEE Photon. Technol. Lett.*, vol. 15, no. 6, pp. 846, Jun. 2003.

[4] **Chang-Soon Choi**, Hyo-Soon Kang, Dae-Hyun Kim, Kwang-Seok Seo and Woo-Young Choi, "60GHz harmonic optoelectronic up-conversion using InAlAs/InGaAs metamorphic HEMT on GaAs substrate," *Japanese Journal of Applied Physics*, vol. 42, no. 6B, pp. L658, Jun. 2003.

[5] Young-Kwang Seo, **Chang-Soon Choi** and Woo-Young Choi, "All-optical signal up-conversion for radio-on-fiber applications using cross-gain modulation in semiconductor optical amplifiers," *IEEE Photon. Technol. Lett.*, vol. 14, no. 10, pp. 1448, Sep. 2002.

[6] **C.-S. Choi**, W.-Y. Choi, M.-H. Joo, J.-H. Song and S. Im, "Optimum B+ implantation conditions for the edge termination of the Au/n-Si Schottky diodes," *Journal of Vacuum Science & Technology B*, vol. 20, no. 2, pp. 613, Mar. 2002.

[7] **Chang-Soon Choi**, Kyung-Whan Kim and Woo-Young Choi, "Design and analysis of a new self-aligned asymmetric structure for deep submicrometer MOSFET," *Solid-State Electronics*, vol. 45, no. 9, pp. 1673, Sep. 2001.

[8] Kyung-Whan Kim, **Chang-Soon Choi** and Woo-Young Choi, "Analysis of a novel self-aligned elevated source/drain MOSFET with reduced gate induced drain leakage current and high driving capability," *Japanese Journal of Applied Physics*, vol. 39, no. 11, pp. 6208, Nov. 2000.

International Conferences

[1] **Chang-Soon Choi**, Jun-Hyuk Seo, Woo-Young Choi, Hideki Kamitsuna, Minoru Ida and Kenji Kurishima, "Radio-on-fiber downlink transmission systems based on optically controlled InP/InGaAs HPT oscillators," will be presented in *IEEE MTT-S Int. Microwave Symp*, Long Beach, USA, 2005

[2] Jun-Hyuk Seo, **Chang-Soon Choi**, Woo-Young Choi, Young-Shik Kang, Yong-Duk Jung and Jeha Kim, "Bi-directional 60GHz radio-on-fiber systems using cascaded SOA-EAM frequency up/down converters," will be presented in *IEEE MTT-S Int. Microwave Symp*, Long Beach, USA, 2005

[3] Woo-Young Choi, **Chang-Soon Choi**, Hyo-Soon Kang, Dae-Hyun Kim and Kwang-Seok Seo, "Fiber-supported millimeter-wave data transmission systems based on InP HEMTs (invite paper)" will be presented in *The 6th Korea-Japan Joint Workshop on Microwave and Millimeter-wave Photonics*, Kyung-ju, Korea, 2005

[4] Jae-Young Kim, **Chang-Soon Choi**, Hong-Seung Kim, Eun-Soo Nam and Woo-Young Choi, "Equivalent circuit models for InP/InGaAs photo-HBTs," will be presented in *The 6th Korea-Japan Joint Workshop on Microwave and Millimeter-wave Photonics*, Kyung-ju, Korea, 2005

[5] **Chang-Soon Choi**, Jun-Hyuk Seo, Dae-Hyun Kim, Kwang-Seok Seo and Woo-Young Choi, "Radio-on-fiber downlink systems based on InP HEMT oscillators," *Contemporary Photonic Technology (CPT)*, Tokyo, Japan, 2004.

[6] **Chang-Soon Choi** and W.-Y. Choi, "Millimeter-wave optoelectronic mixers based on InP HEMTs (invited paper)," *IEEE LEOS Annual Meeting Technical Digest*, pp. 126, Puerto Rico, USA, 2004.

[7] Jun-Hyuk Seo, **Chang-Soon Choi**, Woo-Young Choi, Young-Shik Kang, Yong-Duk Jung and Jeha Kim, "Frequency conversion with cascaded SOA-EAM for bi-directional radio-on-fiber systems," *International Topical Meeting on Microwave Photonics*, pp. 56, Ogunquit, USA. 2004.

[8] **Chang-Soon Choi**, Hyo-Soon Kang, Dae-Hyun Kim, Kwang-Seok Seo and Woo-Young Choi, "Characteristics of InP HEMT harmonic optoelectronic mixers and their applications to 60GHz radio-on-fiber systems," *IEEE MTT-S Int. Microwave Symp. Digest*, pp.401, Fort Worth, USA, 2004.

[9] **Chang-Soon Choi**, Hyo-Soon Kang, Dae-Hyun Kim, Kwang-Seok Seo and Woo-Young Choi, "Millimeter-wave InP HEMT optoelectronic mixers," *The 5th Japan-Korea Joint Workshop on Microwave and Millimeter-wave Photonics*, pp. 19, Otsu, Japan, 2004.

[10] Hyo-Soon Kang, **Chang-Soon Choi**, Dae-Hyun Kim, Kwang-Seok Seo and Woo-Young

Choi, "High conversion gain optoelectronic mixer based on metamorphic *HEMT," International Topical Meeting on Microwave Photonics*, pp. 105, Budapest, Hungary, 2003.

[11] **Chang-Soon Choi**, Woo-Young Choi, Dae-Hyun Kim and Kwang-Seok Seo, "A millimeter-wave harmonic optoelectronic mixer based on InAlAs/InGaAs metamorphic HEMT," *IEEE MTT-S Int. Microwave Symp. Digest*, pp. 1383, Philadelphia, USA, 2003.

[12] Y.-K. Seo, J.-H. Seo, **C.-S. Choi** and W.-Y. Choi, "Remote photonic frequency-upconversion using a semiconductor optical amplifier for WDM/Broadband radio-on-fiber links," *The 4th Korea-Japan Joint Workshop on Microwave and Millimeter-wave Photonics*, pp. 201, Daejun, Korea, 2003.

[13] **Chang-Soon Choi**, Woo-Young Choi, Dae-Hyun Kim and Kwang-Seok Seo, "InAlAs/InGaAs/GaAs metamorphic HEMT as a photodetector and an optoelectronic up-converter," *The 4th Korea-Japan Joint Workshop on Microwave and Millimeter-wave Photonics*, pp. 37, Daejun, Korea, 2003.

[14] Y.-K. Seo, J.-H. Seo, **C.-S. Choi** and W.-Y. Choi, "WDM/Radio-on-fiber distribution using remote photonic frequency upconversion," *Contemporary Photonic Technology (CPT)*, pp. 115, Tokyo, Japan, 2004.

[15] Y.-K. Seo, **C.-S. Choi** and W.-Y. Choi, "All optical signal up-conversion at K-band using SOA," *The 3rd Japan-Korea Joint Workshop on Microwave and Millimeter-wave Photonics*, pp. 119, Tokyo, Japan, 2002.

[16] **Chang-Soon Choi**, Kyung-Whan Kim and Woo-Young Choi, "A new self-aligned asymmetric structure for 0.1μm technology," *IEEE Hong Kong Electron Devices Meeting*, pp. 54, Hong-Kong, 2000.

[17] **Chang-Soon Choi**, Kyung-Whan Kim and Woo-Young Choi, "A study on the characteristics of high performance self-aligned asymmetric structure MOSFET," *Asia-Pacific Workshop on Fundamental and Application of Advanced Semiconductor Device*," pp. 3, Okinawa, Japan, 2000.

Awards

[1] 2004 IEEE MTT-S International Microwave Symposium, Fort Worth, USA,
Student Paper Competition Finalist

Domestic Conferences

[1] **<u>최창순</u>**, 김재영, 김홍승, 남은수, 최우영, “A 1.25Gbps radio-on-fiber transmission in 60GHz band using an InP heterojunction phototransistor,” *Photonics Conference*, 단양대명콘도, 2004.

[2] **<u>최창순</u>**, 강효순, 김대현, 서광석, 최우영, ”Fiber-optic/60GHz broadband transmission systems using InP HEMT phototransistors,” 제 11회 광전자 및 광통신 학술회의, pp. 283, 한국정보통신대학교, 2004.

[3] 서준혁, **<u>최창순</u>**, 최우영, 강영식, 정용덕, 김제하, “전계흡수 변조기를 이용한 광학적 주파수 상/하향 변환기,” 제 11회 광전자 및 광통신 학술회의, pp. 237, 한국정보통신대학교, 2004.

[4] **<u>최창순</u>**, 최우영, 김홍승, 정동윤, 남은수, “Photonic InP/InGaAs HBT for radio-on-fiber application,” *Photonics Conference*, pp. 73, 한화리조트, 2003.

[5] **<u>최창순</u>**, 권용환, 최중선, 서영광, 최우영, “도파로형 광검출소자를 이용한 광전 주파수 하향변환,” 제 10회 광전자 및 광통신 학술회의, pp. 457, 강촌리조트, 2003.

[6] 강효순, **<u>최창순</u>**, 최우영, 장경철, 서광석, “InP HEMT의 광검출 특성,” 광학회 동계학술대회, pp. 146, 인하대학교, 2003.

[7] 강효순, **<u>최창순</u>**, 최우영, 손주혁, 장경철, 서광석, “InP HEMT의 변조된 1.55μm 광신호 검출 특성,” *Photonics Conference*, pp. 719, 용평리조트, 2002.

[8] **<u>최창순</u>**, 강효순, 서영광, 서준혁, 최우영, 장경철, 김대현, 서광석, “60GHz broadband up-conversion using metamorphic HEMT as a harmonic optoelectronic mixer,” *Photonics Conference*, pp. 83, 용평리조트, 2002.

[9] **<u>최창순</u>**, 강효순, 최우영, 김회종, 최원준, 장경철, 김대현, 서광석, “Photoresponse of InAlAs/InGaAs metamorphic HEMT on GaAs substrate with composite channel,” *Photonics Conference*, 용평리조트, 2002.